

We are IntechOpen, the world's leading publisher of Open Access books Built by scientists, for scientists

6,900

Open access books available

186,000

International authors and editors

200M

Downloads

Our authors are among the

154

Countries delivered to

TOP 1%

most cited scientists

12.2%

Contributors from top 500 universities



WEB OF SCIENCE™

Selection of our books indexed in the Book Citation Index
in Web of Science™ Core Collection (BKCI)

Interested in publishing with us?
Contact book.department@intechopen.com

Numbers displayed above are based on latest data collected.
For more information visit www.intechopen.com



Equilibrium Nucleation, Growth, and Thermal Stability of Graphene on Solids

E.V.Rut'kov and N.R.Gall

*Ioffe Physico-Technical Institute of Russian Academy of Sciences,
St.Petersburg, Polytechnicheskaya, 26, 194021,
Russia*

1. Introduction

Graphene and graphite films form on the surface of many metals: Pt(100) [1], Pt(111) [2], Ru(001) [3], Ni(111) [4--6], Pd(100), Pd(111), Co(0001) [7], Mo(110) [8], Mo(100) [9], Fe(100) [10]. Re(1010) [11], Rh(111) [12], Ir(111), Ir(100) [13--15], on polycrystalline Pd [16], and carbides of a number of metals [17, 18].

The simplest way of producing graphene on the surface of a variety of metals consists in exposing a heated metal sample to an atmosphere of hydrocarbons C_xH_y —in most cases, this is benzene C_6H_6 . A critical step in these experiments is to choose correctly the temperature of the heated metal, which, as a rule, should be not below 900--1000 K. C_xH_y molecules striking the heated metal dissociate intensively, with H_2 desorbing, and carbon remaining stuck onto the metal surface; its subsequent fate depends essentially on the actual type of the metal involved. This exposure to hydrocarbons culminates in formation of a continuous two-dimensional film of carbon with graphite structure, i.e., a graphene film. The physics underlying these processes differs radically among different Me-C systems. Consider several characteristic metal-graphene systems which were studied thoroughly under identical conditions.

A. Graphene on Ir(111) and Ir(100) [13—15]

The samples used most frequently in our experiments were thin textured metallic ribbons measuring $(50 \times 0.02 \times 1)$ mm³, with the surface uniform in work function $e\phi = 5.75$ eV, which corresponds to the closely packed (111) face [19]. While the experiments performed with iridium single crystals with (111) and (100) faces did not reveal any radical differences in the results obtained, thin ribbons prove to be much more convenient for the experimentalist.

The major attractive feature of iridium consists in that carbon, unlike other metals, does not dissolve in its bulk, thus simplifying considerably interpretation of the results obtained.

Figure 1 plots the variation of carbon and iridium Auger signal intensity with the time of exposure to benzene vapor at $T = 1650$ K. The Auger signal of carbon is seen to grow until it reaches saturation. Scanning tunneling microscopy demonstrates convincingly formation on the surface of a continuous graphene layer (Fig. 2) [20-23]. Graphene features valence-saturated, passive surface, which effectively terminates dissociation of C_6H_6 molecules.

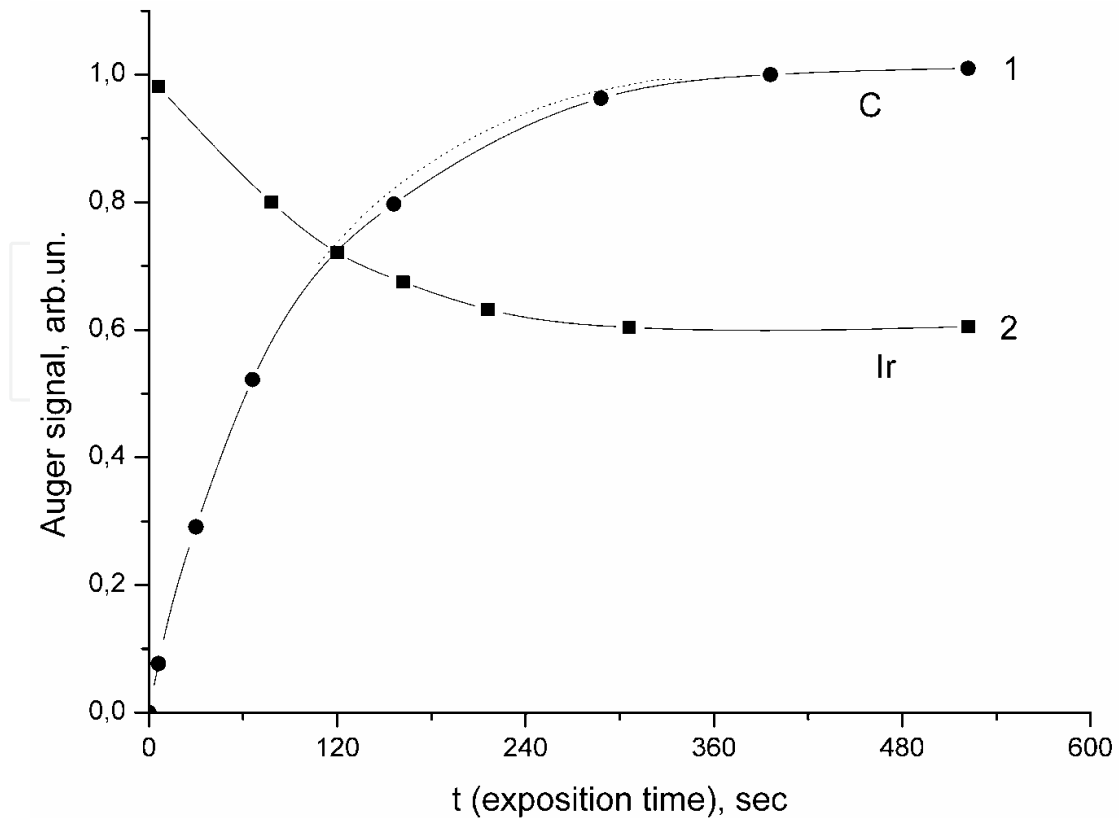


Fig. 1. Auger intensities versus deposition time for iridium ribbon exposure by benzene vapor at 1600 K and $\sim 7 \cdot 10^{-7}$ Torr; 1 - carbon at E = 272 eV, 2 - iridium at E = 176 eV; solid - experimental data, dashed - calculations.

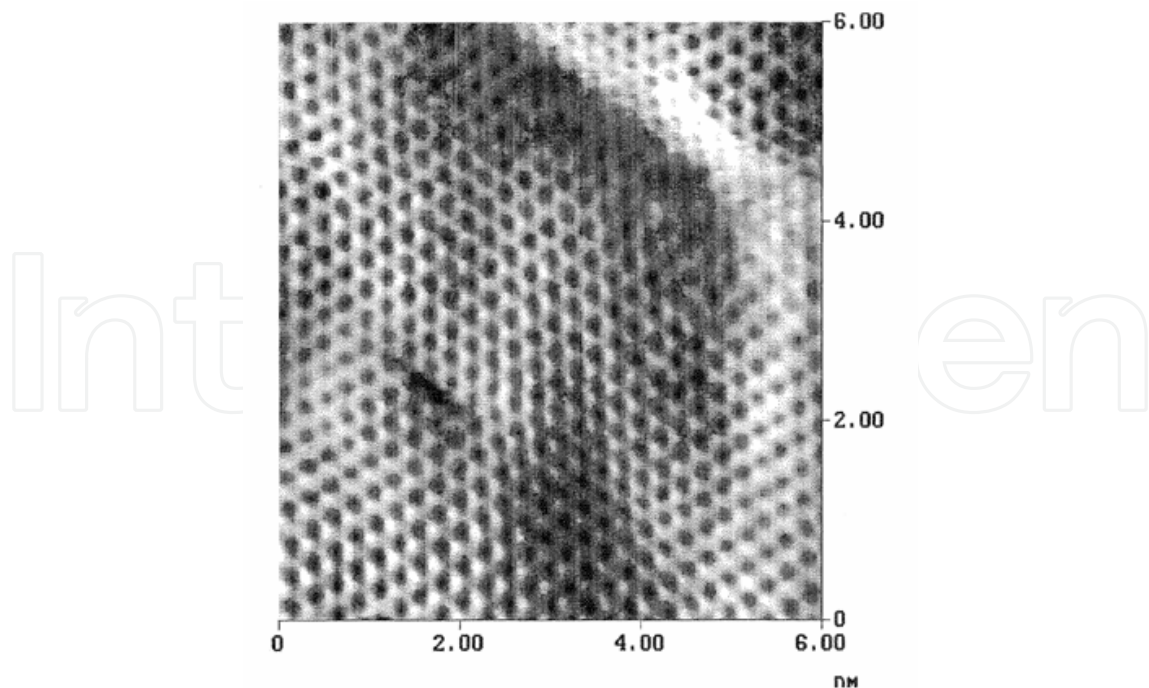


Fig. 2. STM image of a single graphene layer on Ir(111). The image was got using current mode. The layer was intercalated with Cs to saturation. The image size is 10 x 10 nm. The graphitic structure can be clearly seen.

Experiments revealed the growth of a graphene film to proceed through the following stages: adsorbed carbon “gas” → graphene islands in equilibrium with this gas → growth of islands in area → coalescence of the islands to form a continuous graphene layer (see § 5). Graphene islands being catalytically passive, the kinetics of their growth can be described by the equation

$$\frac{dN_c(t)}{dt} = N_{cm}(1 - S_0) \cdot v_c \cdot \eta, \quad (1)$$

where S_0 is the relative area covered by the islands, with $S_0 = 1$ corresponding to a continuous layer (§ 2); $N_c(t)$ is the concentration of carbon atoms on the surface; N_{cm} is carbon concentration in a graphene layer, $N_{cm} = 3.56 \cdot 10^{15}$ at/cm²; v_c is the carbon atom flux incident on the surface; and η is the sticking coefficient of benzene molecules to a graphene-free surface.

In our experiments, the concentration of carbon in the chemisorbed “gas” phase could be neglected [§ 5]; therefore, $\frac{dN_c(t)}{dt} = N_{cm} \left(\frac{dS_0}{dt} \right)$, thus yielding the solution to Eq. (1) in the form

$$N_c(t) = N_{cm} \left[1 - \exp \left(- \frac{v_c \cdot \eta}{N_{cm}} \cdot t \right) \right] \quad (2)$$

The dashed line in Fig. 1 plots relation (2) calculated assuming the carbon Auger signal intensity $I \sim N_c$. The calculated curve is seen to fit nicely to experimental data. Similar results were obtained for other hydrocarbons as well, among them isoprene (C₅H₆), acetylene (C₂H₂), and limonene (C₁₀H₁₀), as well as for single-crystal (100) iridium [§ 15]. The region within which high-quality graphene films can be obtained on iridium is confined to the 1400–1900-K interval; for $T < 1500$ K, one may suggest an increase of the concentration of as-formed graphene islands, with an ensuing growth of defects in the layer produced in the coalescence of these islands (§ 11), while for $T > 1900$ K, desorption of carbon from iridium sets in [14].

B. Graphene on Pt(III), Rh(III), Re(1010) [11, 12, 24]

The above metals do not form bulk carbides [25], and at $T > 1000$ –1100 K carbon atoms start to dissolve intensively in the bulk of the metal. To obtain graphene on Pt(III), both benzene and a calibrated carbon atom flux were employed [26]. Figure 3 displays graphically the variation of carbon Auger signal intensity with the time of carbon atom adsorption at $T = 1475$ K. We readily see that during ~120 s carbon atoms do not accumulate on the surface of platinum (the Auger signal is below the noise level) but dissolve instead actively in its bulk; indeed, desorption can be excluded from consideration because carbon atoms desorb from metal surfaces at high temperatures $T > 1900$ K [27]. After the amount of indiffused carbon has reached the limit of its solubility in platinum, graphene islands will start to form on the surface of the latter, to coalesce finally into a continuous graphene layer ($t = 400$ s, Fig. 3). Significantly, carbonization in contact with benzene vapor produces automatically one graphene layer, just as in the case of iridium. By contrast, the thickness of a film formed under an atomic flux of carbon atoms grows without limit.

Figure 4 presents an Auger spectrum of carbon from graphene atop platinum (1) confronted by that from a graphite film on platinum (2). The Auger spectra displayed exhibit a classical “graphitic” signature (see § 3). In view of the large scatter among available published data, we used a calibrated carbon flux to determine for the Pt–C system the dependence of the

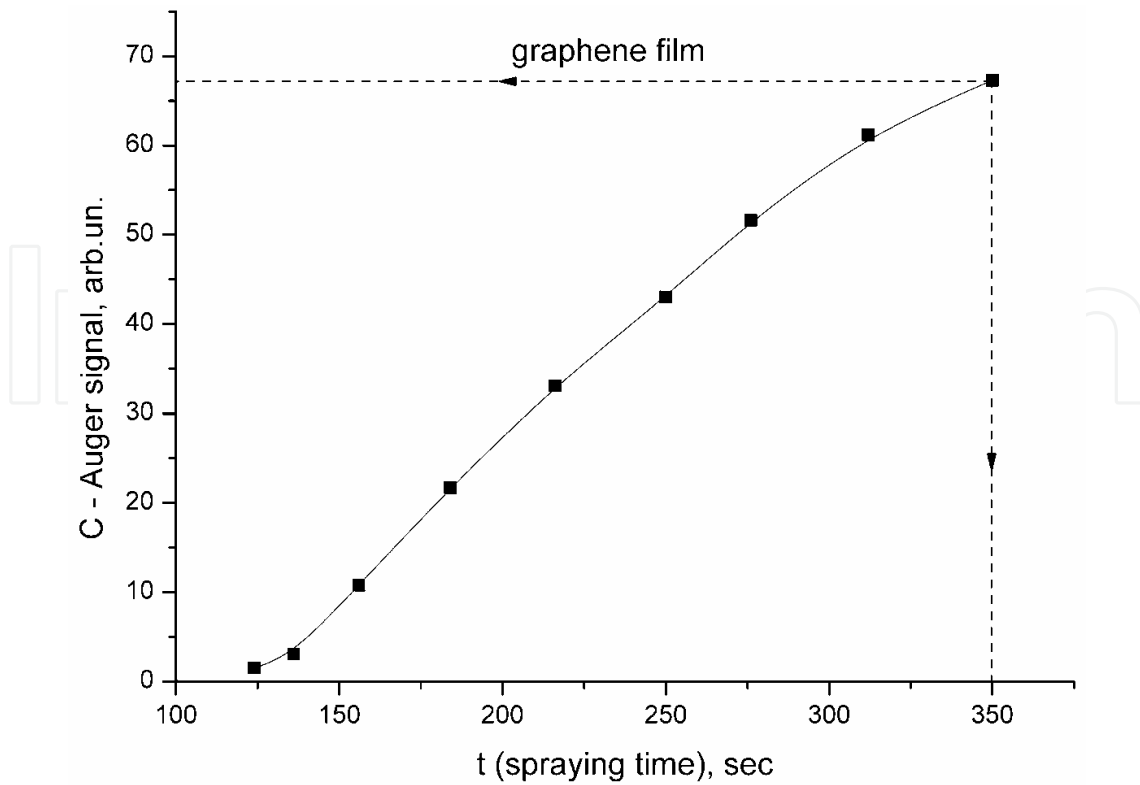


Fig. 3. Carbon Auger signal versus deposition time in atomic carbon deposition onto Pt(111) surface at 1465 K. 67 a.u. corresponds to a single grapheme layer. The deposition flux is $v_C = 3.2 \cdot 10^{13} \text{ cm}^{-2} \cdot \text{s}^{-1}$.

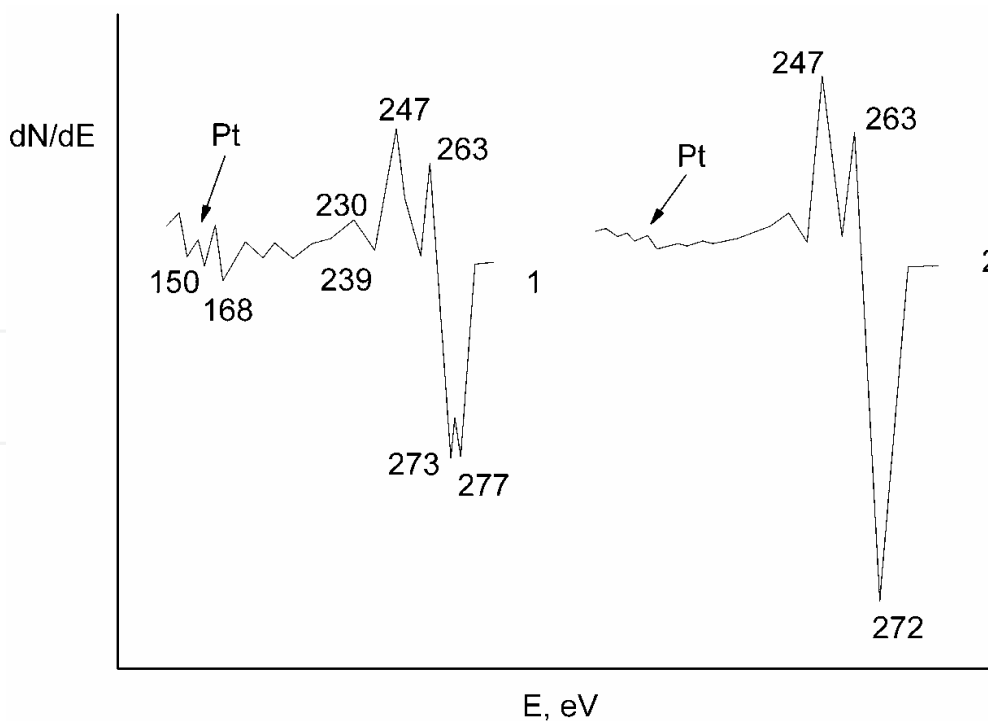


Fig. 4. Carbon KVV Auger spectra for a single graphene layer (1) and 4-layer graphite film (2) on Pt(111). the covers were got using carbon precipitation from the metal bulk at 1300 K. Peaks with energies 150 - 168 eV correspond to Pt Auger transitions.

limiting carbon solubility N_{lim} on substrate temperature from the beginning of appearance of graphene islands on the surface [24]

$$\lg N_{lim} (at. \%) = 2,6 - \frac{7200}{T[K]} \quad (3)$$

Note the low solubility limit of carbon in Pt; indeed, at $T = 1475$ K, $N_{lim} = 2.7 \cdot 10^{-3}$ at. %. Interestingly, although carbon deposition was performed on one side of the platinum ribbon only, on the other side a symmetric pattern was observed, which suggests fast transport of carbon atoms across the bulk of the platinum. Heating of a carbonized sample up to $T = 1800$ K, followed by lowering its temperature to $T = 1475$ K, brings about again fast growth of the graphene layer from the “excess” carbon atoms that have out-diffused from the bulk of the metal onto its surface (§ 8). The operating temperature interval within which graphene can be obtained on platinum is 1000–1900 K. Significantly, if it is needed to “freeze” a graphene layer by dropping sharply the temperature down to room level, one will have to choose the lowest possible carbonization temperature. Otherwise, during the cooling of the ribbon several graphene layers may form from the carbon leaving the metal (§ 8).

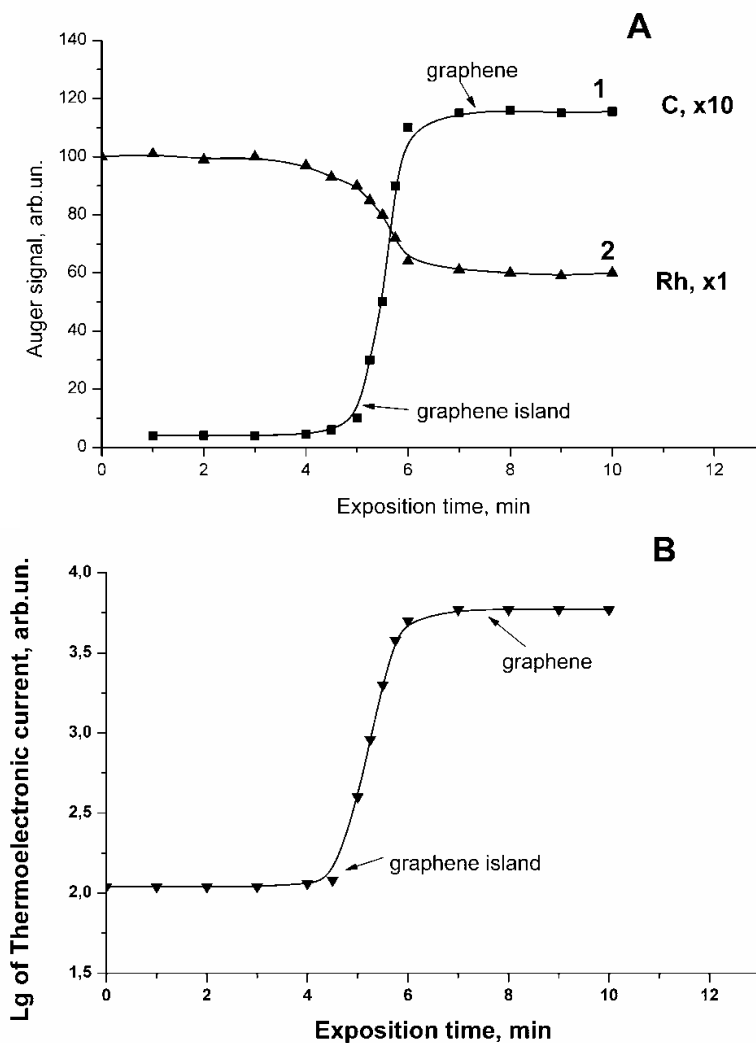


Fig. 5. A: Auger signals of carbon (curve 1), Rh (curve 2); and Fig.5B: thermionic current versus exposition time.

The time needed to load rhodium with carbon at the same temperatures and benzene vapor pressures as in the case of platinum is noticeably longer. Figure 5A demonstrates graphically the variation of the carbon and rhodium Auger signal intensities in the course of carbonization at $T = 1360$ K, and Fig. 5B traces the variation of the thermionic current under the same conditions. The sharp rise of the thermionic current should be ascribed to the formation and growth of graphene islands whose work function $e\phi_1 = 4.35$ eV, to be contrasted with parts of the surface free of islands, where $e\phi_1 = 4.95$ eV (Fig. 5B) [28]. The processes evolving on Rh are similar to those observed on Pt, namely, dissolution of carbon atoms in the bulk of rhodium and their buildup on the surface of the metal \rightarrow formation of graphene islands in equilibrium with the chemisorbed carbon "gas" \rightarrow growth of islands in area culminating in coalescence with eventual formation of a continuous graphene layer, and the carbon Auger signal intensity reaching saturation (Fig. 5A). In contrast to platinum, Auger spectroscopy probes already the carbon "gas" on the surface, whose concentration, for instance, at $T = 1360$ K is $\sim 1 \cdot 10^{14}$ at/cm².

We have succeeded in tracing, just as with platinum, the behavior with temperature of the solubility limit N_{lim} of carbon in rhodium in the 1000--1800-K range:

$$\lg N_{lim}(at. \%) = 2,2 - \frac{4600}{T[K]}. \quad (4)$$

Figure 6 shows graphically the variation of the carbon and rhodium Auger signal intensities with the temperature of a sample carbonized at $T_c = 1400$ K. One could isolate conveniently a few regions in the graph which are of special interest.

A. On the surface-- low-density chemisorbed carbon "gas", which does not affect the rhodium work function $e\phi = 4.95$ eV. Dissolved carbon dose not contribute to the Auger signal intensity of carbon.

B. Nucleation and growth of graphene islands. The surface becomes nonuniform in work function.

C. Termination of formation of a continuous graphene layer on rhodium has come to the end. The surface is again uniform in work function, with $e\phi = 4.35$ eV. The region of existence of a graphene layer is $\Delta T \sim 50^\circ$.

D. Growth of a thick graphite film on Rh through segregation of carbon out of the supersaturated Rh-C solid solution, with the substrate Auger signal intensity dropping below the instrument noise level.

The graph displayed in Fig. 6 is characteristic of nearly all Me-graphene systems, with the exclusion of iridium. It repeats over and over again under increasing or decreasing temperature, without noticeable time delays, which should be assigned to the small thickness of the metal samples used and fast volume diffusion of carbon in metals for $T > 1000$ K.

Regrettably, the strong Auger peak of rhodium at $E = 302$ eV is superimposed on the carbon Auger peak and distorts its shape (Fig. 7, spectrum 1). Therefore, the carbon Auger spectrum assumes a distinct graphitic shape only on formation of several layers of graphene on the surface of rhodium (Fig. 7, spectrum 3).

Formation of a graphene film on Re(1010) takes up still longer metal exposure times in benzene vapor, than is the case with Rh and Pt under the same experimental conditions. Figure 8 displays the kinetics of variation of the Auger spectrum of carbon (1) and rhenium (2) observed under carbonization of a ribbon sample at $T = 1700$ K, The process starts with

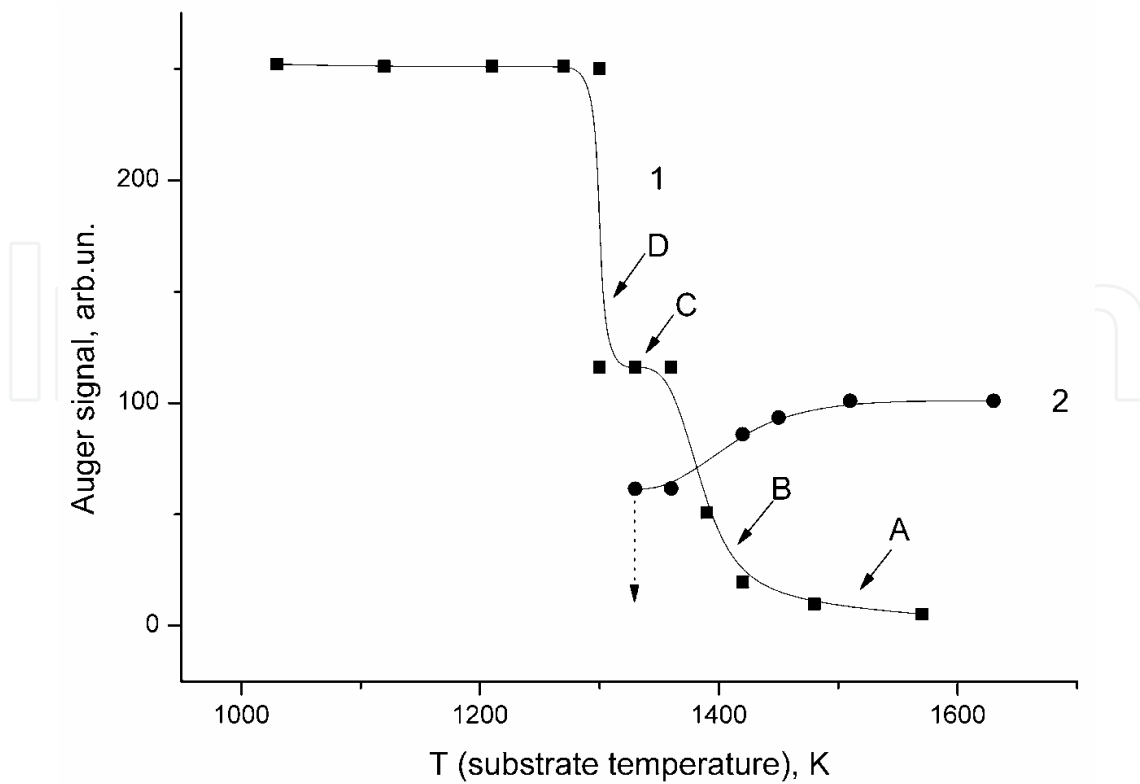


Fig. 6. Auger signals of carbon (1) and Rh (2) versus temperature in sequential annealing of carbonated Rh. Carbonization temperature is $T_C = 1400$ K; time delay at each temperature point is 30 s.

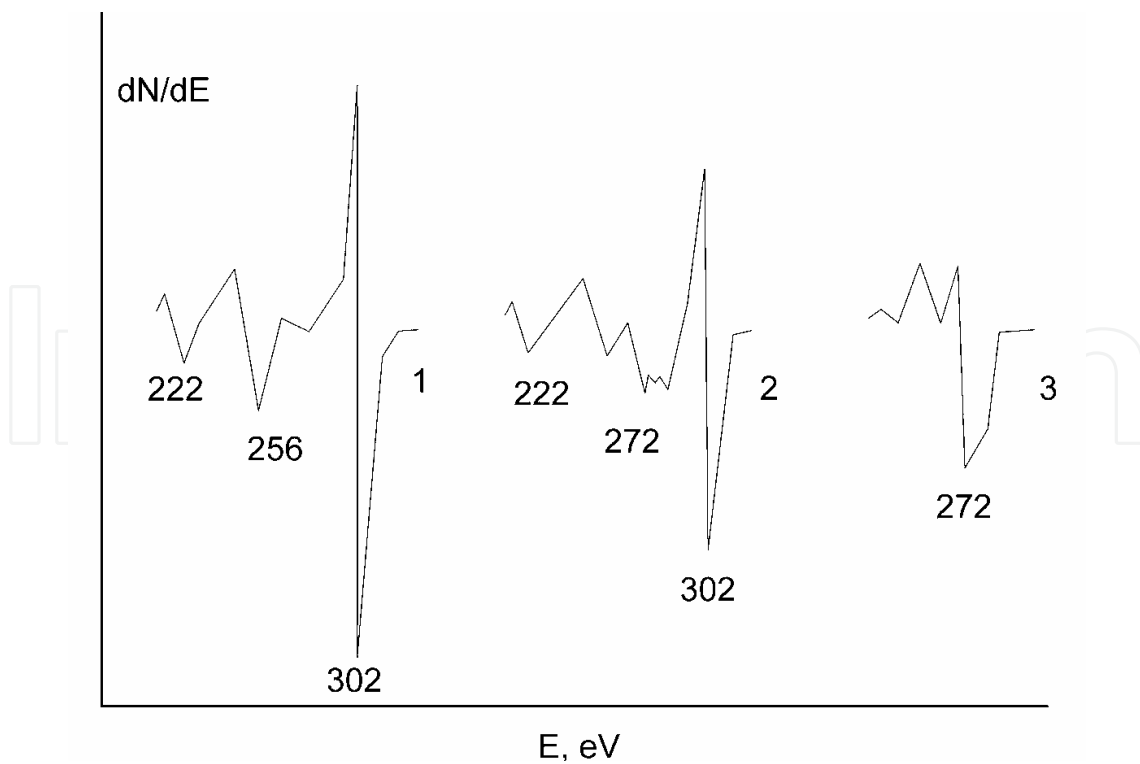


Fig. 7. Auger spectra for pure Rh (1), for Rh with a single graphene layer (2), and for polylayer ($n \sim 8$) graphite film on Rh.

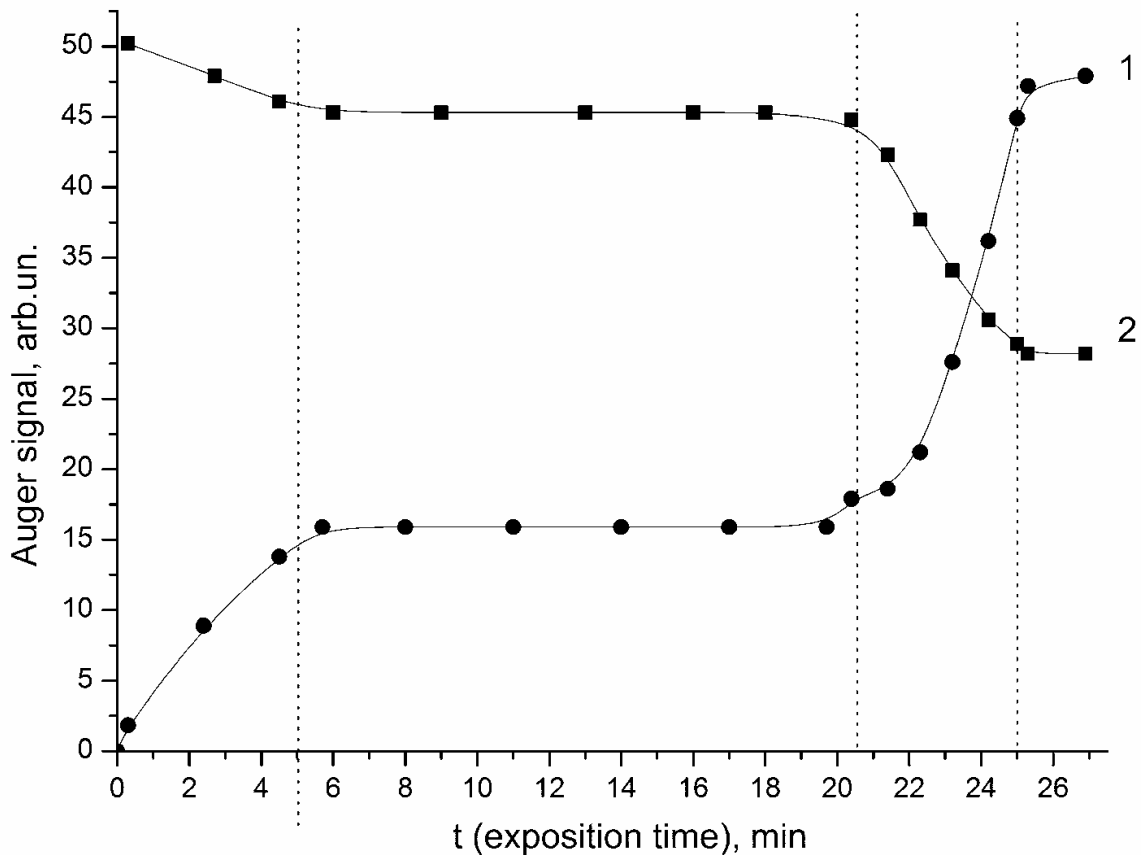


Fig. 8. Auger signals of carbon (1) and Re (2) versus exposure time in carbonization of Re in benzene vapor. Carbonization temperature is $T_C = 1700$ K; benzene pressure is $\sim 1 \cdot 10^{-5}$ Torr

dissolution of carbon in the bulk of the metal, accompanied by its accumulation on the surface. As seen from the graphs, the time $t = 5$ min can be identified with formation on the surface of a stationary carbon coating. Consider some properties of this carbon coating.

1. Concentration of carbon is consistent with the ReC stoichiometry.
2. As carbon deposition continues, the surface concentration $N_s = 1.4 \cdot 10^{15}$ at/cm² does not change for a long time because of all of the evaporated carbon dissolving in the bulk of rhenium.
3. Changing the sample temperature in the 300–1700-K range does not affect the surface concentration of carbon.
4. The Auger spectrum of this coating has a typical “carbide” shape (spectrum 1 in Fig. 9), a feature characteristic of strong Me-C bonding [27]. This coating suppresses the substrate Auger signal intensity only by 10–20%.

We have called this surface compound “surface rhenium carbide”---ReC. According to the diagram of state, volume rhenium carbide should not exist [25]; this restriction does not, however, extend to an interface state. Obviously enough, the surface rhenium carbide resides in dynamic equilibrium with carbon atoms dissolved in the bulk of the metal, so that this carbon phase can likewise be called chemisorbed carbon “gas”. Surface chemical compounds were a subject of a number of our earlier publications [29–33]. For $t \geq 20$ min (Fig. 8), the carbon Auger signal grows somewhat in amplitude to match the coverage

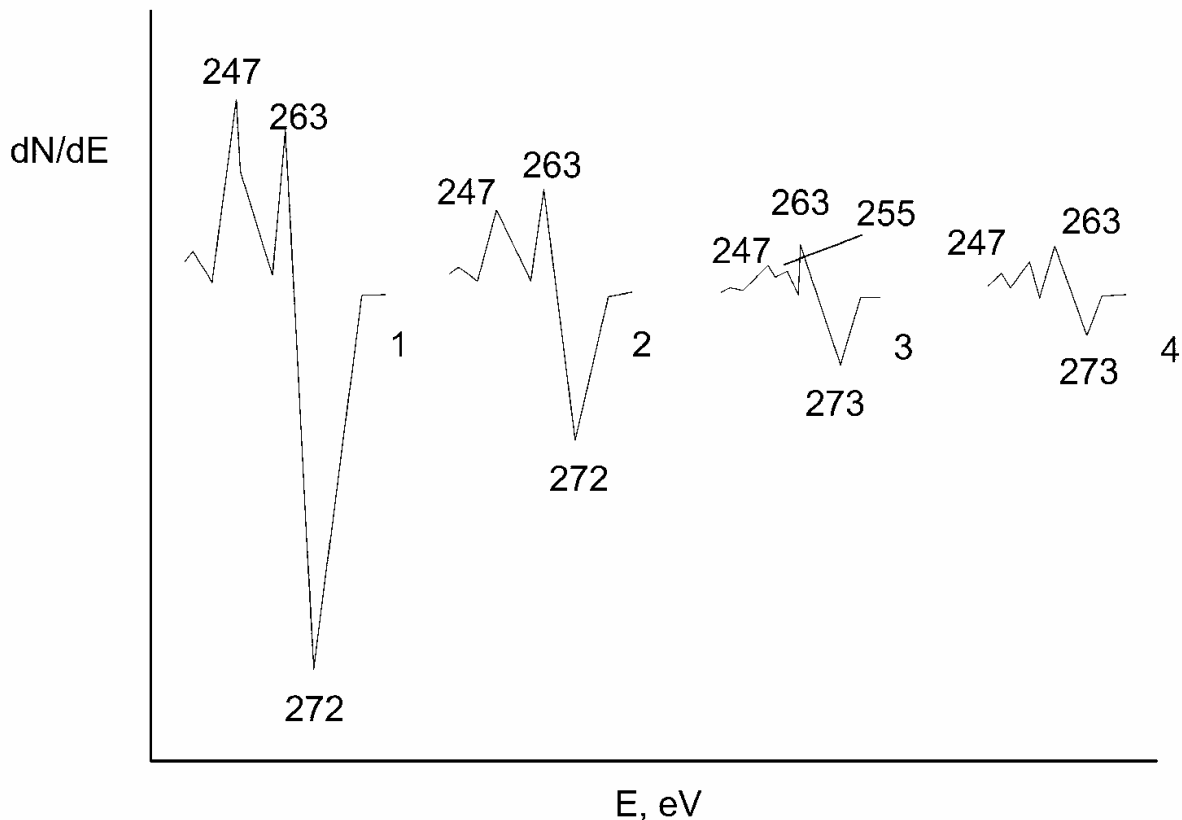


Fig. 9. Carbon KVV Auger spectra for: 1 - Re surface carbide with $N_C = 1.4 \cdot 10^{15} \text{ cm}^{-2}$; 2 - Re surface carbide with $N_C = 2 \cdot 10^{15} \text{ cm}^{-2}$; 3 -- a single graphene layer on Re with the surface carbide behind it; 4 - 7-layer graphite film on Re.

$N_s = 2 \cdot 10^{15} \text{ at/cm}^2$, accompanied by a change in the shape of the Auger spectrum of carbon which remains "carbodic" (spectrum 2 in Fig. 9). For $t > 21 \text{ min}$, the Auger signal of carbon increases noticeably, while that of the substrate decreases by a factor 1.6. For $t \geq 25 \text{ min}$, the Auger signals of carbon and of the substrate change no longer. This stage should be identified with formation of a continuous graphene film on the surface of rhenium, with the carbon Auger spectrum becoming close to "graphitic" in shape (spectrum 3 in Fig. 9); the carbon "gas" confined under the graphene layer amplifies additionally the positive surge of the carbon Auger peak with $E = 263 \text{ eV}$; it is to be confronted with spectrum 4 corresponding to a thick graphite film on rhenium which was obtained through precipitation of carbon from the supersaturated solid solution Re-C by lowering its temperature down to $T = 1300 \text{ K}$.

The process of rhenium carbonization can be visualized not only by AES. Figure 10 displays graphically the variation with temperature of the thermionic current (1) and of pressure (2) in the chamber during carbonization of rhenium at $T = 1780 \text{ K}$. The sharp drop of pressure in the chamber (curve 2) measured by an ionization pressure gauge was caused, as revealed by mass spectrometric measurements, by a change in the composition of the gas atmosphere, because the breakup of benzene molecules on heated rhenium brings about out-diffusion of carbon into the bulk of the metal accompanied by desorption of hydrogen molecules. It is the difference between the ionization coefficients of benzene and hydrogen that accounts for the pressure drop. Interestingly, if, following admission of benzene vapors

into the chamber, one shuts off the pumping and heats rhenium to $T = 1700\text{--}2000\text{ K}$, the benzene vapor in the chamber will become “replaced”, as it were, by hydrogen molecules, a convenient method of obtaining pure hydrogen for experimental purposes indeed! Measurements of thermionic current (curve 1 in Fig. 10) offers a straightforward way to fixing the moment when the limiting concentration of rhenium has been reached and formation of graphene islands has started. Indeed, the start of graphene island formation ($t > 16\text{ min}$) is signaled by a sharp increase of the thermionic emission, because the chemisorbed carbon “gas” raises the rhenium work function from 5.15 to 5.25 eV, while graphene islands lower it strongly to 4.25 eV (§ 7). For $t > 25\text{ min}$, the surface is uniform in work function again, with $e\phi = 4.25\text{ eV}$.

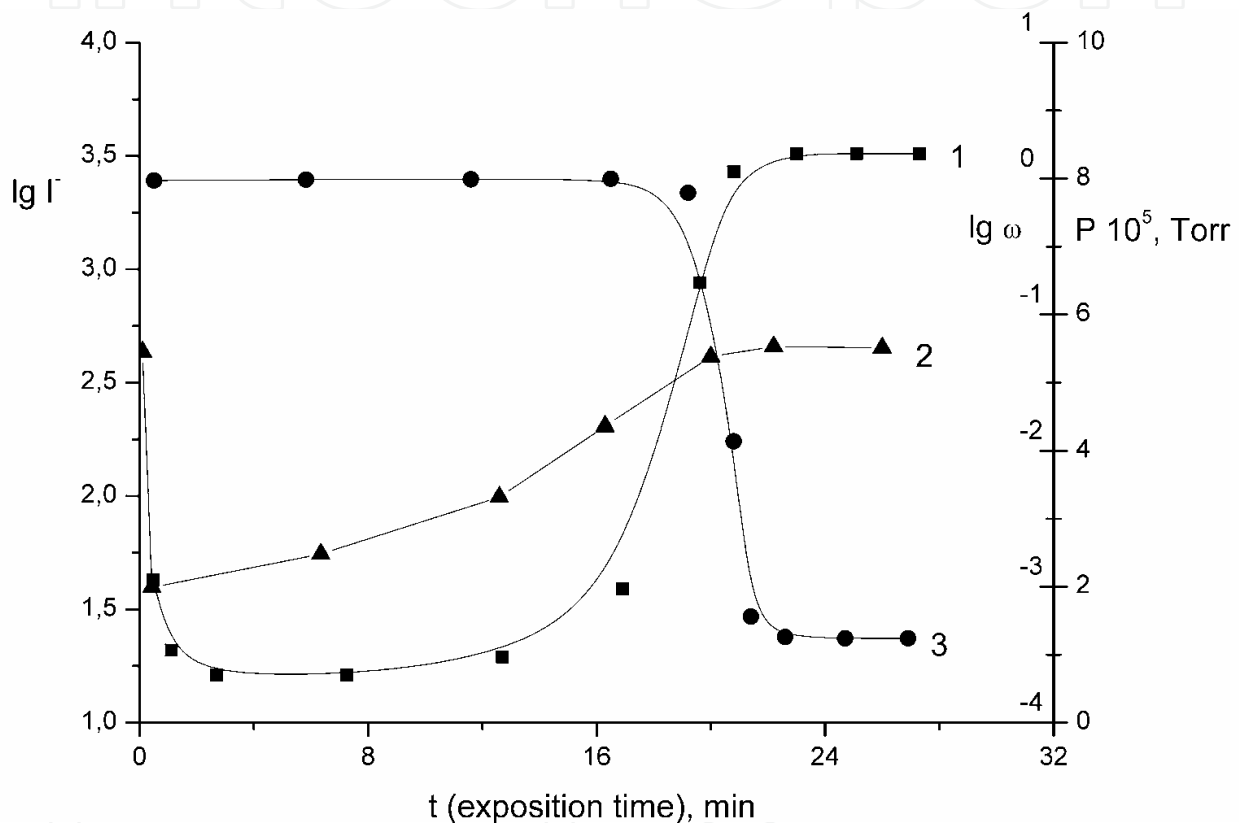


Fig. 10. Thermionic current (1) and $\lg \omega$ for CsCl molecules (3) and the pressure (2) as functions of the exposure time for Re carbonization in benzene vapor at 1780 K. The pressure was measured by ionization manometer calibrated for dry nitrogen.

Just as other Me-C systems, carbonized rhenium can be manipulated purposefully at will by varying its temperature. If the temperature of rhenium carbonized at T_n is raised to $T \approx T_n + 100^\circ$, the graphene layer breaks up in no time and carbon from the graphene phase dissolves in the bulk of the metal leaving on the surface carbon “gas” with a concentration $N_c = 2 \cdot 10^{15}\text{ at/cm}^2$. Lowering the temperature down to $T = T_n$ gives rise to a fast recovery of the graphene layer. Reducing the temperature still lower, to $1100\text{ K} \leq T \leq T_n$, will drive the Re-C solid solution to supersaturation, and carbon will precipitate on the surface forming a graphite film tens of atomic layers thick (spectrum 4 in Fig. 9).

If the temperature of carbonized rhenium $T_n = 1600\text{--}1700\text{ K}$, turning off the ribbon heating current will leave the graphene layer “frozen” on the surface. Carbonization of rhenium at moderate temperatures of $1200\text{--}1500\text{ K}$ can hardly be recommended, because it will result

in formation in the very early stages of graphene islands which will suppress dissociation of benzene molecules, with the ensuing drop of carbon atom flux into the bulk of the metal. Therefore, the process of carbonization may take up several hours [11]. On the other hand, at $T_c = 1100\text{--}1200$ K one may turn off the ribbon heating current after the benzene inlet and prepare a graphene layer with the bulk of the metal remaining practically free of carbon.

A. Graphene on Mo(100) [9, 34]

It is instructive to study the processes involved in graphene formation on carbide-forming metals, for instance, molybdenum. As with rhenium, carbonization of molybdenum passes through a stage of formation of the surface carbide. Figure 11 plots the variation of surface carbon concentration in the course of adsorption of carbon atoms from a calibrated flux striking Mo at $T = 1400$ K. As follows from the overall particle balance, part of the incident carbon atoms dissolve in the bulk of the metal, while the other part remains on the surface. For a total evaporation dose $N = v_c t = 6 \cdot 10^{15}$ at/cm², surface coverage reaches a level $N_c = 1 \cdot 10^{15}$ at/cm², to remain constant thereafter. Knowing the ribbon parameters ($40 \times 0.03 \times 1$) mm³, one readily finds that each atomic plane of the molybdenum ribbon contains dissolved carbon in a concentration $\sim 6 \cdot 10^{10}$ at/cm²; such low concentrations of carbon in the bulk of a molybdenum sample, just as of other Me-C systems, cannot contribute to Auger spectra which originate from surface carbon. All of the newly arriving carbon becomes dissolved in the bulk of molybdenum (Fig. 11). This surface coating has MoC stoichiometry, thus giving us grounds to call it the surface molybdenum carbide, whose Auger spectrum has a “carbide” shape (spectrum 1 in Fig. 12). Variation of the temperature of a molybdenum sample within the 300--1500-K range does not affect in any way the surface concentration of carbon. The chemisorbed carbon atoms from the surface carbide phase are in equilibrium with the atoms of carbon dissolved in the bulk. Surface molybdenum carbide increases noticeably the molybdenum work function from 4.45 to 5.25 eV.

Let us follow the processes occurring on molybdenum surface exposed for a long time to benzene vapors at $T = 1600$ K (Fig. 13). In region I, surface carbide of molybdenum is forming with $\epsilon\phi = 5.25$ eV. Interestingly, this value of $\epsilon\phi$ persists in region II too, which suggests that the surface carbide is sustained there as well. After the carbon solubility limit in the bulk of molybdenum has been reached, in region II starts formation in the near-surface layer of bulk molybdenum carbide, apparently of the Mo₂C composition, as can be inferred from the diagram of state [35]. Bulk molybdenum carbide evolves into the ribbon toward its center. This is what accounts for the variation of the carbon and molybdenum Auger signal stopping in $t > 14$ min, because Auger spectroscopy is capable of probing 3--5 surface layers. That penetration of carbon into the bulk of the ribbon is deep is corroborated by the growth of its resistance and increase by $\sim 200^\circ$ of its radiance temperature. Formation of a volume Mo₂C carbide “poor” in carbon compared with the “carbon-rich” surface carbide MoC was suggested also by experiments on ion etching of carbonized molybdenum, in which after sputtering of the surface carbide the Auger peak of carbon decreased in intensity, whereas that of molybdenum grew to reach new steady-state values identifiable with the volume carbide. Evaluation of the total dose of carbon absorbed by the sample in region II by the time volume carbide evolved to the ribbon center suggests Mo₂C stoichiometry for the volume carbide.

Ion etching revealed that the thickness of the volume carbide layer is $> 10^3$ Å. Formation under the surface carbide in the metal of the volume carbide produces only a weak impact on the “carbide” shape of the Auger peak (compare spectra 1 and 2 in Fig. 12).

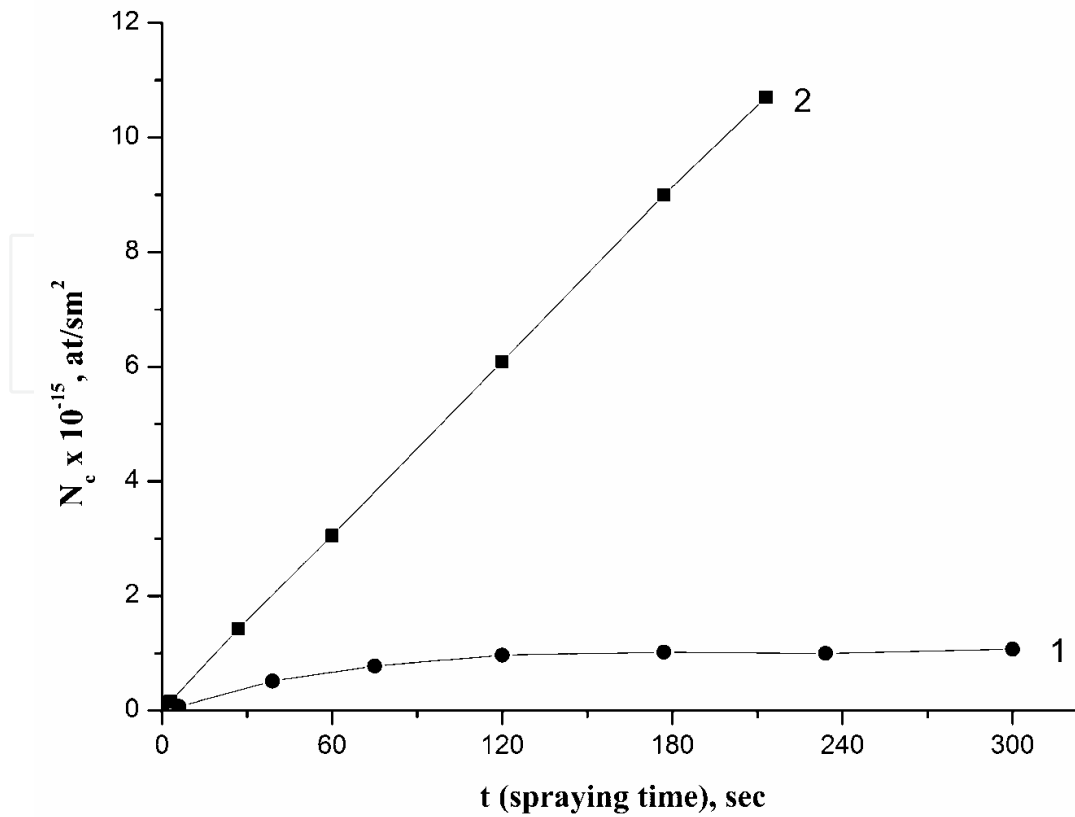


Fig. 11. Carbon surface concentration (1) and the total amount of deposited carbon $N_{\text{tot}} = v_c * t$ (2) in atomic carbon deposition on heated Mo at 1400 K.

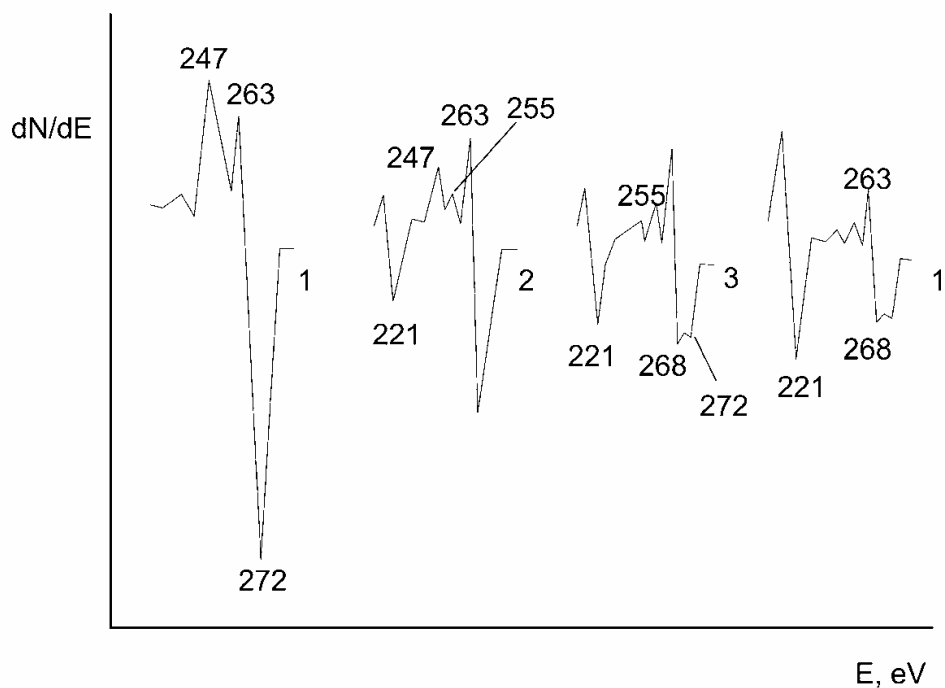


Fig. 12. Auger spectra of various carbon forms on Mo(100) surface: 1 – surface carbide MoC; 2 – bulk carbide MoC₂; 3 -- a single graphene layer with the bulk carbide MoC₂ behind it; 4 - 8-layer graphite film.

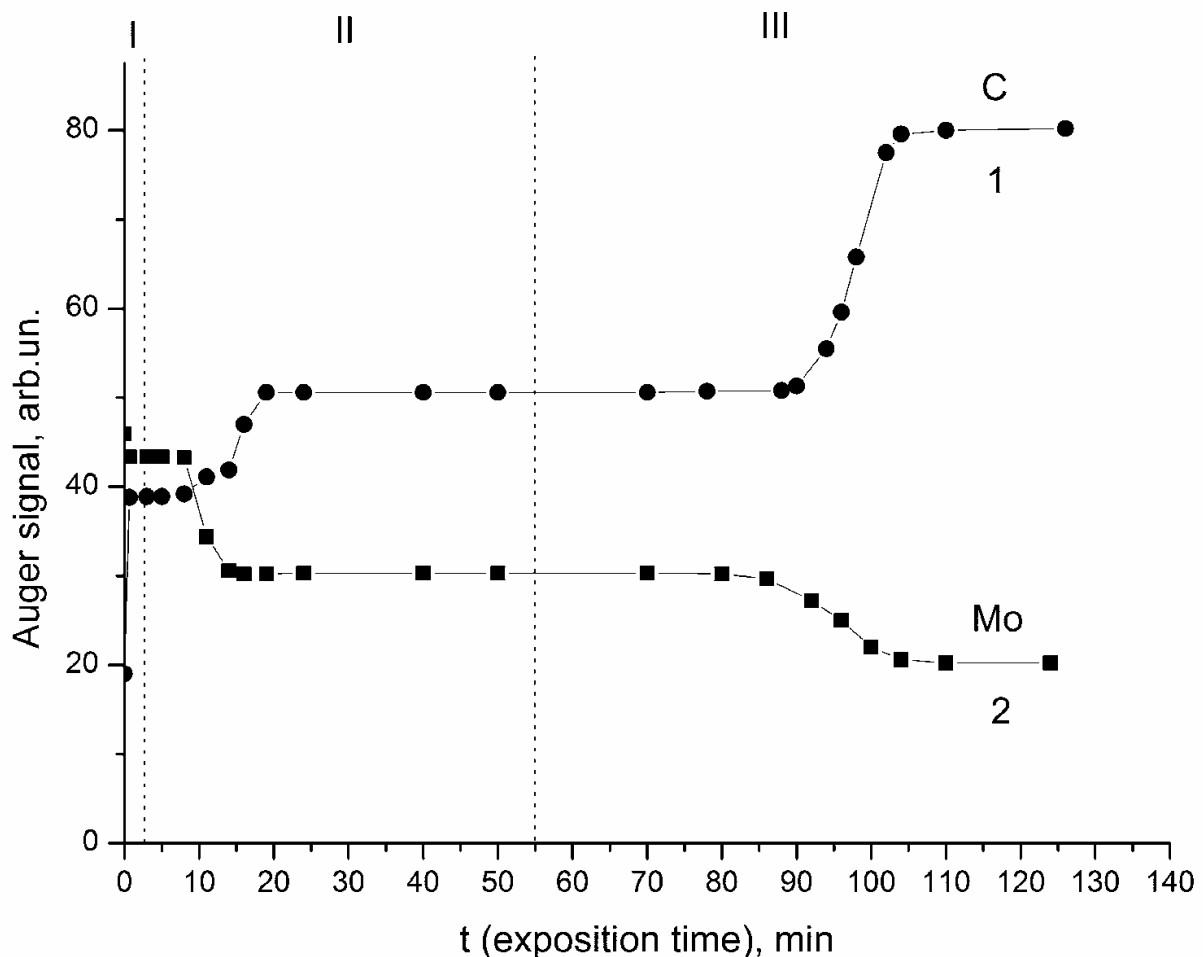


Fig. 13. Auger signals of carbon (1) and Mo (2) versus exposure time in carbonization of Re in benzene vapor. Carbonization temperature is $T_c = 1700$ K; benzene molecular flux is $\sim 2 \cdot 10^{15} \text{ cm}^{-2} \cdot \text{s}^{-1}$

Interestingly, if the volume carbide formed in the near-surface region of the ribbon at a low temperature, for instance, at $T = 1000$ K, is heated to $T \geq 1300$ K, it breaks down, and the excess carbon becomes incorporated in the Mo-C solid solution, with the surface carbide remaining on the surface.

If we continue the exposure of the molybdenum ribbon to benzene vapors after the volume carbide Mo_2C has formed throughout the bulk of the sample, a graphene layer will grow above the surface carbide (region III in Fig. 13). This is accompanied by a decrease of the molybdenum Auger signal by a factor 1.6, a feature characteristic of screening by one graphene layer (see § 4).

Spectrum 3 in Fig. 12 was obtained in Auger probing of a graphene film on molybdenum. We note immediately an unusual shape of the carbon Auger peak, which is actually a superposition of the Auger peaks of graphene and the signal of surface (MoC) and volume (Mo_2C) carbides.

Molybdenum carbonized at T_c was subjected to different heat treatments. When heated to $T > T_c + 70^\circ$, graphene was found to dissolve in the bulk of the metal. Subsequent lowering of the temperature down to $T < T_c - 30^\circ$ initiated growth on the surface of a thick graphite film,

the molybdenum Auger peak disappears, and the Auger peak assumes the “graphitic” shape (spectrum 4 in Fig. 12). For $T \leq 1100$ K, carbon stops to evolve because of the diffusion becoming “frozen”.

Dissolution of carbon from graphene in molybdenum at temperatures T rising above T_c and its precipitation below T_c resemble very much similar processes occurring in the Re-C, Pt-C, and Rh-C systems. The MoC system differs essentially only in that rhenium, platinum, and rhodium do not support carbide formation, while molybdenum has the volume carbide, which is the first to become augmented by carbon following formation of the surface carbide MoC.

It thus appears proper to expect that after formation of the volume carbide carbon will dissolve in it just as it does in the metal, up to the solubility limit. Then lowering of the temperature to $T < T_c$ will bring about supersaturation of the solid solution of carbon in the volume carbide, while the excess carbon atoms will start construction of a graphene film on the surface without involvement of carbon atoms from the volume carbide.

D. Graphene on Ni(III)

Unlike the Re-C and Mo-C systems, nickel can be readily carbonized at comparatively low temperatures $T = 1100 - 1400$ K, despite the high solubility limit of carbon in this metal (0.3 to 3 at. % in the temperature region specified). This should be assigned to the diffusion of adatoms from the surface into the bulk of nickel being a process fast enough to preclude formation of a “protective” graphene film, as this is observed to occur in the Re-C system. To estimate the average depth x of penetration of carbon atoms from nickel into the ribbon in time t , we use the relation $\bar{x} = \sqrt{2Dt}$ [37], in which $D = D_0 \exp[-E/kT]$ is the diffusion coefficient, and E is diffusion activation energy. It is known that for volume diffusion of carbon in nickel $E \approx 1.5$ eV, and $D_0 \approx 0.1$ cm²s⁻¹ [36]. Then for $T = 1200$ K and the exposure time of nickel to benzene vapors $t = 100$ s we obtain

$$\bar{x}(\text{cm}) = \sqrt{2D_0 t \exp(-E/kT)} = 3 \cdot 10^{-3} \text{ cm} ,$$

a value close to one half the thickness of the ribbon used in the experiments. Just as in the Ir-C, Re-C, Mo-C, Pt-C, and Rh-C systems, carbonization culminates in formation of a graphene film. That the film formed is indeed graphene, is attested by the “graphitic” shape of the carbon Auger spectrum (spectrum 2 in Fig. 14), by characteristic splittings of the Auger spectrum of carbon initiated by intercalation of cesium atoms under graphene (spectrum 5 in Fig. 14) - see below § 7, as well as by the good fit of the calculated to experimentally observed drop of the substrate Auger signal intensity by a factor ~ 2 for $E_{Ni} = 61$ eV caused by one graphene layer.

The variation in intensity of the carbon and nickel Auger peaks brought about by heating and cooling of nickel carbonized at $T_c = 1365$ K is shown graphically in Fig. 15. If the ribbon temperature is increased, at $T > T_c + 40^\circ$ graphene breaks down and escapes from the surface altogether, leaving a small carbidic Auger peak of carbon (spectrum 1 in Fig. 14), whose intensity and shape practically do not vary with further increase of temperature. The concentration of carbon in this state $N_c \approx (2-3) 10^{14}$ at/cm²; this may be the Ni₆C surface carbide, because for the Ni(III) face $N_{Ni} = 1.86 10^{15}$ at/cm². Obviously enough, surface carbide of nickel resides in equilibrium with the carbon dissolved in the bulk of the metal, as is the case with other systems forming surface carbides (WC, MoC, ReC). After the

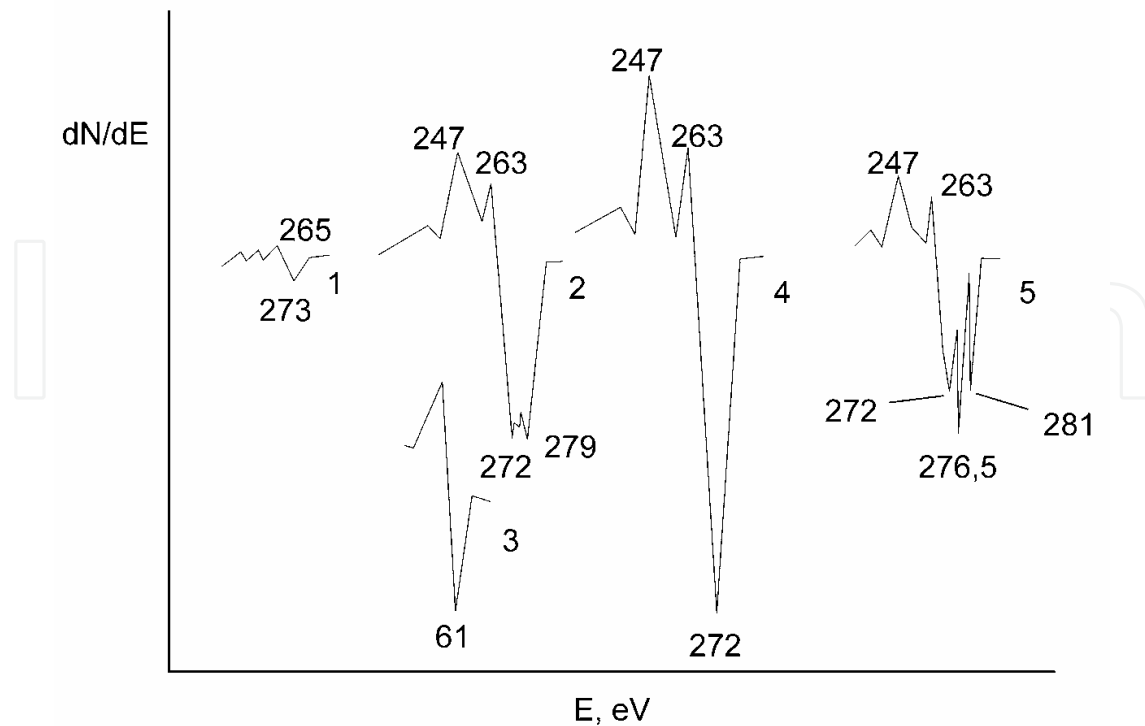


Fig. 14. Auger spectra of various carbon forms on Ni(111) surface: 1 – surface carbide of Ni; 2 – a single graphene layer; 3 Ni Auger peak at $E=61$ eV under it; 4 – 6-layer graphite film; 5 – the spectrum of a graphene layer after intercalation with Cs.

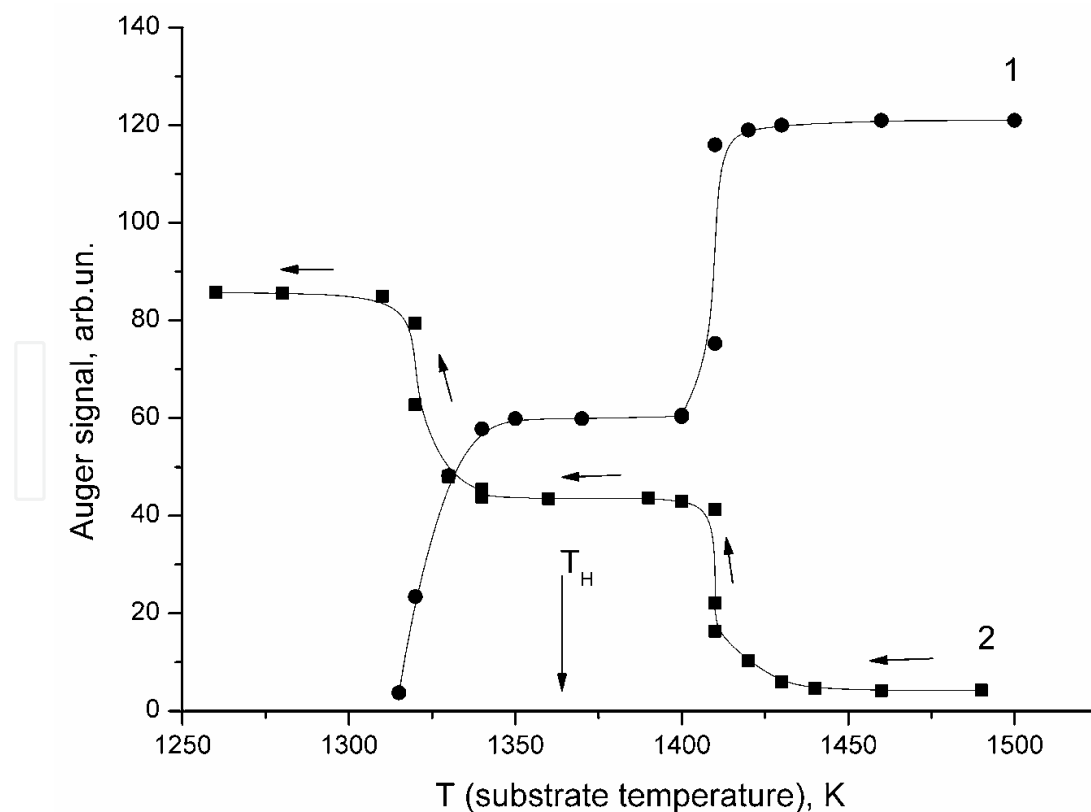


Fig. 15. Auger signals of Ni (1) and carbon (2) versus temperature in temperature decreasing. Carbonization temperature is $T_C = 1375$ K; time delay at each temperature is 30 s.

temperature has been lowered down to $T = T_c = 1365$ K, a layer of graphene forms again on the surface. As the temperature is lowered down to $T < T_c - 30^\circ$, a thick graphite film starts to grow, with its thickness clearly larger than 6--7 layers, because Auger spectroscopy does not sense the substrate (Fig. 15). The Auger spectrum of carbon exhibits a distinct "graphitic" shape (4 in Fig. 14).

Because the solubility limit N_{lim} of carbon in nickel is well known [35], for instance, at $T = 1365$ K it is $N_{lim} \approx 2$ at. %, while at $T = 900$ K, $N_{lim} \approx 0.15$ at. %, one readily finds that at $T = 900$ K a graphite film about 100 atomic layers thick should form on each side of a nickel ribbon $30 \mu\text{m}$ thick through segregation on the surface of "excess" carbon atoms.

We did not study the low-temperature ($T < 900$ K) region of volume nickel carbide formation.

§ 2. Probing a surface with CsCl molecule flux

A simple method is proposed for detection of graphene
on a metal and determination of the relative area
occupied by graphene islands

It was shown [27] that a graphene film is valence-saturated and passive, and that it suppresses dissociation of a variety of molecules which on a clean metal proceeds very efficiently (see § 7). If we direct a flux of CsCl molecules on a metal heated above 900 K, the molecules will dissociate, with one of the products of this reaction, the cesium atoms, desorbing from the surface as Cs^+ ions with a 100% probability; indeed, on all the metals under study here the cesium ionization potential $V = 3.89$ eV is much lower than the surface work function φ , i.e., $V \ll \varphi$ - the case of "easy" surface ionization indeed [39]. On a continuous graphene film, only residual dissociation is observed, at a level of 0.01--0.1 %, depending on the metal, and it originates apparently from substrate defects or edges of the merged graphene islands. Therefore, by measuring the cesium ion current I_0^+ from a clean metal surface and the ion current I^+ from a surface coated by islands one can readily find the fraction n of the surface occupied by graphene islands:

$$n = \left(1 - \frac{I^+}{I_0^+} \right). \quad (1)$$

Experiments revealed that only graphene is capable of reducing radically the dissociation efficiency of CsCl molecules. On a clean metal, on surface and volume metal carbides, and on continuous carbon films formed at $T < 900$ K (see § 11) the dissociation efficiency is 100%. As this should be expected, n does not depend on substrate temperature, and the effects associated with CsCl molecules sliding off the edges of graphene islands onto the metal could be neglected because of the migration path length of CsCl molecules in their lifetime on graphene is extremely short [40]. Besides, as demonstrated for the Ir(III)-graphene system, the carbon Auger signal intensity for graphene islands growing at $T = 1600$ K is directly proportional to the fraction n of the area occupied by the islands.

In addition to CsCl, the island-occupied fraction n of the area can be derived by probing the surface by a variety of atoms, for instance, by K and Na. On the iridium surface coated by chemisorbed carbon "gas" with $e\varphi \approx 6.0$ eV, K and Na desorb only in the form of ions---another illustration of "easy" ionization; in this case, the measured I_0^+ ion current will be [39]

$$I_0^+ = e \cdot \nu \cdot s, \quad (2)$$

Where e is the electronic charge, ν is the density of the atom flux, and s is the area of the emitting surface of the sample; in our experiments, $s = 0.005 \text{ cm}^2$.

For atoms desorbing from a surface bearing graphene islands the measured current I^+ can be written as [39]

$$I^+ = e \cdot \nu \cdot s \cdot (1 - n) + \frac{e \cdot \nu \cdot s \cdot n}{1 + A \cdot \exp\left(\frac{e(V - \varphi)}{kT}\right)} = I_0^+ (1 - n) + \frac{I_0^+ \cdot n}{1 + A \cdot \exp\left(\frac{e(V - \varphi)}{kT}\right)}, \quad (3)$$

where A is the ratio of the partition functions of the atomic and ionic states of the ionizing atoms, V is the ionization potential of K or Na atoms, φ is the work function of graphene islands on iridium ($e\varphi = 4.45 \text{ eV}$), k the Boltzmann constant, and n is fraction of surface area occupied by graphene islands.

Having measured I_0^+ and I^+ , one can find from Eqs. (2) and (3) n , i.e., the fraction of iridium surface area occupied by graphene islands.

These two methods correlate well with one another, with the data scatter not over 10%, thus providing support for the physical model reproducing the relations in the metal-graphene islands system.

The first method is certainly simpler and can be realized readily with any high-vacuum equipment; significantly, it allows one to follow in real time the nucleation, growth, and destruction of graphene islands on various metals.

Note also one more significant aspect of the method based on probing the surface with CsCl molecules, more specifically, the high sensitivity to the integrity of a graphene film; indeed, a film rupture of only $\sim 0.1\%$ of the total graphene area is signaled reliably by a growth of the Cs^+ ion current. Apart from this, residual dissociation of CsCl molecules on thick graphite films decreases still more by a hundred times compared with graphene. This may be considered as one more evidence in support of the assumption of residual dissociation of molecules occurring at the edges of merged islands in the graphene layer.

For illustration, curve 3 in Fig. 10 plots the variation of the dissociation efficiency of CsCl molecules ($\log \omega$) in the course of rhenium carbonization ($\omega = I^+/I_0^+$). The steep growth of the thermionic current, which signals the appearance of graphene islands, is seen to coincide with the sharp drop of the CsCl dissociation efficiency.

§ 3. Electronic Auger spectroscopy of carbon

The rich variety of chemical realizations of carbon exhibits an astounding diversity of its Auger spectra, both in shape and energy position, which is revealed most clearly by high-resolution Auger spectroscopy.

Our studies have amassed a vast collection of Auger spectra of carbon in its various chemical states [41]. The experiments were conducted under identical conditions with a high-resolution prism electronic Auger spectrometer ($\Delta E/E \leq 0.1\%$). The characteristic features and the main parameters of the instrument were basically determined by the prism type of its energy analyzer, more specifically, a prism analyzer with deflecting electric field [42]. As a rule, the primary electron beam with a current $\sim 5 \mu\text{A}$ bombarded the operating

surface of a sample, 1 mm² in area, from which the Auger electrons were collected. The large distance (~ 74 mm) between the sample and the energy analyzer permitted obtaining, without any loss in sensitivity, carbon Auger spectra of ribbon samples heated up to $T = 2500$ K, an aspect which in more than one case turned out to be of crucial significance for correct unraveling of the physical-chemical processes occurring in a Me-C system. For instance, if we carbonize rhenium at $T = 1850$ K and measure the carbon Auger spectrum directly at this temperature, the spectrum will have a typically graphitic shape (Fig. 9, spectrum 3). By contrast, if the ribbon is temperature is lowered down to room level, a layer of graphite will form on the surface during the cooling (Fig. 9, spectrum 4). Now if we measure the Auger spectrum at $T = 1900$ K, the shape of the Auger spectrum will be purely carbidic due to the chemisorbed carbon "gas" involved (Fig. 9, spectrum 2).

Figure 16 displays some carbon Auger spectra obtained both from pure carbon materials and from carbon in its various chemical compounds. We see that even morphologically close forms of carbon, single-crystal and polycrystals of graphite, differ markedly in the shape of their Auger spectra. A fullerite film produces a spectrum approaching that of graphite polycrystals while differing strongly in the position of the negative spike of the carbon Auger peak, 272 eV for the graphite polycrystals, to be contrasted with 269 eV for the fullerite (spectra 2 and 7 in Fig. 16).

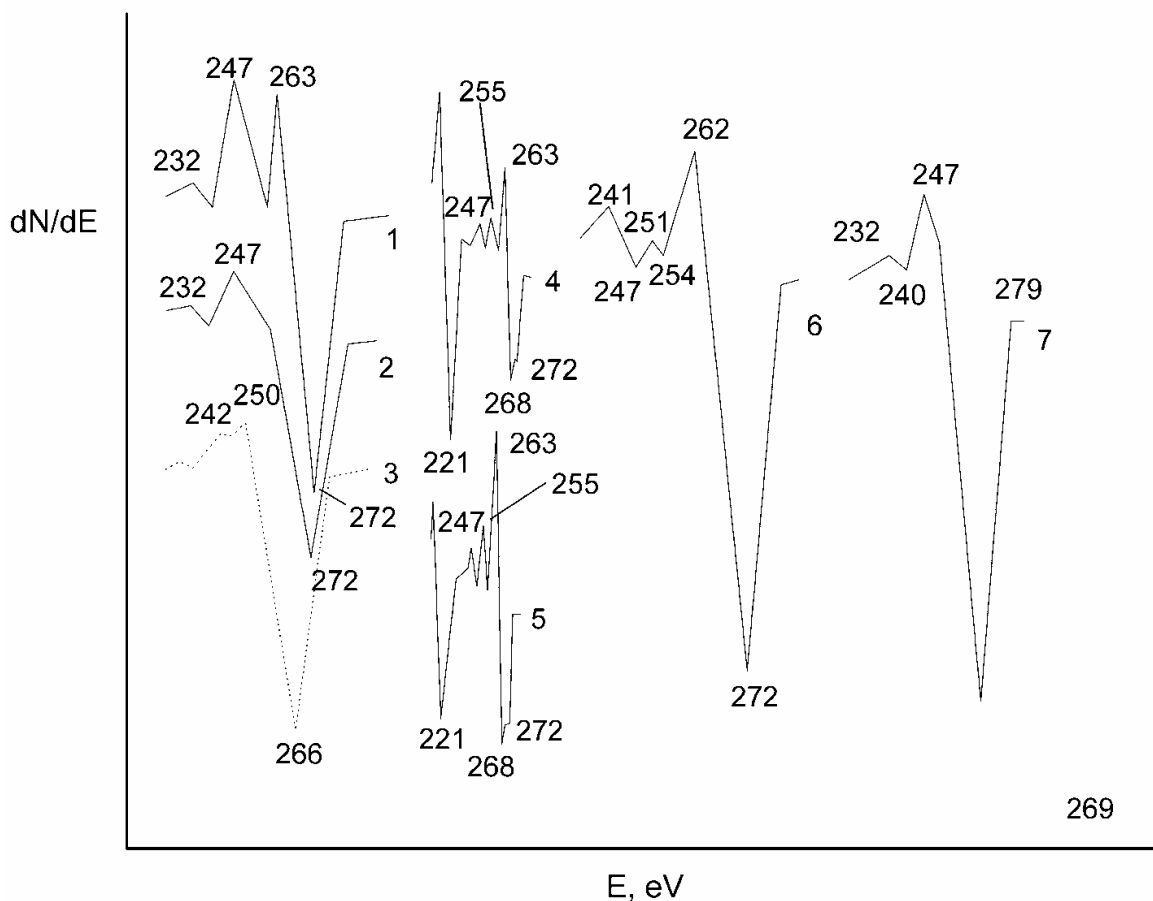


Fig. 16. Carbon KVV Auger spectra for various chemical forms of carbon: 1 - graphite single crystal, 2 - polycrystalline graphite; 3 - diamond, 4 - surface carbide MoC; 5 - bulk carbide MoC₂; 6 - silicon carbide SiC; 7 - fullerite.

A continuous graphene film formed on Ir(III) in exposure to benzene vapors at $T_c = 1600$ K offers a convenient means of calibration relating the Auger peak intensity of carbon with its amount present on the surface. A convenient reference for calibration of carbon in the carbide state is the readily obtained surface tungsten carbide WC containing $N_c = 1 \cdot 10^{15}$ at/cm² [43]. The two calibrations correlate nicely with one another as well.

Summing up, we can say that high-resolution Auger spectroscopy is a valuable complementary tool in diagnostics of surface processes evolving in a carbon layer on metals (see the subsequent Sections).

§ 4. The structure and two-dimensional pattern of graphene films on metals

A graphene film on a metal is indeed two-dimensional!

There can be no doubt whatsoever that a carbon film prepared by exposing a heated metal to hydrocarbon vapors does indeed have graphite structure; this can be readily demonstrated in a direct experiment with the use of scanning tunneling microscopy (Fig. 2, § 2). Indirect supportive evidence for this comes from Auger electron spectroscopy measurements, as well as from a number of properties of graphene films correlating closely with those of graphite single crystals, in particular, valence bond saturation of a layer of graphene, its chemical passivity [27], and the possibility of intercalating the film with foreign atoms [13].

One can hardly question the statement that the graphene films obtained in this way are continuous---this is argued for by scanning tunneling microscopy measurements [20-23] and probing the surface with CsCl molecules. Besides, the graphene surface is uniform in work function (§ 7).

Consider some evidence for the graphene film being indeed two-dimensional:

1. Figure 17 plots the variation of the carbon Auger peak intensity with the relative area of graphene islands, with carbon atoms deposited on the iridium (III) face at $T = 1500$ K. At this temperature, carbon adatoms are confined primarily to graphene islands.

We readily see that the carbon Auger peak intensity is directly proportional to the relative area of graphene islands. This suggests convincingly that the incident carbon does not form a three-dimensional structure, and that it is distributed in one layer, i.e., that the graphene islands are actually two-dimensional. The two-dimensionality of graphene islands was demonstrated in a similar way for the Pt-C and Ni-C systems.

2. Compare now the experimentally observed attenuation of the iridium Auger peak produced by graphene-initiated screening with the corresponding calculations. We assume that the Auger electron emission is isotropic, and that the attenuation of the primary electron beam intensity by graphene may be neglected. Then the attenuation of the iridium Auger peak by a graphene film with thickness x can be derived readily from the relation

$$\frac{1}{\delta(\text{Ir},\text{C})} = \frac{I'_{\text{Ir}}}{I_{\text{Ir}}} = \exp\left[-\frac{x}{\lambda(E_{\text{Ir}})} \cdot \frac{1}{\cos\theta}\right], \quad (1)$$

where $\lambda(E_{\text{Ir}})$ is the average mean free path length of the iridium Auger electrons with the energy $E = 171$ eV in graphite, and $\theta = 10^\circ$ is the angle between the energy analyzer

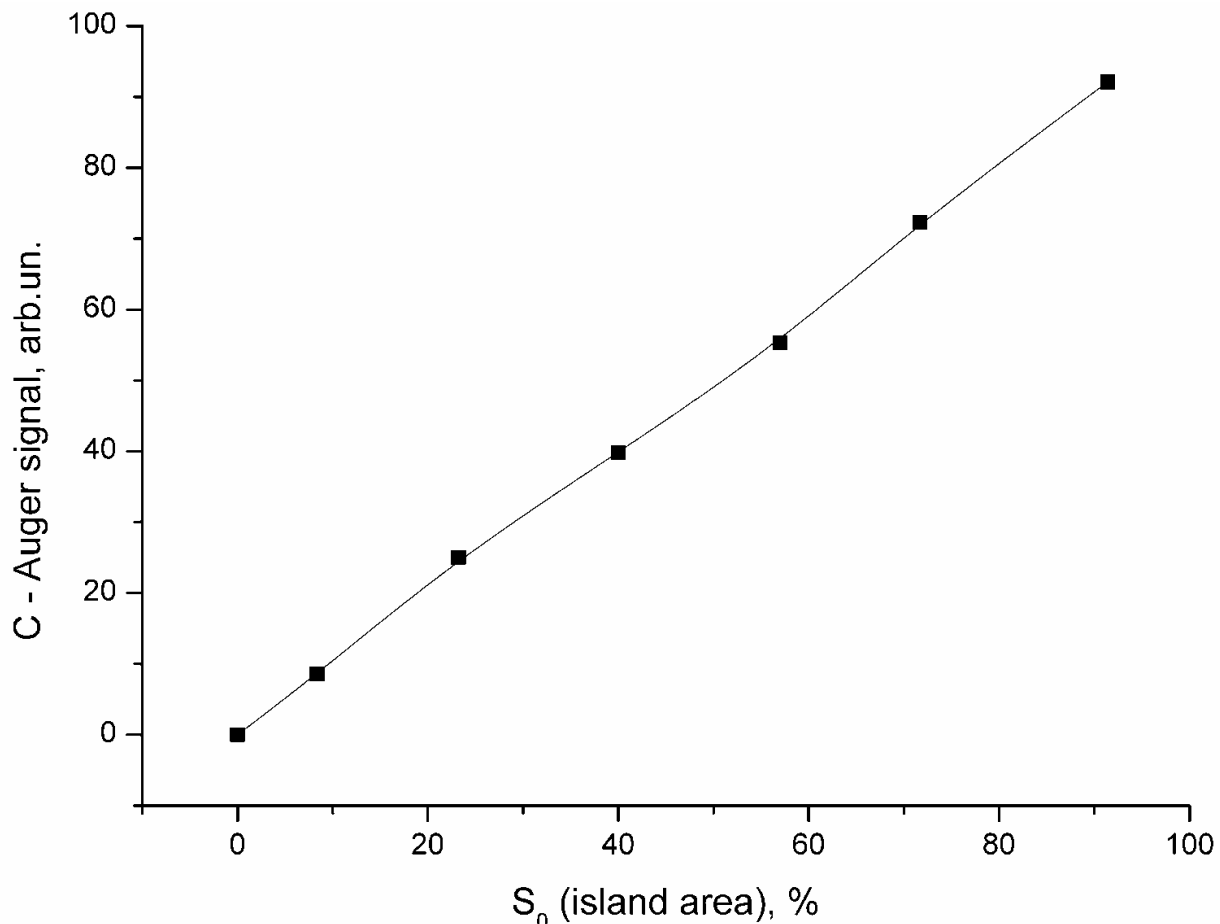


Fig. 17. Carbon KVV Auger signal versus relative area of grapheme islands in deposition of atomic carbon onto Ir(111) surface at 1500 K. The deposition flux is $v_C = 3.2 \cdot 10^{13} \text{ cm}^{-2}\cdot\text{s}^{-1}$.

axis and normal to the sample surface. Putting $x = 3.35 \text{ \AA}$, which is the interplanar distance in graphite and deriving $\lambda(E_{Ir}) = 5.0 \text{ \AA}$ from the $\lambda = f(E)$ relation constructed for a number of materials including graphite, we come to $\delta(\text{Ir}, \text{C}) = 1.8$. The experimentally found attenuation of a factor 1.6 turns out to be close to the calculated value. We may add that for a graphite film two monolayers thick the same calculation yields a factor 3 for the attenuation.

A comparison of the values of attenuation of the substrate Auger signal intensity by a graphene layer performed for other Me-C systems with close Auger peak energies of the metal (Re, Mo, Pt) yields an experimental value $\delta = 1.6 \pm 0.1$. We note also that one layer of C_{60} fullerene molecules on Ir(III) with a concentration $N_{\text{C}_{60}} = 2 \cdot 10^{14} \text{ mol/cm}^2$ reduces the substrate Auger signal ~ 4 times [44].

3. That the graphene layer on iridium is monatomic is argued for also by a comparison of Auger peak intensities from a graphene film, I'_c , and graphite, I''_c obtained under identical experimental conditions with calculations. Neglecting the dependence of electron backscattering from the material and setting $\cos\theta = 1$, we come for a thick film of graphite on iridium to

$$I''_c = \kappa \int_0^h \exp\left[-\frac{x}{\lambda(E_c)}\right] dx = \kappa \lambda(E_c), \quad (2)$$

where $\lambda(E_c) = 6.2 \text{ \AA}$ is the average mean free path length of carbon Auger electrons with $E_c = 272 \text{ eV}$ in graphite [44]. For the carbon Auger peak intensity from a graphite monolayer $h = 3.35 \text{ \AA}$ thick we obtain

$$I'_c = \kappa \int_0^h \exp\left[-\frac{x}{\lambda(E_c)}\right] dx = 0,42\kappa\lambda(E_c). \quad (3)$$

The calculated ratio $I''_c/I'_c = 2.4$ is close to the experimental value 2.5. It is worth reiterating that a continuous graphene film on a metal can be obtained in any high-vacuum instrument without any effort expended, without special diagnostics of the surface---indeed, all one needs to do is expose the metal heated enough to benzene vapors. Table 1 presents for illustration the time needed for a graphene layer to form on various metals at $T = 1700 \text{ K}$ and $P_{C_6H_6} \sim 1 \cdot 10^{-6} \text{ Torr}$ for thin metal ribbons $20\text{--}30 \text{ }\mu\text{m}$ thick.

Me	Ir(III)	Pt(III)	Rh(III)	Re(I0I0)	Mo(I00)
t, c	~ 10	~ 20	~ 300	~ 1500	70000

Table 1

Figure 18 plots the times needed for formation of a graphene layer on rhenium heated to $T_c = 1730 \text{ K}$; at each point, the temperature was first raised to 1900 K , and lowered

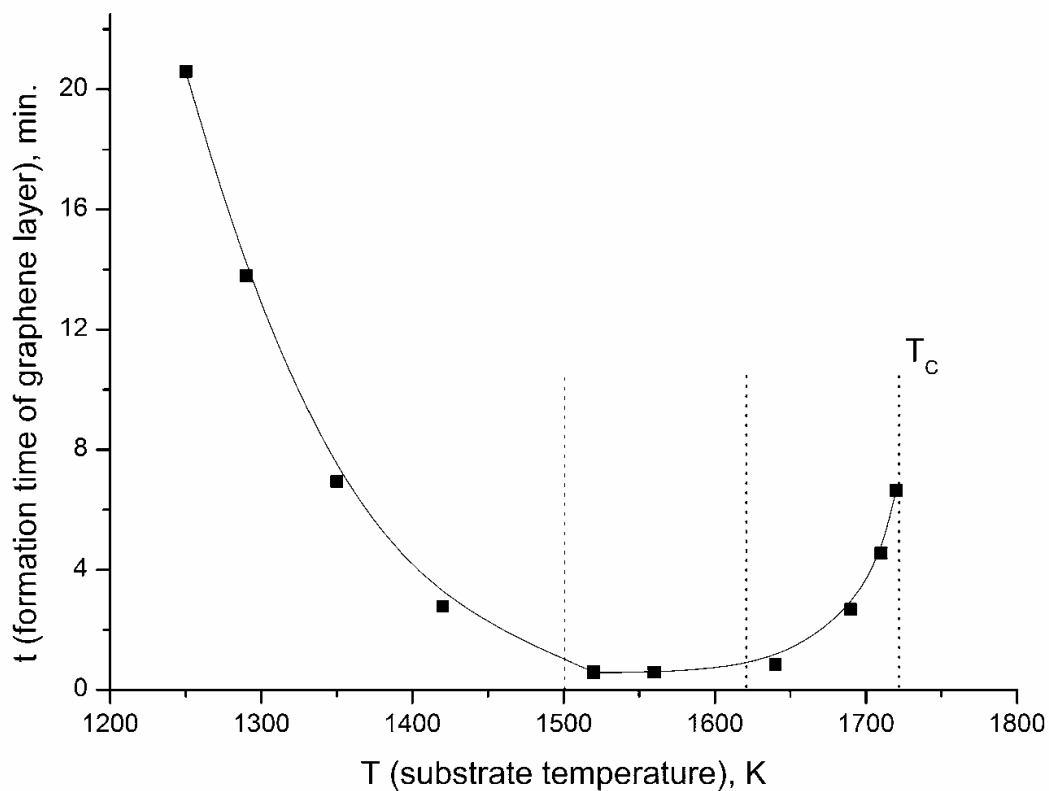


Fig. 18. Time of single graphene layer formation on Re due to carbon precipitation from the metal bulk versus surface temperature. Carbonization temperature is $T_c = 1730 \text{ K}$; The layer was considered as completed when the thermionic current become corresponded to the work function $e\phi = 4.25 \text{ eV}$

subsequently to the required level. The growth of the formation time at low temperatures should be assigned to freezing of the volume diffusion of carbon atoms, and its increase at high temperatures can be traced to intensive dissociation of graphene islands.

§ 5. Two-dimensional phase transition in a carbon layer on metals

A graphene film on a metal grows by formation of graphene islands, which expand in area and coalesce to produce a continuous layer.

It is known that many films coating the surface of solids undergo first-order phase transitions. In the course of such a phase transition, the originally uniform adsorbate layer becomes nonuniform, with the surface breaking up to form islands containing adsorbate with different adatom densities. An apparently pioneering experimental study [45] based on the use of an ion projector revealed the presence on a tungsten surface of two-dimensional Zr islands produced in a phase transition in the adfilm, with the same process observed to occur [46--48] in zirconium, hafnium, and platinum films coating the surface of a number of refractory metals. The theory of the phase transition involved and a review of the experimental studies amassed was dealt with in Ref. [49]. Phase transitions were observed to evolve in platinum metal-carbon systems [50--52], in sodium adlayers on W(100) [53], in barium adlayers on metal substrates [54], and, probably, in gold and copper films grown on single-crystal graphite [55]. Even in two-dimensional films of charged adatoms one may expect, despite the repulsive character of their interaction, a first-order phase transition, including a condensation-type one, as this was shown theoretically [56--57]. Phase transitions in such systems set in as the density of the film increases, thus reducing the effective charge of the adatoms.

A first-order phase transition in a carbon adlayer on a metal was first observed in the iridium-carbon system [50--52], the associated ideology having been underpinned by statistical theory of lattice gas and exposed in considerable detail in Ref. [27]. The onset of a phase transition depends essentially on several factors, among them the nature of the adsorbate and substrate atoms, the strength of lateral interaction among the adatoms, and charge state of the adatom. For carbon atoms having electronegativity close in magnitude to that of substrate atoms of transition metals (W, Ir, Re) one may expect the carbon adatom to either be uncharged or have a weak negative charge. On the other hand, the binding energy coupling carbon atoms is high, for instance, in molecules of organic compounds the energy of a single C-C bond is 3.6 eV, that of the double C=C bond, 6.32 eV, that of the ternary bond C≡C, 8.65 eV, and the sublimation heat of carbon is also large--7.44 eV [59]. Assuming a noticeable migration mobility of carbon adatoms, one may therefore expect formation of closely packed carbon islands. A condensation-type first-order phase transition would make a Me-C film system nonuniform in its emission characteristics. Therefore, phase transitions can be revealed by methods sensitive to nonuniformities in emission, such as field-emission microscopy, low-energy electron diffraction, and a method combining thermionic emission with surface ionization of hard-to-ionize elements (TESI).

A study of high-temperature ($T \sim 1600$ K) adsorption of carbon atoms on iridium made by TESI [50--52] reported on a first observation on a metal surface of a first-order phase transition of the two-dimensional condensation type which gives rise to coexistence on the surface of two carbon phases, more specifically, two-dimensional graphene islands and

chemisorbed carbon atoms (two-dimensional carbon “gas”). For the substrate the above authors conveniently chose iridium, a metal which does not dissolve carbon in its bulk, a factor which alleviated markedly interpretation of the results obtained.

The phase transition in a carbon adlayer on metals having presently become universally recognized, it deserves a particular place in our analysis here. The TESI method, first proposed in Ref. [60] and developed in a later publication [27], is based essentially on determination of the work function from measurement of the thermionic and ion currents generated through surface ionization of the probing atomic beam [39]. By measuring the thermionic and ion currents at a constant emitter temperature and different coverages of the substrate by carbon, one can readily calculate by the total current method the variation of the thermionic, $\Delta\varphi_e$, and ionic, $\Delta\varphi_i$, work functions. A comparison of $\Delta\varphi_e$ with $\Delta\varphi_i$ provides a good means to judge the nonuniformity of the carbon layer. Indeed, thermionic current I_e from a uniform emitter is given by the Richardson relation [60]

$$I_e = A_0(1 - \bar{R}) \cdot S \cdot T^2 \exp[-\varphi_e / kT], \quad (1)$$

where A_0 is a universal constant, R is the coefficient of thermoelectron reflection from the potential barrier on the sample surface, S is the emitting surface area, and k is the Boltzmann constant.

The positive ion current from a surface produced by surface ionization is given by the Saha – Langmuir relation [39]

$$I_i^+ = \frac{eSv}{1 + A \cdot \exp\left[\frac{V - \varphi_i}{kT}\right]}, \quad (2)$$

where v is the density of the flux of atoms with ionization potential V striking the surface, and A is the partition function ratio of the atomic and ionic states of the ionizing atoms.

Examining Eqs. (1) and (2), we see that thermionic emission “senses”, as it were, the surface areas with the lowest work function, while the ion current produced by the atomic flux probing the surface is, by contrast, sensitive to those with the highest work function. When $\varphi_e = \varphi_i$, we infer that the sample surface is uniform in the work function.

Figure 19 displays graphically the variation of the φ_e and φ_i work functions in the case of carbon atoms adsorbed on Ir(III) at $T = 1700$ K with the surface coverage by carbon θ ($\theta = 1$ corresponds to a carbon concentration $N_{cm} = 3.56 \cdot 10^{15}$ at/cm²). Three regions stand out in the graph:

I--- the surface is uniform in work function, $\varphi_e = \varphi_i$;

II---the surface is nonuniform in emission, and $\varphi_e < \varphi_i$;

III---the surface is again uniform in work function, $\varphi_e = \varphi_i$.

The presence in the carbon adlayer of regions with different work functions (region II in Fig. 19) is attributed [50--51] to a first-order two-dimensional phase transition. In region I in Fig. 19, carbon resides in the phase of two-dimensional chemisorbed “gas”, i.e., it is spread uniformly over the surface, and $\varphi_e = \varphi_i$. In region II, a phase of condensed carbon (graphite islands with $\theta_c = 1$), which is in dynamic equilibrium with the carbon “gas”, is forming on the iridium surface. The nonuniformity of the surface in work function in region II finds convincing support in the strong anomalous electronic Schottky effect. As the total carbon concentration on the iridium surface increases, the different adsorbate phases undergo

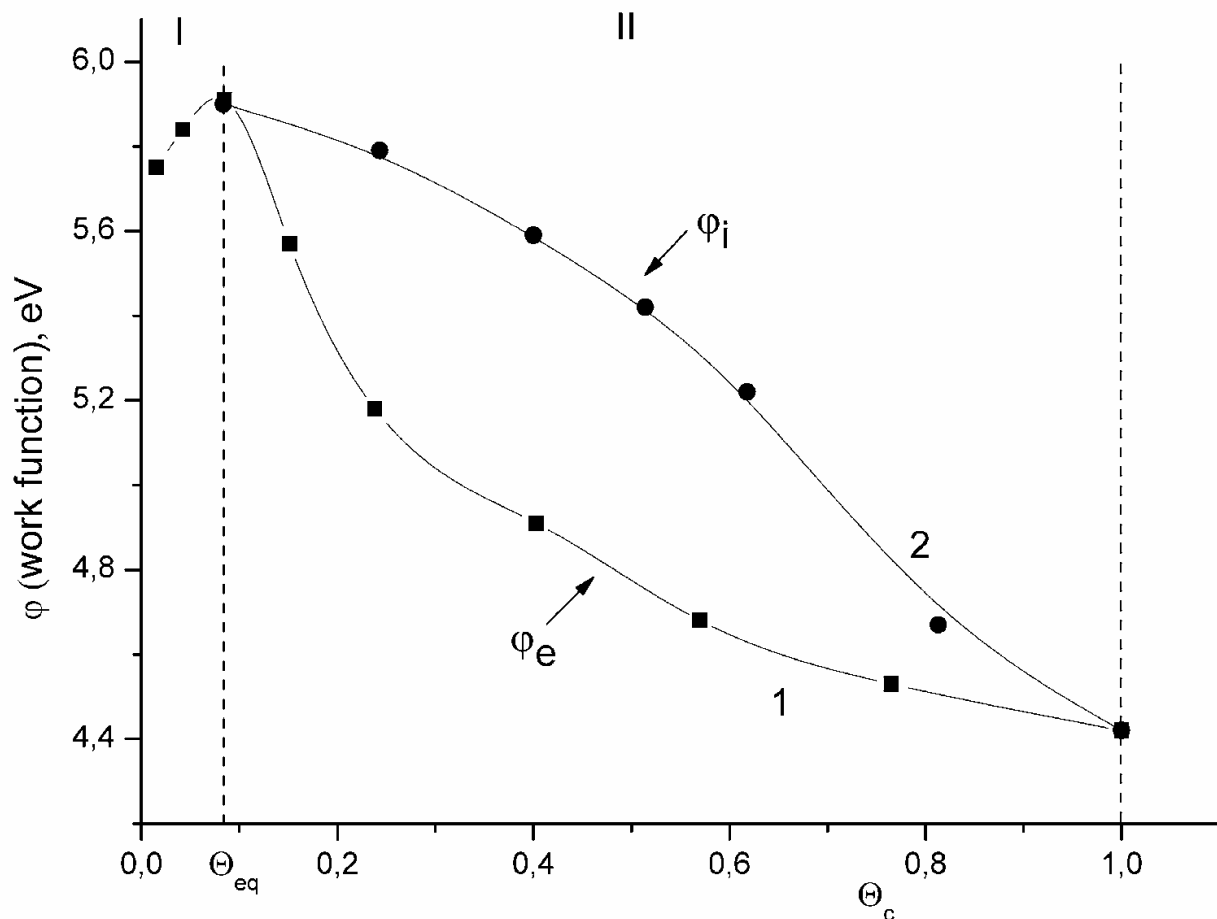


Fig. 19. Variations of 'electron' φ_e (1) and 'ionic' φ_i (2) work functions measured from thermionic current and from In^+ ion probing respectively, with surface carbon cover θ_c . $\theta_c = 1$ corresponds to a continuous graphene layer; $T = 1700$ K

redistribution in occupied area, with the graphene islands growing in area, thus reducing the area covered by the carbon "gas". Merging islands produce a graphene film---region III in Fig. 19---which is uniform in work function. Obviously enough, the ratio of the areas occupied by the different carbon phases depends not only on the amount of the adsorbate present but on the substrate temperature as well.

A two-dimensional phase transition was subsequently found to occur in the Ni-C system [5] and explored in detail in our studies of the growth of graphene films on Ir, Pt, Ni, Rh, Re, and Mo [41].

For the first time in Me-C systems, the equilibrium carbon coverage $\theta_{eq}(T)$ in the state of chemisorbed carbon "gas" on Ir(III) was determined in the phase transition in a carbon layer which involved formation of graphene islands [14]. Consider two methods of $\theta_{eq}(T)$ determination.

Determination of $\theta_{eq}(T)$ by Auger electron spectroscopy. Chemisorbed carbon "gas" is known to increase the work function of the iridium surface; indeed, at $T = 1800$ K the work function grows from 5.75 to 5.95 eV (Fig. 19). The maximum in the $\varphi = f(\theta_c)$ plot signifies reaching a critical coverage by carbon θ_c which initiates a phase transition with formation of graphene islands residing in dynamic equilibrium with their carbon "gas" whose coverage $\theta_{eq} = \theta_c$. Formation of graphene islands with $\varphi = 4.45$ eV brings about a sharp growth (by

orders of magnitude) of the thermionic current. To determine $\theta_{\text{eq}}(T)$, carbon atoms were deposited at different iridium temperatures in the 1600--1900-K region until φ_{max} was reached, which was signaled by the thermionic current, and the carbon concentration N_c on the surface was found by AES, with subsequent calculation of $\theta_{\text{eq}} = N_c/N_{cm}$ ($N_{cm} = 3.56 \cdot 10^{15}$ at/cm²). The measurements were performed repeatedly at each T . The averaged values of $\theta_c = \theta_{\text{eq}}$ are plotted vs. temperature in Fig. 20.

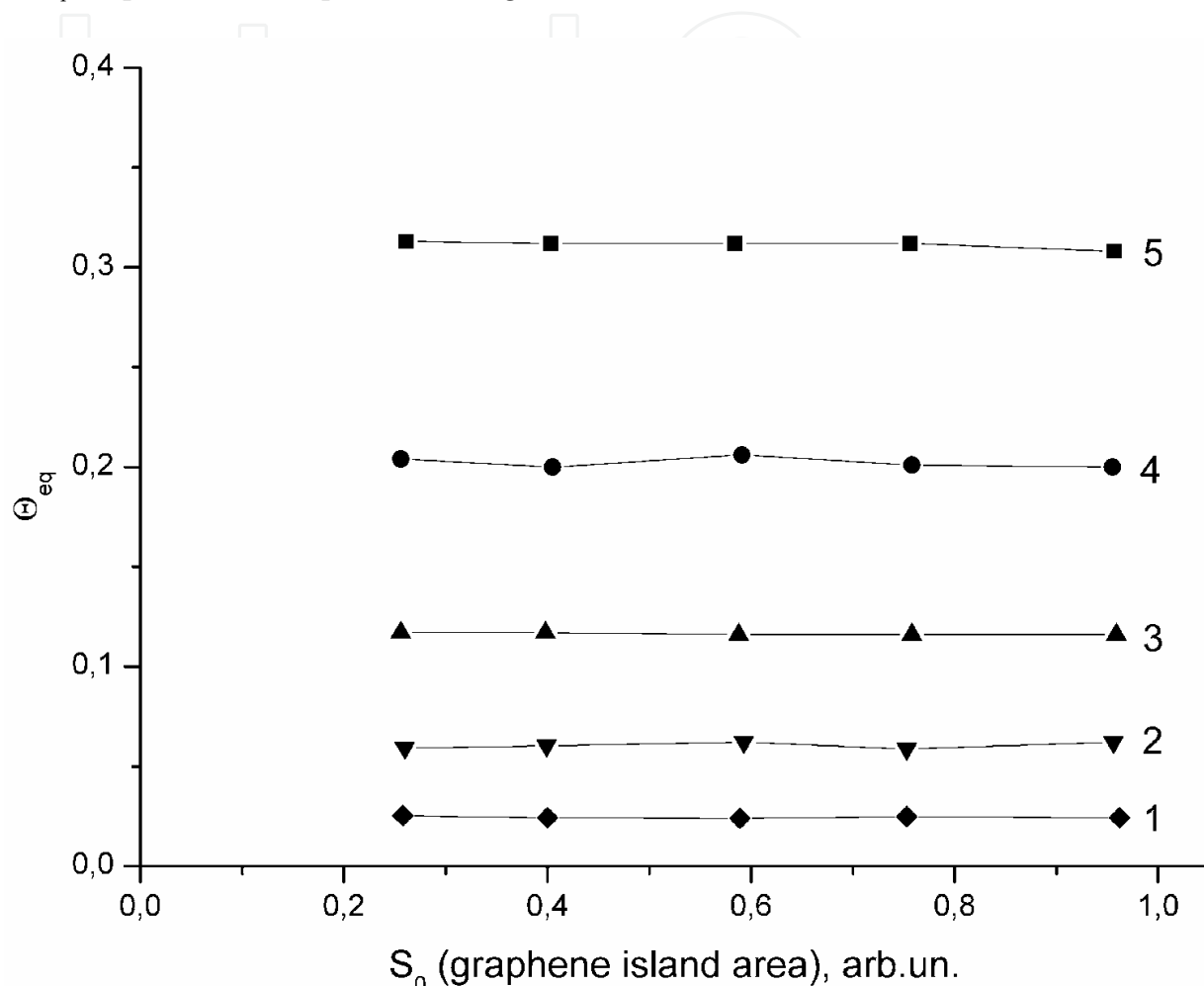


Fig. 20. Equilibrium surface carbon covers θ_{eq} as functions of relative grapheme area S_0 for Ir-C system at various temperatures (K): 1 - 1670; 2 - 1760; 3 - 1840; 4 - 1915; 5 - 1975.

Determination of $\theta_{\text{eq}}(T)$ from dissociation of CsCl molecules. The method draws essentially from the possibility of deriving the relative area of graphene islands from dissociation of CsCl molecules (see § 2). Graphite islands with a relative area $S_0(T_C)$ were produced at $T_C = 1600$ K on the surface of an iridium ribbon by exposing it to benzene vapors. At $T_C = 1600$ K, $\theta_{\text{eq}} \sim 0.01$, and carbon adatoms are concentrated primarily within graphene islands; therefore, lowering the temperature below T_C does not change the relative area of the graphene islands. After this, benzene vapors were pumped out, and the temperature of iridium was raised in steps to T_1, T_2, \dots, T_i . As the temperature increased, the graphene islands dissociated, and their relative area decreased, while the chemisorbed carbon "gas" became, accordingly, denser. The graphene islands recovered finally their area after the temperature had been lowered down to T_C .

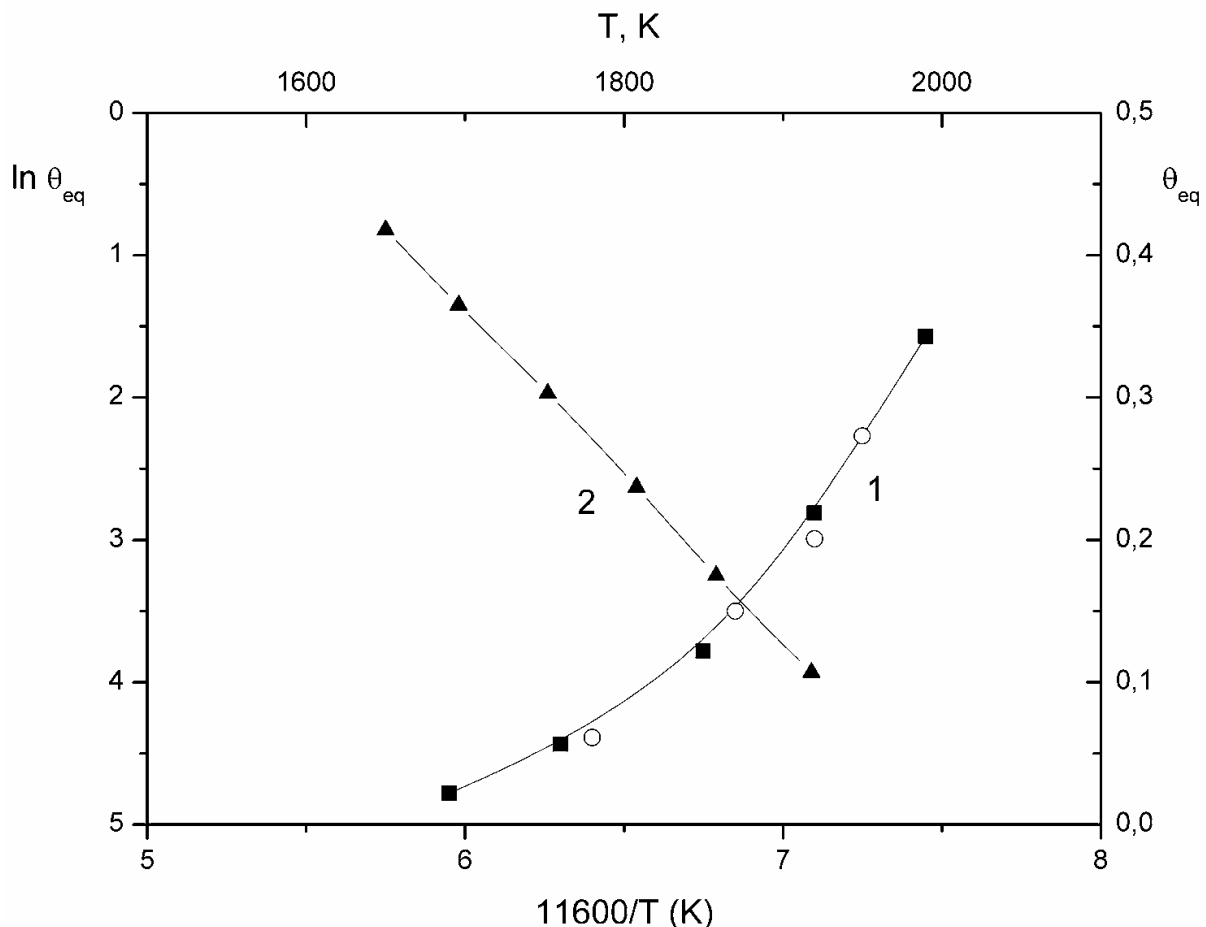


Fig. 21. Equilibrium carbon cover θ_{eq} as function of T (1) and $\ln\theta_{eq}$ as function of $1/kT$ (2) for 2D carbon gas in equilibrium with grapheme islands. black dots - by CsCl dissociation, light dots - by AES.

It was demonstrated convincingly [14] that the carbon “gas” covers the total surface, i.e., that it resides under the graphene islands as well. But then $\theta_{eq}(T_i) - \theta_{eq}(T_C) = S_0(T_C) - S_0(T_i)$, and, recalling the small value of $\theta_{eq}(T_C)$, we come to

$$\theta_{eq}(T_i) \approx S_0(T_C) - S_0(T_i). \quad (3)$$

Figure 20 illustrates the experiments performed at different T_i within the 1670--1970-K region, as well as for different original values of $S_0(T_C)$ in the 0.25--0.95 interval. It was found that the magnitude of $\theta_{eq}(T_i)$ does not depend on the initial relative area of graphene islands. The $\theta_{eq}(T_i)$ plot is displayed in Fig. 21, curve 1. The results of θ_{eq} determination by this method and with the use of AES are seen to correlate closely. If we construct the $\ln\theta_{eq} = f(1/kT)$ plot using experimental data, the result will be a straight line (Fig. 21, curve 2)

$$\theta_{eq} = D \cdot \exp\left(-\frac{\Delta E}{kT}\right) = 2 \cdot 10^5 \exp\left(-\frac{2,3eV}{kT}\right). \quad (4)$$

Consider now this relation. Let N_1 be the linear concentration of carbon along the perimeter of the graphene islands. Then for the carbon atom flux from the island into the adsorbed “gas” phase outside the island we obtain

$$\nu_1 = N_1 \cdot W_0 \cdot \frac{1}{2} = \frac{1}{2} N_1 \cdot C \exp\left(-\frac{E_{det}}{kT}\right), \quad (5)$$

where $W_0 = C \exp(-E_{det}/kT)$ is the probability for an edge carbon atom to become detached from the island, C is the prefactor, E_{det} is the binding energy of the edge carbon atom with the island, and the coefficient $1/2$ reflects the probability for the carbon atom that has been detached from the island to end up either outside the graphene island or under it. Assuming dynamic equilibrium, for the flux of carbon atoms from the adsorbed “gas” phase outside the graphene islands onto the island we obtain

$$\nu_2 = N_1 \cdot \theta_{eq} \cdot W_{tr} \cdot \frac{1}{4} = \frac{1}{4} N_1 \cdot \theta_{eq} \cdot A \exp\left(-\frac{E_{tr}}{kT}\right), \quad (6)$$

where $W_{tr} = A \exp(-E_{tr}/kT)$ is the probability for a carbon adatom to transfer (or better to say, to be reattached) from the phase of surface “gas” to that of the graphene island, A is the prefactor, and E_{tr} is the binding energy for activation of this transition, and the $1/4$ coefficient accounts for possible adatom migration hops in the four equally probable directions.

At equilibrium, $\nu_1 = \nu_2$, and

$$\theta_{eq} = 2 \cdot \frac{C}{A} \cdot \exp\left[-\frac{(E_{det} - E_{tr})}{kT}\right] \quad (7)$$

Confronting now Eq. (7) with (4), we obtain $E_{det} - E_{tr} = 2.3$ eV, and $(C/A) \sim 10^5$. Equation (7) deserves a careful study because it provides an insight into the actual meaning of the quantities entering it for determination of $\theta_{eq}(T)$. Indeed, knowing the energy of detachment of an edge carbon atom from a graphene island on iridium, $E_{det} = 4.5$ eV (§ 7), one immediately comes to $E_{tr} = E_{det} - 2.3 = 4.5 - 2.3 = 2.2$ eV. A question arises now as to why we have obtained such a large value of $E_{tr} \gg E_M$, where E_M is the activation energy for carbon adatom migration over iridium equal to 0.7 eV [27]. To get an answer to this question, consider Fig. 22. For a newly arrived carbon atom to become incorporated into a graphene island, the edge atom has to transfer from the chemisorbed state I (B) to the physisorbed state II (C) identifying incorporation into the graphene island; said otherwise, this atom has to rupture its bonds to the surface atoms of iridium. In this case, $E_{tr} = 2.2$ eV is the energy which has to be expended to transfer a carbon atom from the state of surface “gas” to its “just” position in the graphene island, while $E_{det} = 4.5$ eV is the energy required to detach an edge carbon atom from an island accompanied by its transition to the “adsorbed gas state” (Fig. 22). The position of a metal-linked edge carbon atom in an island is nothing more than an intermediate state of an adatom in the process of growth or dissolution of graphite islands.

Regrettably, attempts at studying the two-dimensional phase transition in a carbon layer in other Me-graphene systems to the extent this was done for the iridium substrate failed, because the processes involved in carbon dissolution in the bulk of a metal play a substantial role. Nevertheless, for some temperatures it was found possible to derive by AES the concentration of chemisorbed carbon “gas” at which graphene islands start to nucleate on other metals as well (Table 2). We readily see that the carbon concentration depends crucially on the substrate material used; indeed, the highest density has the carbon “gas” on Re(1010), while on Pt(III) AES does not sense the carbon “gas”, because its concentration is below the Auger spectrometer sensitivity to carbon.

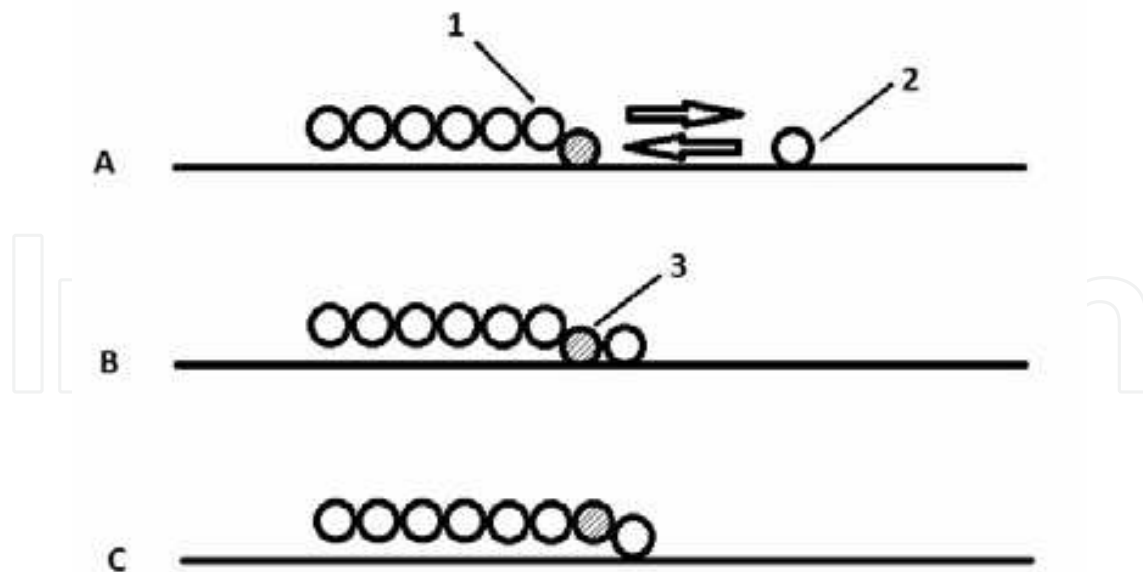


Fig. 22. A model scheme showing graphene island growth on metal surface by attaching a chemisorbed carbon atom from 2D carbon 'gas': 1 - carbon atom in the grapheme island; 2 - chemisorbed carbon atom; 3 - edge carbon atom.

Подложка	Ni (111)	Re(10-10)	Pt(III)	Rh(III)	Ir(III)
T, K	1370	1700	1700	1400	1700
at/cm ²	(2-3) · 10 ¹⁴	2 · 10 ¹⁵	< 5 · 10 ¹³	~ 6 · 10 ¹⁴	~ 7 · 10 ¹³

Table 2

Chemisorbed carbon "gas" is involved in two extremely essential operations in the adlayer. First, it participates actively in the dissolution and growth of graphene islands. Second, it acts as an intermediate link in the transport of carbon between the surface and the bulk of the metal where carbon atoms are dissolved. If there were no carbon "gas" on the surface, carbon atoms dissolved in the bulk of the metal just could not diffuse over its surface.

High-temperature, high-resolution AES offers a possibility of visualizing the process of the phase transition in the carbon adlayer on iridium. As shown above, this possibility rests on the extremely high sensitivity of the shape of the carbon Auger spectrum to the phase in which adatoms reside on the surface. Figure 23 illustrates the reversible transformation in a heating-cooling cycle of the Auger peak of carbon adsorbed on iridium, which is initiated by the substrate temperature variation in the 1600--1960-K interval. The total carbon concentration on the surface is $N_c = 1.2 \cdot 10^{15}$ at/cm² ($\theta_c \approx 0.3$). At $T = 1600$ K, virtually all of the carbon on the surface is confined to graphene islands, and the carbon Auger peak approaches the shape characteristic of graphene. At $T = 1950$ K ($\theta_{eq} = 0.27$), a sizable part of carbon is bound in chemisorbed "gas", and its Auger peak is close to being "carbide"; there is nothing strange in it, because the activation energy for desorption of a carbon atom from the surface of iridium, which is 6.3 eV (see § 7) testifies to strong metal-carbon bonding.

Literature has virtually neglected a relevant problem of paramount importance, namely, the very beginning of nucleation of graphene islands. Indeed, the transition from a single chemisorbed carbon atom to a graphene island should contain an intermediate stage of clustering of two, three and so on carbon atoms together. It appears reasonable to expect

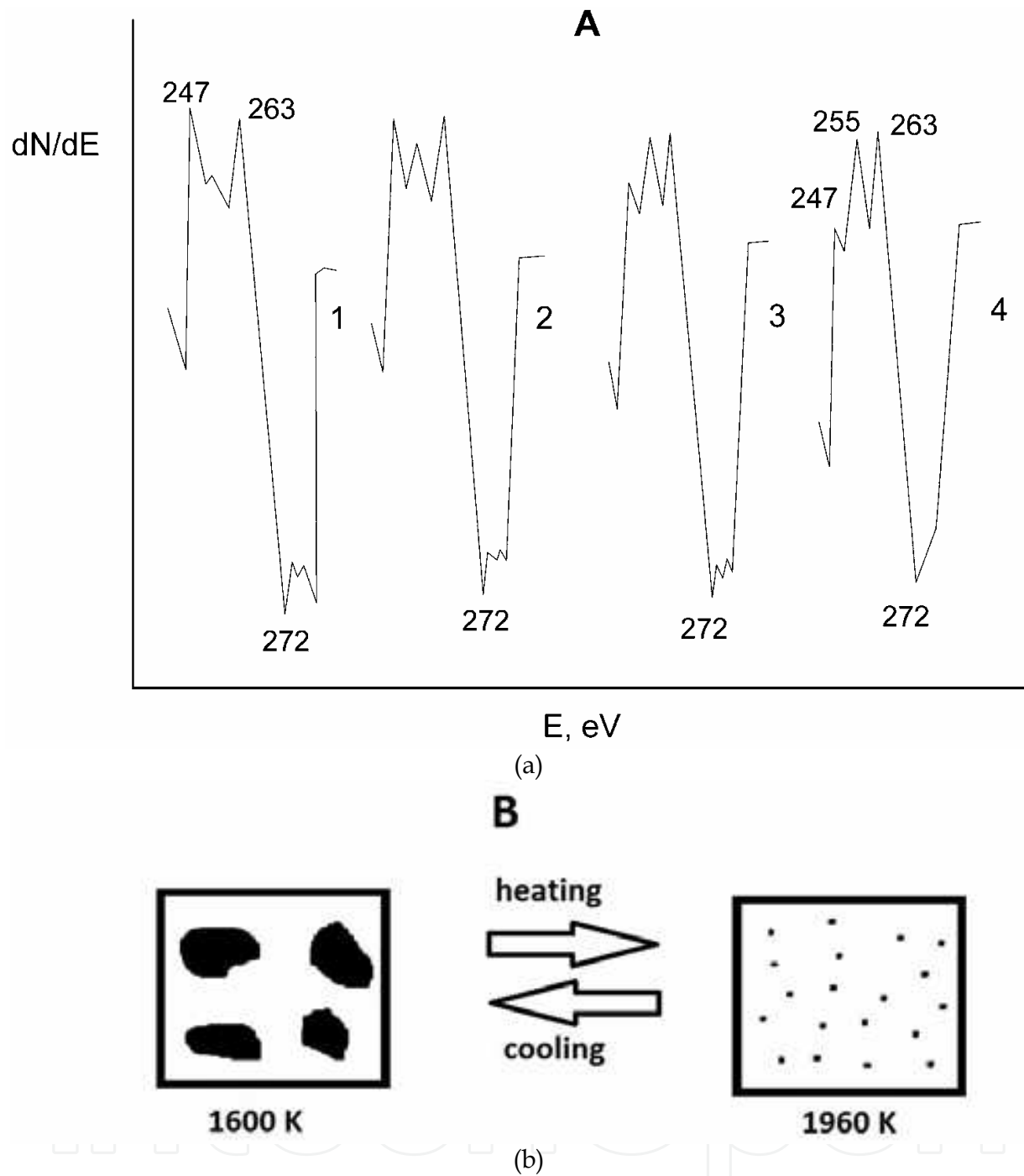


Fig. 23. Phase transition between graphene and carbon chemisorbed 2D 'gas' on Ir (111). The total amount of carbon on the surface $N_C = 1.2 \cdot 10^{15} \text{ cm}^{-2}$ is unchanged. A - transformation of carbon KVV Auger spectra with temperature T (K): 1 - 1600; 2 - 1800; 3 - 1850; 4 - 1960. B - a model scheme illustrating the process.

that a cluster will acquire the right to be called a graphene island after it has combined several tens of carbon atoms together. Relevant theoretical calculations do indeed yield for such a cluster a figure of ~ 50 atoms, of which only its central part will be a proper graphene island [61]. While visualize the process of growth of carbon cluster structures would not be an easy thing to do, that they should exist cannot probably be questioned.

Another, and possibly not less serious, problem is how to deal with the edges of graphene islands, on which the carbon atoms have dangling bonds. It appears reasonable to suggest that edge carbon atoms form strong chemical bonding to the surface atoms of metals. This is suggested by the following observations. First, thermal stability of graphene islands is different and lies in the 900--1600-K interval for various metals (§ 7); bonding of an edge carbon atom in an island to the metal weakens its coupling to the "parent" island, and it is this that brings about its destruction. To cite just one example, on nickel graphene islands break up already at $T \sim 900$ K, while the most heat-resistant islands turned out to be those on iridium, with their temperature of destruction being above 1600 K (§ 7). It is pertinent to note here that a thick (more than 3 layers) graphite film on iridium dissolves at $T > 2300$ K, because the three edges of the top graphene layer do not bond chemically to the metal, and the binding energy of the edge carbon atom to its parent layer is ~ 6 eV [27].

Second, intercalated cesium, i.e., cesium located under a graphene island, for instance, on rhenium, desorbs only for $T > 2200$ K (sic !), because it remains imprisoned under the graphite traps---islands whose edges are coupled to the metal (§ 7). By contrast, cesium present on the surface of graphene or a metal can be readily removed at $T \sim 800$ K [62].

The various chemical states of carbon translate into varying patterns of the Auger spectrum of carbon as it is adsorbed, for instance, on iridium at $T = 1950$ K (Fig. 24). The spectra are seen to change, which reflects the constantly changing carbon redistribution among its different states. For a relative island surface area $S_0 = 0.3$ -- 0.4 , the shape of the carbon Auger

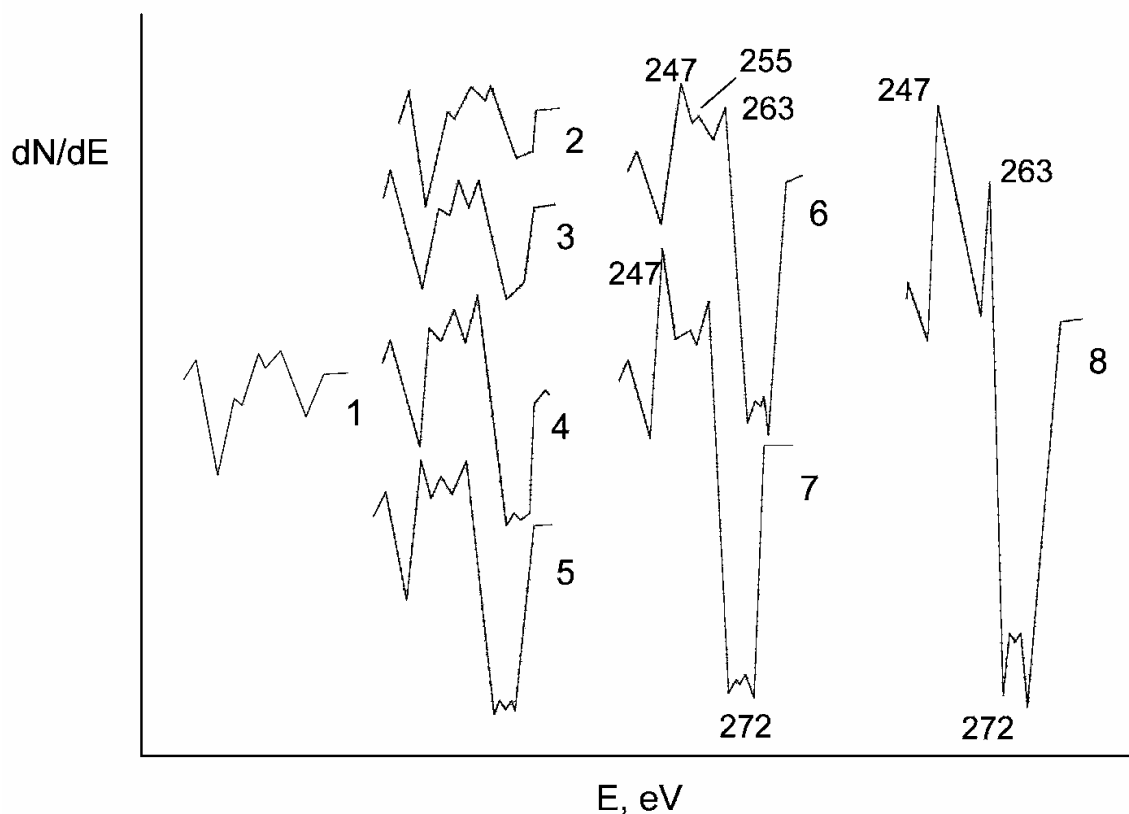


Fig. 24. Carbon KVV Auger spectrum transformation in deposition of atomic carbon on the Ir(111) at 1950 K for various covers of 2D carbon 'gas' θ_C and relative graphene areas S_0 (relative un.):

No	1	2	3	4	5	6	7	8
θ_c	0.12	0.24	0.21	0.27	0.27	0.27	0.27	0.27
S_0	0	0	0	0.11	0.27	0.33	0.43	0.73

All Auger spectra were measured at 1900K.

spectrum is still not pure graphene-like. Even after the temperature has been lowered down to $T \leq 1600$ K, with practically all of the carbon “gas” confined to the islands, the Auger spectrum of carbon will not have the pure graphenic shape, which should be assigned to the graphene island edges being bound chemically to the substrate. In some simpler cases, for instance, with surface carbides of the metal present, the shape of the carbon Auger peak does not change, and only the intensity of the carbon Auger signal undergoes variation.

§ 6. The nature of graphene island coupling to the metal

The central part of the islands is coupled to the metal by weak van der Waals-type forces, and the island edges are coupled to the metal.

As already mentioned, graphene films form on many metals and their carbides with strongly different crystal geometries of their surfaces. There is an intriguing point, however: only the crystal geometry of the Ni(III) face coincides perfectly with the structure of graphene layers [56]. We are thus facing a paradoxical situation: formation of a chemisorbed graphene layer on metal surfaces should be an extremely uncommon event. This point was discussed in Ref. [27] where it was suggested that because of the graphene layer being valence saturated, it should be physisorbed on a metal surface, i.e., coupled to it only by the van der Waals forces of polarization nature, without electron exchange, and, hence, should be separated from the surface by a resultant distance characteristic of these forces.

This suggestion is corroborated by our studies of intercalation of graphene layers on a metal with foreign atoms and C_{60} fullerene molecules [41], the situation where adatoms build up spontaneously, and in sizable amounts, under the graphene layer, and, thus, force the layer away from the surface of the metal to a distance comparable with the diameter of the intercalated atoms or molecules. Apart from this, experimental studies of surface migration of Si atoms on Ir(III) revealed that the kinetics of surface diffusion under a graphene layer remains the same as on a pure metal [63].

Graphite is known to have layered structure with a large interplanar distance, $2R_{vdW} = 3.35$ Å, accounted for by van der Waals coupling without electron exchange. Within a layer, carbon atoms are coupled by strong covalent bonding, with the distance between atoms $2R_c = 1.42$ Å. Treated in the context of the ideology developed in Ref. [27], the layered structure of graphite suggests that the graphite layer is valence-saturated. In a graphite crystal, by contrast, each layer is permanently in contact with an identical valence-saturated layer. The situation is radically different with a graphite layer forming on a metal whose surface atoms have many free electrons capable of forming chemical bonding with graphite. If a graphite layer is physisorbed on a metal surface, there is no electron exchange between them, and the layer should evolve in the way it would on the surface of a graphite single crystal, i.e., exist in the form of a “plate” $2R_{vdW} = 3.35$ Å thick (Fig. 25) whose central plane is spaced from the plane passing through the centers of the metal surface atoms of radius R_M by a distance

$$L_{\text{phys.}} = R_{vdW} + R_M. \quad (1)$$

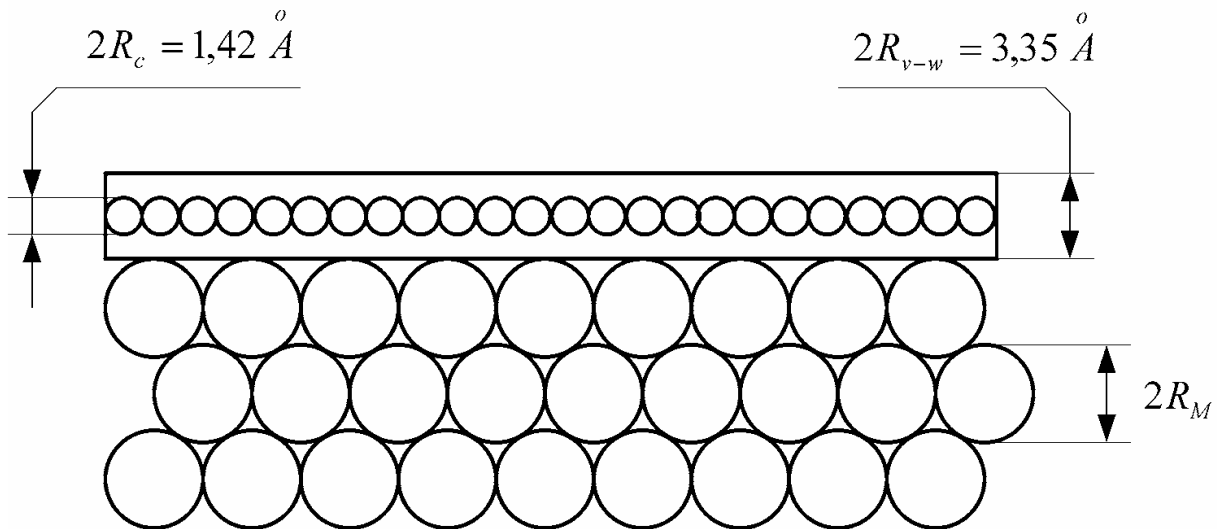


Fig. 25. A model scheme showing the structure of a graphene layer on a metal: R_C - carbon atomic radius, R_m - metal atomic radius, $2R_{v-w}$ - interlayer distance in graphite.

In the case of chemisorption, i.e., in the presence of electron exchange, the graphite layer would be pressed to the metal surface, with the distance between the center of carbon atom of radius R_C in the island and that of the surface metal atom

$$L_{chem.} = R_C + R_M. \quad (2)$$

There are three publications of interest in this respect. The first study [64] used SEELFS (surface-extended energy-loss fine-structure spectroscopy) to investigate the structure of a graphene film on the Ni(III) face whose crystal geometry matches nicely that of graphene. From SEELFS measurements one has succeeded in deriving an essential distance $L_{exp} = 2.80 \pm 0.08$ Å. Significantly, the physical meaning of L_{exp} is, however, not disclosed in the paper. Let us analyze now this quantity following the review of A. Ya. Tontegode [27]. The author of the review estimated and compared the distances involved in chemisorption, L_{chem} , and physisorption, L_{phys} , with the experimental value $L_{exp} = 2.80$ Å reported in Ref. [64]. The distance L_{chem} was estimated from geometric parameters, with carbon atoms placed into the hollows separating nickel atoms, with due account taken for the known radii $R_C = 0.71$ Å and $R_{Ni} = 1.24$ Å [65]. The calculations yielded $L_{chem} \leq 1.6$ Å. For physisorption we have

$$L_{phys.} = R_{vdW} + R_{Ni} = \frac{3,35}{2} + 1,24 = 2,91 \text{ Å} \quad (3)$$

Because $L_{exp} \sim L_{phys}$ and considerably larger than L_{chem} , a conclusion was drawn [27] that a graphene layer is physisorbed on nickel. That the Ni--Ni distance in an atomic surface layer is constant, an observation made by LEEDS, likewise argues for the absence of electron exchange between a graphite layer and a metal surface. The physisorptive nature of the graphite-metal coupling is corroborated by another study [6] which shows that the best agreement between the dependences of diffraction intensities on electron energy obtained experimentally and by calculation performed under certain assumptions is reached for a separation of graphene from the nickel surface of 3.4 Å. Strange though as this may seem, the paper that reported this result did not comment on this either.

The third study [66] probed the system consisting of a graphene film on Pt(III) by a LEED method developed to study structures of incommensurate adlayers. The analysis offered three interplanar spacings: $L_1 = (3.70 \pm 0.05) \text{ \AA}$, $L_2 = 2.45 \text{ \AA}$, and $L_3 = 1.25 \text{ \AA}$, as well as the metal-carbon bond length $L_4 = (2.03 \pm 0.07) \text{ \AA}$. It was found possible to interpret these results by assuming that sandwiched between the graphite monolayer and platinum there are chemisorbed carbon atoms; indeed, the distance $R_{Pt} + R_C = 1.38 + 0.71 \text{ \AA} = 2.09 \text{ \AA}$ [66], which is close to L_4 ; L_3 can be identified with the distance between the centers of chemisorbed carbon atoms sitting in the hollows between platinum atoms and the centers of surface Pt atoms. The distance $L_2 = 2.45 \text{ \AA}$ approaches the sum $R_C + R_{vdW} = R_C + R_{vdW} = 0,71 \text{ \AA} + \frac{3,35 \text{ \AA}}{2} = 2.39 \text{ \AA}$, and the distance $L = 3.70 \text{ \AA}$, equal to the sum $(L_2 + L_3)$, is then the separation between the centers of platinum surface atoms and those of carbon atoms in the graphene film. Drawing from these data, A. Ya. Tontegode [27] came to the conclusion that the good agreement between L_2 and the sum $R_C + R_{vdW}$ gives one solid enough grounds to suggest that the graphite-metal bonding is actually physisorptive in character. The conclusion drawn in Ref. [66] assumes this bonding to be rather intermediate in character between "chemisorption" and "physisorption". But if this coupling is indeed of a mixed nature, valence electrons of carbon atoms chemisorbed on platinum should have been able to penetrate into the π electron zone of graphene, with the result that the distance L_2 should be smaller than the sum $R_C + R_{vdW}$.

Obviously enough, the physisorptive character of coupling between the graphene film and the surface of a metal should produce a substantial impact on the various physico-chemical processes occurring in an adlayer, more specifically, segregation of atoms from the bulk of the metal onto the surface, migration-based processes in the adlayer, in the initial stages of growth of carbon films, adsorption-desorption phenomena, and chemical reactions. A physisorbed graphite monolayer, i.e., a graphene film on a metal, may be identified, in a certain sense, with a graphite cell (a two-dimensional graphite "plate"). This novel approach has revealed a new intriguing direction in the investigation of intercalation, namely, study of the relations governing intercalation in the metal-graphene system.

Thus, the above experimental findings suggest the following simplified model representation of the processes evolving in the Me-graphene system (Figs. 26A and 26B).

1. Chemisorbed carbon "gas" increasing the work function of the metal surface by a few tenths of an eV. Carbon atoms of this phase are coupled to the metal by a strong covalent bonding $\geq 6 \text{ eV}$ (§ 7)---see item 1 in Fig. 26A.
2. Chemisorbed carbon "gas" under the graphene islands [15]---item 2 in Fig. 26A; if present in a high enough concentration, this "gas" distorts the shape of the Auger spectrum of carbon of the graphene films (see, e.g., spectra 3 and 4 in Fig. 9).
3. Graphene island whose central part is coupled to the metal by weak, van der Waals-type forces; this is what makes it possible, for instance, for foreign atoms to penetrate easily under a graphene film---item 3 in Fig. 26A.
4. Edge, non-graphite carbon atoms chemically bound to the metal surface; on iridium, for instance, this energy is $\sim 2.2 \text{ eV}$ (§ 5). Different binding energies coupling edge atoms in an island to different metals account for the strongly different temperatures at which graphene islands break up (§ 7)---item 4 in Fig. 26A.
5. Carbon atoms dissolved in the bulk of the metal; as a rule, at $T > 900\text{--}1000 \text{ K}$ diffuse easily over the bulk of the metal---item 5 in Fig. 26A.

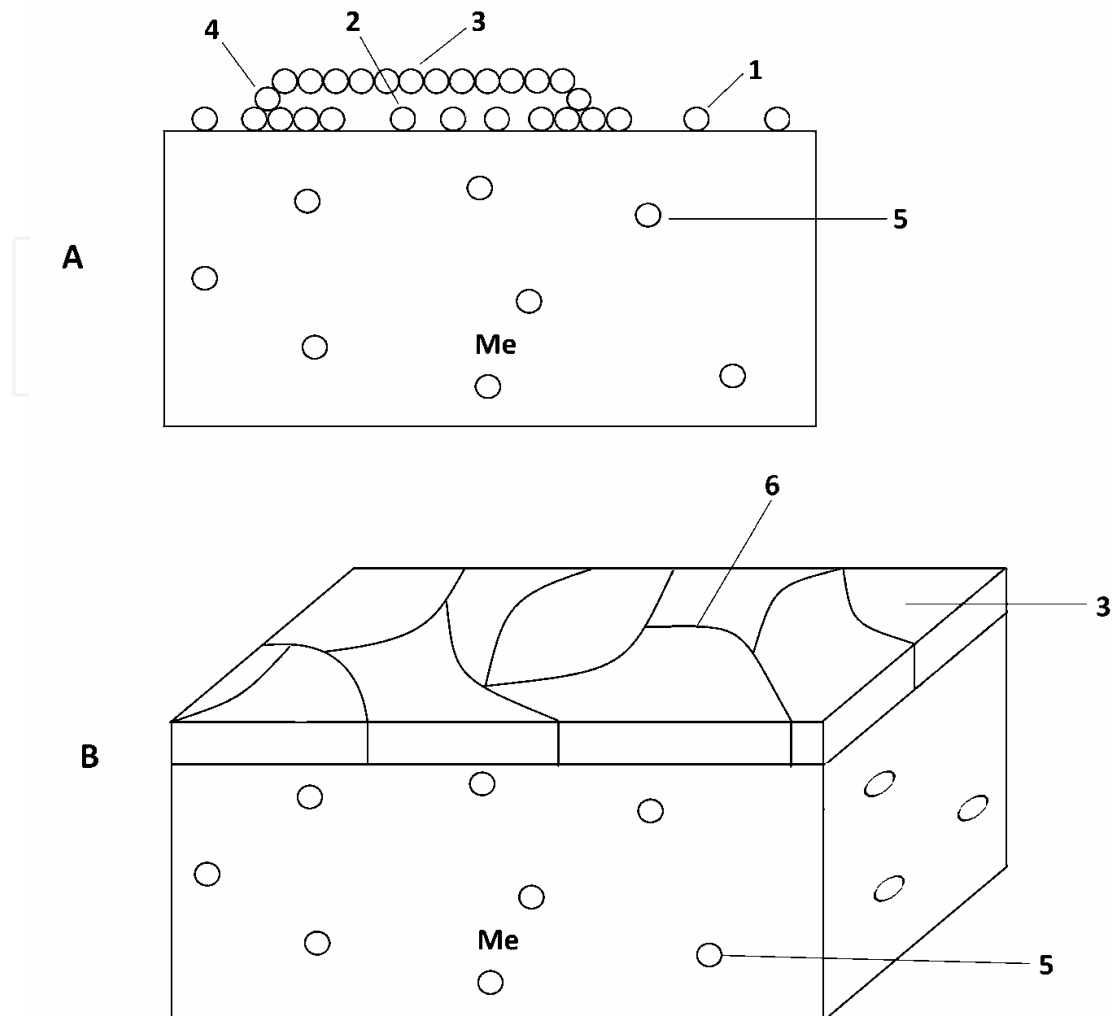


Fig. 26. A model scheme showing the graphene layer on a metal: 1 - chemisorbed carbon 'gas' upon the metal and under the graphene layer (2); 3 - carbon atom in the graphene island; 4 - non-graphitic edge carbon atom; 5 atomic carbon dissolved in the metal bulk; 6 - edges of the merged graphene islands.

Figure 26B displays a model representation of formation of a continuous graphene film from merged islands. It is assumed that the edges of coalesced islands are actually layer defects which are responsible for residual dissociation of CsCl molecules, and that through these defects foreign atoms penetrate under the layer; and it is at the defect edges that nucleation of the second layer of graphene is initiated when carbon atoms segregate onto the surface from the supersaturated Me-C solid solution (§ 9).

§ 7. Properties of graphene films on metal surfaces

Valence saturation and passivity of graphene
give rise to some intriguing properties.

1. Concentration of graphene islands on iridium

As derived from graphene island oxidation. Oxidation of carbon in its various chemical states on the surface of iridium was studied in considerable detail in Ref. [67]. It was shown that at

300 K only the edges of graphene islands become decorated; in fact, oxygen does not adsorb to the passive surface of the central part of an island. As the temperature increases, the edge atoms of carbon in an island escape from the surface in the form of CO and CO₂. Consider the results obtained in Ref. [67]. At $\theta_c = 0.5$, i.e., at $S_0 = 0.5$, the total concentration of carbon atoms in the islands is $N_c(\text{tot}) = N_{cm} \theta_c = 1.8 \cdot 10^{15}$ at/cm². One temperature flash produced after a sample with graphite islands has been maintained in an oxygen atmosphere at 300 K removes $N_c(\text{edge}) \approx 1.7 \cdot 10^{14}$ at/cm² atoms from the surface. Assuming graphene islands to have a simple, e.g., circular shape of radius R , we come to

$$N_c(\text{tot}) = \frac{\pi R^2}{a^2} \cdot f, \quad (1)$$

$$N_c(\text{edge}) = \frac{2\pi R}{a} \cdot f, \quad (2)$$

where $S \approx a^2$ is the area occupied by a carbon atom with a diameter a , and f is the graphene island concentration on the surface. Solving Eqs. (1) and (2), we obtain

$$f = \frac{N_c^2(\text{edge})}{N_c(\text{tot})4\pi}. \quad (3)$$

Substitution of the above experimental data yields an estimate for the island concentration $f \approx 3 \cdot 10^{12}$ cm⁻². In the case under consideration, the number of carbon atoms in an island will be $\sim 7 \cdot 10^2$. Straightforward calculation shows that 13 adsorption-desorption cycles would be required to “consume” such islands with the use of oxygen. This number 13 matches very well with the estimate [67] that 12 ÷ 13 cycles should suffice to clean completely the iridium surface of graphene islands covering an initial relative area $S_0 = 0.5$.

As derived from potassium atom adsorption. The idea underlying the method involves adsorption of potassium atoms at 300 K on an iridium surface with graphite islands to saturation. A temperature flash (Fig. 27) desorbs first potassium atoms from the central part of graphene islands ($T_{max} \sim 700$ K), followed by desorption from the parts of uncovered metal areas ($T_{max} \sim 800$ K), and only after that, at comparatively high temperatures, from the edges of graphene islands ($T_{max} \sim 1100$ K) (for more details, the Reader can be referred to Ref. [62]). The adsorption capacity of phase “2” in Fig. 27 associated with decoration of graphene island edges by potassium atoms depends on the area of graphene islands. Figure 28 displays in graphical form the dependence of the maximum filling of this phase by potassium atoms on the relative area occupied by the graphene islands. Assuming in a first approximation the maximum concentration of potassium atoms along the island periphery to be equal to the concentration of edge carbon atoms, one may safely use Eq. (3) to estimate f . It turned out that $f \approx 3 \cdot 10^{11}$ cm⁻² for $S_0 = 0.4$ – 0.6 . As the relative island area increases, f decreases. Indeed, for $S_0 = 0.8$ we obtain $f \approx 1 \cdot 10^{10}$ cm⁻², which should probably be assigned to coalescence of the islands setting in as their relative area becomes large enough.

Experiments revealed that the concentration of graphene islands on iridium does not depend on the intensity of the carbon atom flux striking the surface. This suggests that the nucleation is not homogeneous. There are firm grounds to believe that graphene islands nucleate at defects in the iridium substrate, e.g., at the edges of atomic steps.

Thus estimation of the concentration of graphene islands on iridium for the case of the islands occupying a relatively small part of the total surface area yields $f \approx 10^{11}$ – 10^{12} cm⁻².

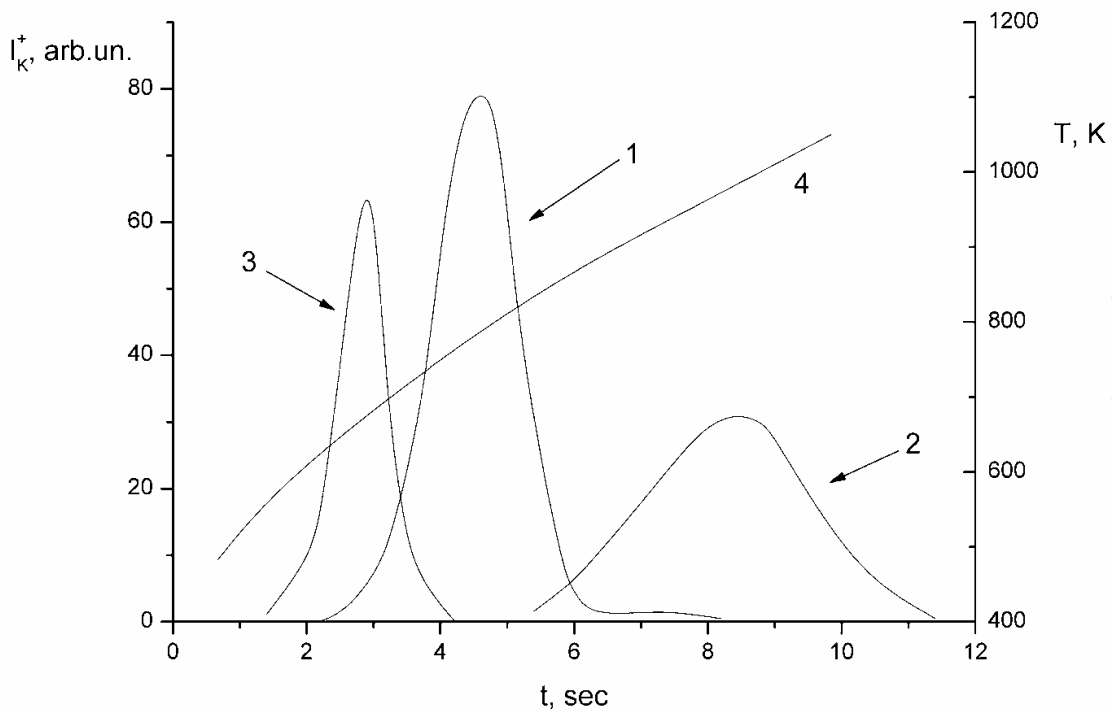


Fig. 27. Thermal desorption spectra for K⁺ ions from Ir(111) (1); from Ir covered with graphene islands at $S_0 = 0.5$ (2), and from grapheme (3). the substrate was pre-exposed to atomic K with the flux $v_K = 2.8 \cdot 10^9 \text{ cm}^{-2}\cdot\text{s}^{-1}$ for 30 sec. 4 - temperature versus time dependence.

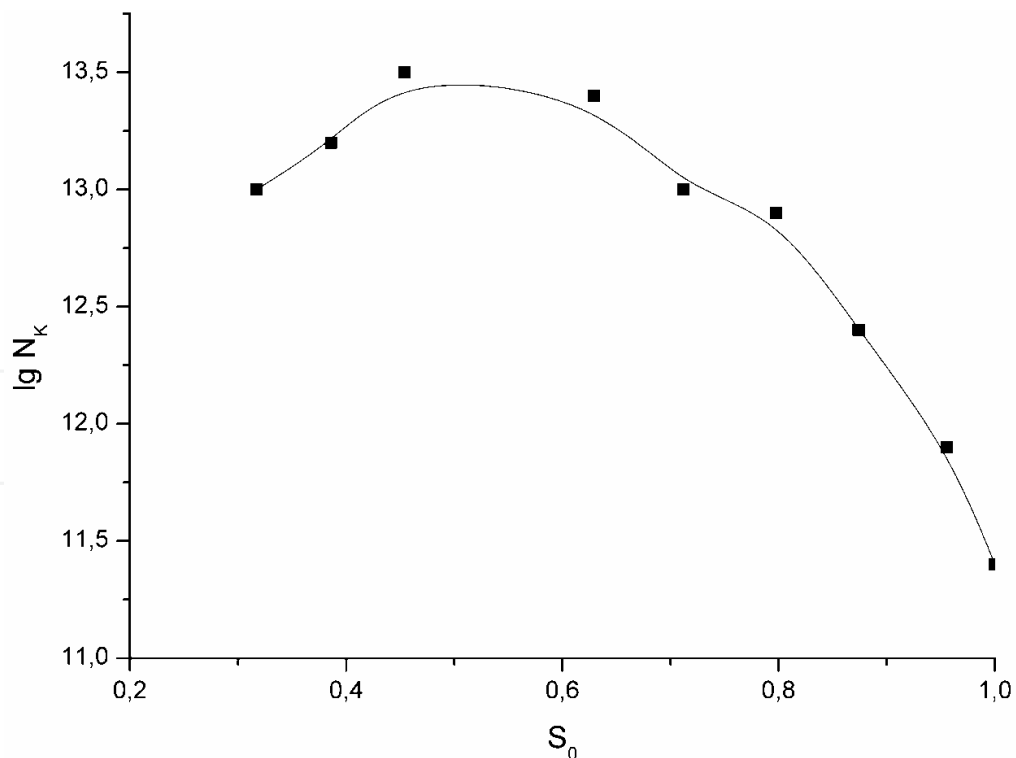


Fig. 28. The maximal concentration of the atomic K on the periphery of the graphite islands as function of relative grapheme area on Ir(111). the temperature of K adsorption is 960 K, $v_K = 1 \cdot 10^{12} \text{ cm}^{-2}\cdot\text{s}^{-1}$, exposition time is 10 min for each point.

2. Specific features of exchange and catalytic reactions on graphene

The activity of catalysts in heterogeneous reactions involved in dissociation of molecules is intimately related with the valence state of atoms in the surface layer of a metal. In the representation adopted in Refs. [27], in order for an adsorbed molecule on the surface of a solid to be capable of dissociating, the atoms making up the molecule should bond to the atoms of the surface catalyst, which reduces the dissociation energy and increases the reaction rate. While the dissociation energy of a CsCl molecule, for instance, is $E_0 = 4.56$ eV in free space, on the surface of metals (Ir, W, Re and others) it decreases strongly down to $E_0 < 0.3$ eV [27].

The surface of a clean metal has a large number of valence bonds, which makes metals efficient catalysts in dissociation reactions. One may expect the efficiency of such reactions to drop markedly (catalyst poisoning) when an adsorbate film of an element of Subgroup IV÷VIIIb of the Periodic System forms on the metal surface [27].

Indeed, heterogeneous catalytic reactions of dissociation of As, Sb, P, Se, Te films were found to exhibit poisoning [68].

Deposition of carbon on the metal surface is a widely recognized process. There were reports of the poisoning effect a carbon film produces in a catalytic reaction of ammonium decomposition on platinum [69, 70], as well as on other metals (Ni, Rh, Ta, W) [70], when carbon is adsorbed in large amounts.

While the poisoning effect of carbon was pointed out in many publications, nevertheless, a systematic study of the effect exerted by controllable amounts of carbon on metal surfaces on the efficiency of heterogeneous reactions of dissociation of a number of salt molecules did not appear until a series of publications [50,71,72], as well as of reviews [27]. An approach most widely used in the above studies involves application of surface ionization (SI) techniques to probe one of the dissociation products of MX molecules. SI of a MX molecule proceeds in two stages:

1. Catalytic dissociation of the molecule, $MX \rightarrow M + X$;
2. Ionization of the metal atom $M \rightarrow M^+ + e$.

(Here M stands for the atom of the metal, and X, for that of a halogen).

The easily measurable current of the M^+ ions (with the mass spectrometric technique employed) provides information on the process of catalytic dissociation of MX molecules on the surface. The above publications made use of the degree of dissociation ω as a quantitative characteristic of the catalyst (metal) activity:

$$\omega = \frac{v_{MX} - v'_{MX}}{v_{MX}}, \quad (4)$$

where v_{MX} is the flux density of MX molecules striking the substrate surface, v'_{MX} is the density of the desorbing molecule flux, and $(v_{MX} - v'_{MX})$ is the fraction of the flux of molecules that has dissociated on the surface. It is assumed that the experimental conditions are stationary, with the flux of molecules incident on the surface equal to that desorbing from it, and no elastic scattering of molecules from the surface present, the points borne out in a special experiment [72].

The role played by the two carbon phases on iridium surface in dissociation of CsCl molecules was studied in Ref. [51]. It was demonstrated that carbon present in the phase of two-dimensional chemisorbed "gas" does not affect in any way the efficiency of the CsCl dissociation reaction, and that $\omega = 1$ just as in the case of clean iridium. Carbon present in

the phase of two-dimensional graphene islands reduced drastically the efficiency of CsCl dissociation, the degree of dissociation decreasing after formation of a graphene film down to $\omega = 10^{-3}$ (at $T = 1700$ K) or $\omega = 10^{-5}$ (at $T = 900$ K). That it was the poisoning action of the graphene phase of carbon on the CsCl dissociation reaction was corroborated by studies of both with carbon layers on other substrates---Rh [27], Pt [73], Pd [74], Re [74], and with other salts---KNO₃, KCl, K₂SO₄, RbCl, HCOOK [27].

The virtually total suppression of dissociation of CsCl molecules on graphene islands, combined with their complete dissociation on surface areas of either a clean metal or a metal containing chemisorbed carbon "gas" suggested a simple method of determining the relative area of two-dimensional graphene islands by measuring the current of Cs⁺ ions produced in SI of one of the dissociation products, namely, Cs atoms (§ 2).

TDS, AES, and LEED were applied to probe the role played by the carbide and graphene carbon phases in the breakup of molecules of the HCOOH and DCOOH formic acid [75]. The carbon was deposited on the surface by exposing heated nickel to C₂H₄ vapor. It was found that exposure to C₂H₄ vapor at $P_{C_2H_4} \sim 10^{-7}$ Torr and $T = 525$ K produced surface nickel carbide with the (2 × 1)C structure as revealed by LEEDS, and at $T = 600$ K, the (4 × 5)C surface carbide. The concentration of surface carbon was estimated as $\sim 9 \cdot 10^{14}$ at/cm², a figure fairly close to that of surface nickel atoms on (110). It was demonstrated that surface carbide did not poison the catalyst; indeed, HCOOH (or DCOOH) molecules dissociated, which was inferred from the release of the various reaction products: H₂, CO₂, CO and H₂O. By contrast, formation of graphene on nickel in C₂H₄ vapor at $T \sim 800$ K reduced dramatically the probability of dissociation of HCOOH molecules, which implies poisoning of the catalyst.

The part played by the same, carbide and graphite, phases of carbon on Ni(100) in the kinetics of hydrogenation of CO ($CO + 3H_2 \rightarrow CH_4 + H_2O$) was studied in Ref. [76]. It was found that carbon is produced at $T = 600$ K in the surface carbide phase in the $2CO \rightarrow CO_2 + C$ reaction, and that it plays a major role in the reaction involved in methane formation. The carbide-contained carbon is chemically active and could be readily removed from the sample by heating it up to 700 K in a hydrogen atmosphere ($P_{H_2} \sim 100$ Torr). Surface graphite was produced by exposing nickel heated to 700 K to a CO atmosphere ($P_{CO} \sim 24$ Torr). The graphite film completely poisoned the catalyst, with the methane production reaction becoming suppressed.

One studied also [77] hydrogenation of CO on Fe(110) which contained carbon deposits of different origin, among them a CH_x phase, carbon-hydrogen carbide phase, and graphite phases differing in the content of intercalated hydrogen. It was found that the CH_x and carbide-carbon phases participated actively in hydrogenation. The graphite phase suppressed the hydrogenation process completely.

An interesting analysis reported in Ref. [78] provided an explanation for the observation that palladium membranes used to prepare chemically pure hydrogen lost their hydrogen permeability after carbonization. Penetration of hydrogen through a membrane involves the stage of H₂ dissociation at the front face of the palladium membrane, followed by dissolution of H atoms in the bulk of the metal, after which the H atoms associate on the rear side of the membrane, to be desorbed in the form of H₂ molecules. It appeared only reasonable to suggest [72] that suppression of hydrogen permeability of the palladium membrane is initiated by termination of the dissociation of H₂ molecules at the front side of the membrane, when it becomes coated by a valence-saturated graphite film.

As pointed out in the review article [27] and suggested by the results of the above studies, it is only in the form of graphite that carbon poisons the metal catalysts used in dissociation-based catalysis.

The graphene surface on metals turned out a convenient substrate for studying exchange chemical reactions. The Ir-graphene system appears to be a particularly suitable combination, because the properties of graphene on iridium are both well studied and readily controllable.

Interaction among particles of different origin on the surface of solids has become a subject of considerable interest. These studies, besides being very instrumental in development of the theory of elementary processes on the surface, pave a way to emerging applications. It is known, for instance, that deposition of a small amount of an alkali metal onto the surface of metal catalysts enhances considerably the yield of products of molecule dissociation.

The favorable effect of atoms of alkali elements adsorbed on metals is attributed to the change in elementary properties the adsorbed molecules undergo when close to alkali atoms [].

For adsorbents with a passive surface, the corresponding aspects have been studied to a considerably lesser extent, although substrates used intensively in heterogeneous catalysis are passive toward dissociation of molecules. The first observation of the substitution reaction $K + RbCl \rightarrow KCl + Rb$ taking place on the carbonized surface of the Pt + 8%W under combined adsorption of K and RbCl molecules was announced in Ref. [79]. The exchange reaction initiated by combined adsorption of CsCl and Na on the same surface and the kinetics of this process were described in Ref. [80].

The results reported in [79,80] are complicated by superposition on the substitution reactions of a quite pronounced intrinsic dissociation of CsCl or RbCl molecules on the heavily defected alloy surface coated by a carbon film.

A study was made of the role played by the properties of an alkali metal (Na, Li and K), as well as of atoms in different valence states (Ba, Tm, Pt) in the reaction with CsCl molecules on the surface of graphene on iridium (Ir-C) [81--84]. Carbon in the graphene layer does not react chemically with atoms of alkali metals and molecules of alkali halide salts. It can be added than within the operating temperature range background dissociation of CsCl molecules on graphene is low ($\omega \approx 10^{-5}$).

The interaction of CsCl molecules with Ir-C was studied in considerable detail [27]; it was shown that the molecules do not scatter elastically from Ir-C [72]. Cs atoms released in exchange reactions of dissociation are detected by the surface ionization technique with the highest possible sensitivity; indeed, virtually each Cs atom desorbing thermally from Ir-C becomes ionized [39]. This offers a possibility of studying elementary events of interaction at low coverages of the adsorbent by reagents.

In the above studies, the surface was bombarded by stationary fluxes of particles of a variety of compositions, and from the surface desorbed fluxes of reacted and unreacted particles. The total number of atoms in the incident fluxes is equal to their total number in the desorbing fluxes. Significantly, at a constant T the coverage by each species of particles is constant. The surface is hit by fluxes of molecules, v_{CsCl} , and atoms, v_z , where z stands for K, Na, Li etc. Part of the particles can desorb in the neutral and charged states (v'_{CsCl} , v'_z , v'_{z+}). Chemical interaction among the particles may bring about either catalytic dissociation of CsCl molecules at active z centers



or a substitution reaction



For direct determination of reaction type on the surface, introduce a characteristic κ which is actually the coefficient of utilization of z atoms:

$$\kappa = \frac{v'_{\text{Cs}^+}(T)}{v_z}. \quad (7)$$

In the reaction of type (5), the active z centers are not expended, so that $\kappa_{\text{max}} = 1$. In the case of z atoms in the valence state m , the limiting value of κ will be $\kappa_{\text{max}} = m$, because $m\text{CsCl} + z \leftrightarrow z\text{Cl}_m + m\text{Cs}$. Thus, to determine the type of the reaction, one has to measure the v'_{CsCl} and v'_z, v_z fluxes.

To study the reaction kinetics and compare the efficiencies of the reactions between CsCl molecules and z atoms, introduce the efficiency of interaction η

$$\eta(T) = \frac{v_{\text{CsCl}} - v'_{\text{CsCl}}(T)}{v_{\text{CsCl}}} = \frac{v'_{\text{Cs}^+}(T)}{v_{\text{CsCl}}}, \quad (8)$$

$\eta(T)$ defines the fraction of the molecules taking part in the reaction. The quantities $\eta(T, v_z, v_{\text{MX}})$ are calculated theoretically [85], so that the parameters of exchange interaction can be derived from $\eta(T)$ relations for the given v_z and v_{MX} .

Studies of reactions within a broad interval of substrate temperatures and a wide range of fluxes of interacting particles revealed that the Z atoms and CsCl molecules adsorbed on a graphene layer on iridium are involved in an exchange reaction; in the case of Na, K, and Li it is one-stage with $\kappa_{\text{max}} = 1$, for Ba it is two-stage with $\kappa_{\text{max}} = 2$, and for Tm, a three-stage one with $\kappa_{\text{max}} = 3$ (Tm is in this case in the highest possible valence state of 3). Experiments with all alkali metals were conducted in not very different conditions:

Reaction	T, K	$v_{\text{CsCl}}, \text{sm}^{-2} \cdot \text{s}^{-1}$	$v_z, \text{sm}^{-2} \cdot \text{s}^{-1}$
K + CsCl	760 - 1050	$5 \cdot 10^{11} - 4 \cdot 10^{13}$	$1 \cdot 10^{10} - 2 \cdot 10^{13}$
Li + CsCl	800 - 1000	$3 \cdot 10^{11} - 2 \cdot 10^{13}$	$1 \cdot 10^{11} - 5 \cdot 10^{12}$
Na + CsCl	750 - 950	$5,3 \cdot 10^{11} - 3,4 \cdot 10^{13}$	$3 \cdot 10^{10} - 9 \cdot 10^{12}$

Table 3

Experimental studies permitted one to obtain $\log \eta(T)$ and $\kappa(T)$ relations for different fluxes of atoms and molecules incident on the surface. Figure 29 plots typical $\log \eta(T)$ and $\kappa(T)$ graphs for the case of potassium atoms. The growth of η observed to occur with decreasing T is initiated by the increase of particle concentration on the surface and of the migration path lengths during their lifetime in adsorbed state (the fluxes striking the surface are constant).

The kinetics of the exchange reaction was considered in terms of the model describing formation of activated MXZ complexes in encounters of adsorbed particles migrating over the surface, and subsequent breakup of these complexes

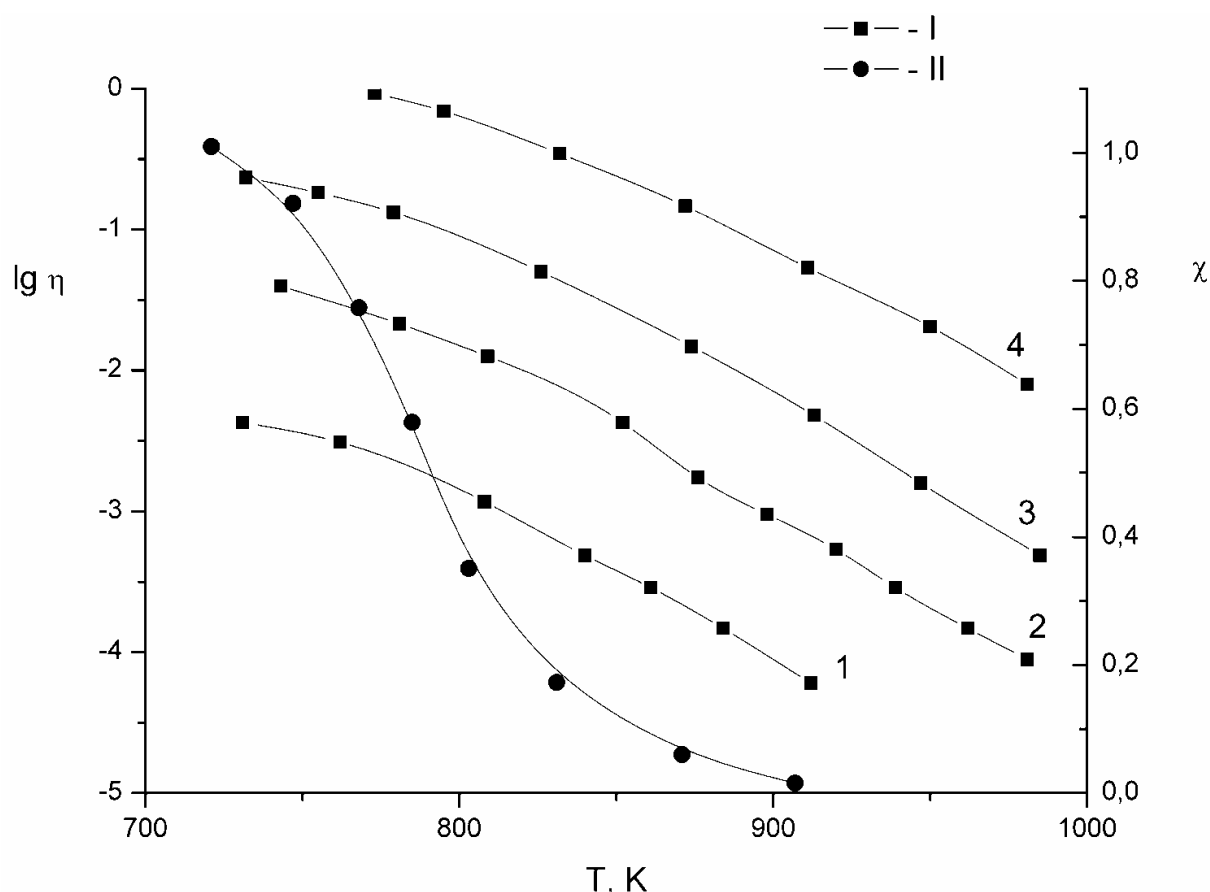
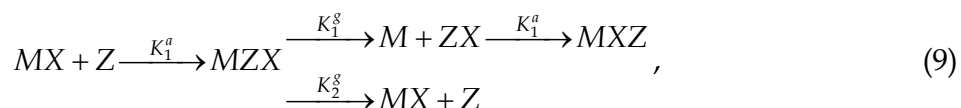


Fig. 29. The dependencies of $\lg \eta$ (I) and η (II) for the reaction $K + CsCl$. The fluxes were $v_{CsCl} = 3.2 \cdot 10^{12} \text{ cm}^{-2} \cdot \text{s}^{-1}$ and v_K ($\text{cm}^{-2} \cdot \text{s}^{-1}$): 1 - $1.3 \cdot 10^{10}$; 2 - $1.4 \cdot 10^{11}$; 3 - $7.5 \cdot 10^{11}$; 4 - $8 \cdot 10^{12}$. Dots show experimental data, solid lines are calculated.



where k_1^a and k_2^a are the rate constants for association of particles into an activated complex MXZ , and k_1^g and k_2^g , those for its dissociation over all possible channels. One succeeded in deriving analytical expressions for the reaction efficiencies that account for the experimental results obtained [81]. The observed increase in the efficiency of the reactions between Li, Na, K atoms and CsCl molecules in the $Li \rightarrow Na \rightarrow K$ sequence matches with the model of local interaction between alkali metal atoms and MX molecules, which provides a reasonable description for the promoting effect alkali metals exhibit in heterogeneous catalytic reactions [81].

We note that the phase state of particles on the surface is essential not only for the kinetics of the reactions proceeding on the surface but for the character of the reaction itself. For instance, in the case of two-dimensional barium islands it was found that the reaction with CsCl molecules involves edge barium atoms only; interestingly, in some temperature regimes one observes not an exchange catalytic reaction but rather catalytic dissociation of CsCl molecules, with the magnitude of κ becoming as large as a few hundred [84]. By properly applying "chemical surface ionization" on passive surfaces with the use of

exchange reactions, one can increase the sensitivity of surface-ionization detection of atoms of a variety of elements. A major requirement is that these atoms are chemisorbed rather than physisorbed on the passive surface of graphene.

3. Thermionic properties of graphene films

It appears only natural to expect that studies of thermal emission from graphene films should reveal the specific characteristics of the metal, which would become manifest, for instance, in the work function of graphene. The work function of graphene films on metals was derived from thermionic emission both by the total current technique and from Richardson graphs [60], as well as by probing the surface with a beam of K, Na, Ba, In atoms [39]. The ribbon temperature was chosen such that its decrease would not initiate growth of the second layer of graphene through segregation of carbon from the bulk of the metal. The results obtained are summarized in Table 4. On all substrates, the graphene surface was uniform in work function. $\text{Re}(10\bar{1}0)$

Substrate	Ir(111)	Pt(111)	Rh(111)	Re(10 $\bar{1}$ 0)
ΔT , K	1800÷1200	1500÷1200	1300÷1150	1700÷1150
$(\varphi \pm 0,05)$ eV	4,45	4,55	4,35	4,25

Table 4.

Apart from this, for the Rh-graphene and Re-graphene systems one determined the work function by measuring the total thermionic current from graphene islands as a function of their relative area S_0 , which was derived by the well-known method involving probing the surface with a flux of CsCl molecules (§ 2). As expected, the work function of islands remained constant with variation of their area from $S_0 = 0.1$ to $S_0 = 1$ (monolayer coverage). Interestingly, the work function of graphene on a metal is affected by atoms of alkali and alkaline-earth metals buried under the graphene film in intercalated state. Indeed, a monolayer of K or Cs adatoms confined under a graphene film on Ir(111) reduces the graphene work function by $\Delta\varphi \approx 0.3\text{--}0.4$ eV; by contrast, the same amount of K or Cs on the surface of graphene lowers the work function by $\Delta\varphi \approx 2.0\text{--}2.5$ eV. A barium monolayer buried under graphene reduces the work function by $\Delta\varphi \approx 0.65$ eV.

4. Thermal stability of graphene films

It appears only natural to expect that as the temperature is increased, graphene islands that formed on a metal surface at T will start to break up eventually at some higher temperature $T_d > T$. Experiments showed that for the four metals studied (Re, Ir, Ni, Pt) the temperature interval within which the graphene islands break up, ΔT_d , lies substantially lower than the temperature of mechanical disintegration of the substrate or of the onset of noticeable desorption T_{des} of carbon atoms from the surface of refractory metals (usually, $T_{des} \geq 2000$ K). On platinum, nickel and rhenium breakup of graphene islands brings about a decrease of the total amount of carbon on the surface. This should apparently be attributed to dissolution of the carbon atoms that have broken off the edge of a graphene island in the bulk of the metal. The only exclusion is iridium, in which carbon practically does not dissolve for $T \leq 200$ K, with the carbon material produced in the breakup of islands persisting on the surface in the form of chemisorbed carbon "gas" [41].

We believe that the elementary event involved in the breakup of a graphene island consists in detachment of a single carbon atom from the edge of this island, followed by its transition to the chemisorbed state on the metal surface. Simplifying the real pattern, we are going to assume that the graphene islands are disc-shaped and have equal areas S_1 . Then the number n_1 of carbon atoms confined to a single island will decrease with time with the temperature increasing up to $T > T_d$ by the law

$$-\frac{dn_1(t)}{dt} = n_b(t) * W = n_b(t)C \exp[-E_{det} / kT], \quad (10)$$

where $n_b(t)$ is the number of carbon atoms in the boundary layer of the island at time t , W is the probability of two-dimensional sublimation, C is the prefactor, and E_{det} is the activation energy for two-dimensional sublimation, or, said otherwise, the energy required to detach an edge carbon atom from the island.

We also assume for the sake of simplicity that the packing of carbon atoms in an island does not differ from that in the basal plane of graphite and that it is independent of the island size, in which case $S_1 \approx an_1$, where a is the area per one carbon atom. Assuming further that $n_b = 2\pi r/d$, where r is the radius of the disc-shaped carbon island, and d is the effective carbon-atom diameter in the graphene lattice, $d = \sqrt{4a/\pi}$, and taking into account that

$$r = \sqrt{\frac{n_1 a}{\pi}} = \sqrt{\frac{aN}{\pi m}},$$

where N is the total number of carbon atoms in all islands per 1 cm², and m is the island concentration, we come to

$$n_b = \frac{\pi}{\sqrt{m}} \sqrt{N(t)}.$$

Now we use Eq. (10) to obtain

$$\frac{dN}{\sqrt{N}} = -\pi\sqrt{m}C \exp[-E_{det} / kT] dt. \quad (11)$$

Equation (11) can be solved for an arbitrary t subject to the initial condition that at $t = 0$, $N = N_0$

$$1 - \sqrt{\frac{N}{N_0}} = -\frac{\pi\sqrt{m}C \exp\left[-\frac{E_{det}}{kT}\right]}{2\sqrt{N_0}} \cdot t. \quad (12)$$

The ratio $N/N_0 = S(t)/S_0$, where S_0 is the area occupied by islands at $t = 0$, is found experimentally by the CsCl dissociation method described above. Having now a set of relations $(1 - \sqrt{S(t)/S_0}) = f(t)$, one can find from the $\log t = f(1/kT)$ equation the energy required to detach a carbon atom from a graphene island for each value $S = \text{const}$. Now knowing E_{det} , one readily derives from Eq. (12) the value of \sqrt{mC} .

As an illustrative case, consider the process of breakup of graphene islands on Re(10-10). A clean rhenium sample was exposed for a short time ($t \sim 10\text{--}30$ s) to benzene vapor ($P_{C_6H_6} \sim 1 \cdot 10^{-7}$ Torr) at $T = 1050$ K. This initiated fast formation of graphene islands on the surface,

while the bulk of the metal remained practically free of carbon. Experiments demonstrated that carbon resides at this temperature on the surface in graphene islands only, because single carbon atoms dissolve rapidly in the bulk of the metal [41]. Nevertheless, to make the experiment as pure as possible, the sample was annealed for several minutes at $T = 1050$ K after the benzene had been pumped off; in this process, the island did not break up, and the small amount of carbon that could build up in the near-surface region was dispersed throughout the volume of the metal, thus reducing the probability of segregation of carbon from the bulk back onto the surface. After this, the rhenium temperature was raised to $T_d \geq 1200$ K and one measured the kinetics of island breakup, i.e., determined the $S/S_0 = f(t)$ relation. The islands broke up completely (Fig. 30). Note that the breakup curves reproduced well enough from one experiment to another although the volume of the sample was not freed from the carbon that had accumulated there. This suggests that at the temperatures ΔT chosen the carbon concentration in the bulk of rhenium is far from the solubility limit, carbon diffuses freely over the metal lattice, and the reverse flux of carbon from the bulk onto the surface may be neglected.

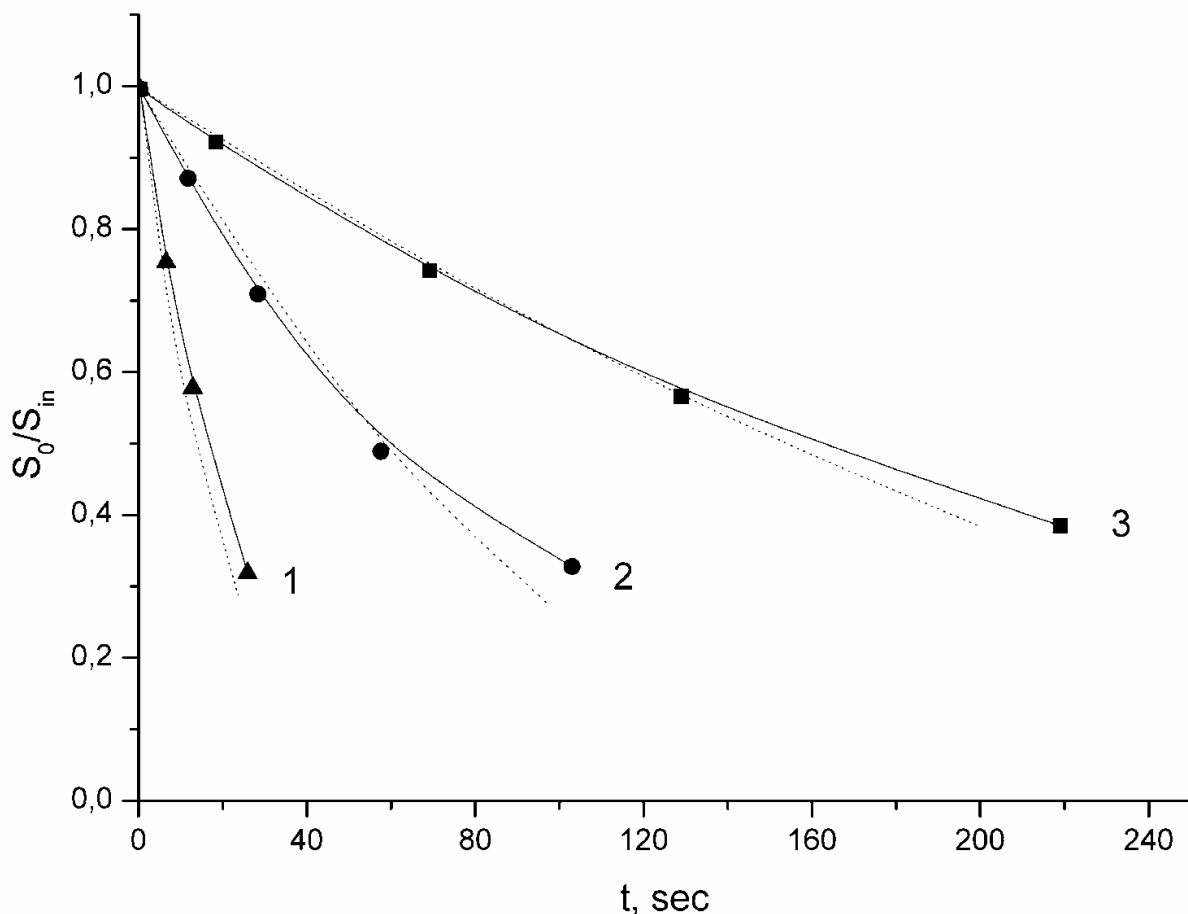


Fig. 30. Equilibrium relative areas of grapheme islands versus annealing time at Re surface at annealing temperatures (K): 1 - 1280; 2 - 1240; 3 - 1215. The value $S_0/S_{in} = 1$ corresponds to the initial area of grapheme islands $S_{in} = 30\%$. Dots show experimental data, solid lines are calculated.

The experimental data were treated in the following way. The curves of Fig. 30 were used to construct $\log t = f(1/kT)$ curves for different $S = \text{const}$, whence one could derive the carbon

detachment energy from the island, $E_{det} = (3.0 \pm 0.2)$ eV. We note that S/S_{tot} varied in the experiments within the 0.2--0.6-interval, and $S/S_{tot} = 1$ correspond to a graphene film with $N_c = 3.56 \cdot 10^{15} \text{ cm}^{-2}$. Next one constructed the graph

$$S(t) / S_0 = (1 - Bt)^2 ,$$

where

$$B = \frac{\pi \sqrt{m} C \exp[-E_{det} / kT]}{2 \sqrt{N_0}} . \quad (13)$$

The value of B was chosen so as to fit the calculated $S/S_0 = f(t)$ relations to experiment (dotted line in Fig. 30). The knowledge of B permitted one now to find from Eq. (13) the product of the prefactor by the root of the number of islands $\sqrt{m}C = 3 \cdot 10^{18} \text{ cm}^{-1}\text{s}^{-1}$. Our studies of the topography of the graphene film on Re(10-10) made by scanning tunneling microscopy permitted estimation of the concentration of graphene islands at close to monolayer coverages, which turned out to be $m \sim 10^{12} \text{ cm}^{-2}$ [86]. Knowing m , one can readily estimate $C \sim 10^{12} \text{ s}^{-1}$.

In a similar way we studied the breakup of graphene islands on Ni(111) and Pt(111). The only difference consisted in the temperature interval ΔT_d within which the islands broke up. The results of the experiments are summed up in Table 5. The values of $\sqrt{m}C$ thus obtained were found to be of the same order of magnitude as those derived for the rhenium sample.

Me	E_{det} , eV	ΔT_d , K
(111)Ni	2.5	950-1050
(1010)Re	3.0	1200-1300
(111)Pt	3.2	1300-1400
(111)Ir	4.5	1650-1850

Table 5

Graphene islands on iridium start to break up at $T_d \geq 1600$ K, which suggests a substantially stronger binding energy of the edge carbon atom to the island compared with the substrates considered earlier. Because the carbon atoms that have detached from the island do not dissolve in the bulk of iridium and do not desorb, the total carbon concentration on the surface does not change, so that as the area of the graphene islands decreases as a result of their thermal destruction, the concentration of carbon atoms in the chemisorbed carbon "gas" phase grows. This, in its turn, gives rise to an increase of the flux of carbon atoms from the chemisorbed "gas" phase to graphene islands. Therefore destruction at a given $T_d = \text{const}$ culminates in the onset of dynamic equilibrium, in which the flux produced in two-dimensional sublimation becomes equal to that of carbon deposited on the islands from the chemisorbed "gas" phase. After this, the island area will no more change (Fig. 31) staying at a certain level depending on T_d . If we reduce the temperature to $T < 1600$ K, the island area recovers to the former level $S = S_0$, with all of the carbon "gas" transferring again to the graphene islands. To be able to neglect the reverse flux of carbon from the chemisorbed "gas" phase, only the very beginning of the $S/S_0 = f(t)$ curves was taken into account. The results of these experiments are also listed in Table 5.

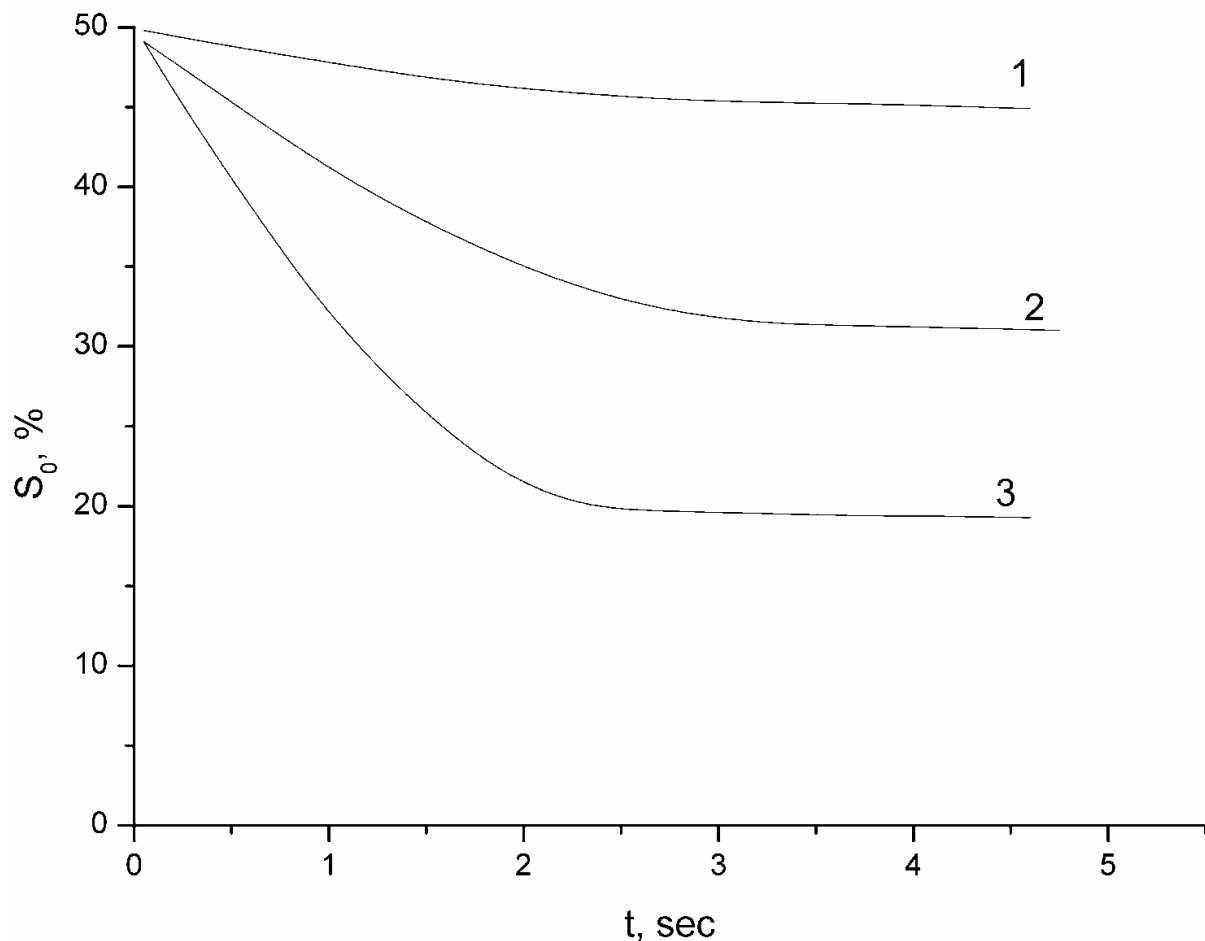


Fig. 31. The dependence of relative graphene island area on Ir versus annealing time at various T , K: 1 - 1715; 2 - 1840; 3 - 1940.

As seen from the table, in contrast to bulk graphite, for which the detachment energy of an edge carbon atom in a layer is ~ 6 eV ($T_d > 2300$ K) [27], in the case of graphene islands adsorbed on metallic surfaces the detachment energy can be markedly lower. It appears reasonable to assume that the valence-active edges of graphite islands form strong chemisorption bonding with atoms of the metallic substrate, which weakens the C-C bonds of an edge carbon atom to neighboring atoms and weakens strongly, in its turn, the destruction temperature of graphene islands on a metal (see Table 5). Experiments show that the easiest to destroy are graphene islands on nickel; this correlates with the observation the nickel, of all the substrates studied, is the only carbide-forming metal. The most thermally stable turned out to be graphene islands on iridium; iridium does not form carbides, practically does not dissolve carbon in its bulk, and, apparently, is the least capable of forming C-Me chemical bonds. Interestingly, if one forms, for instance, on Ir(111) a graphite film a few atomic layers thick by deposition from an atomic flux at $T \approx 1700$ K (Fig. 32), the temperature at which a graphite layer breaks up and, accordingly, carbon escapes from the surface, grows to $T_d > 2300$ K, which corresponds to $E_{det} \sim 6$ eV, a value identified with thermal destruction of bulk graphite. Indeed, in this case no edge atom of the top graphite layer can contact the metal and, hence, there are no grounds to expect that active C-Me chemisorption bonds will reduce the activation energy for detachment of an edge atom from the graphite island.

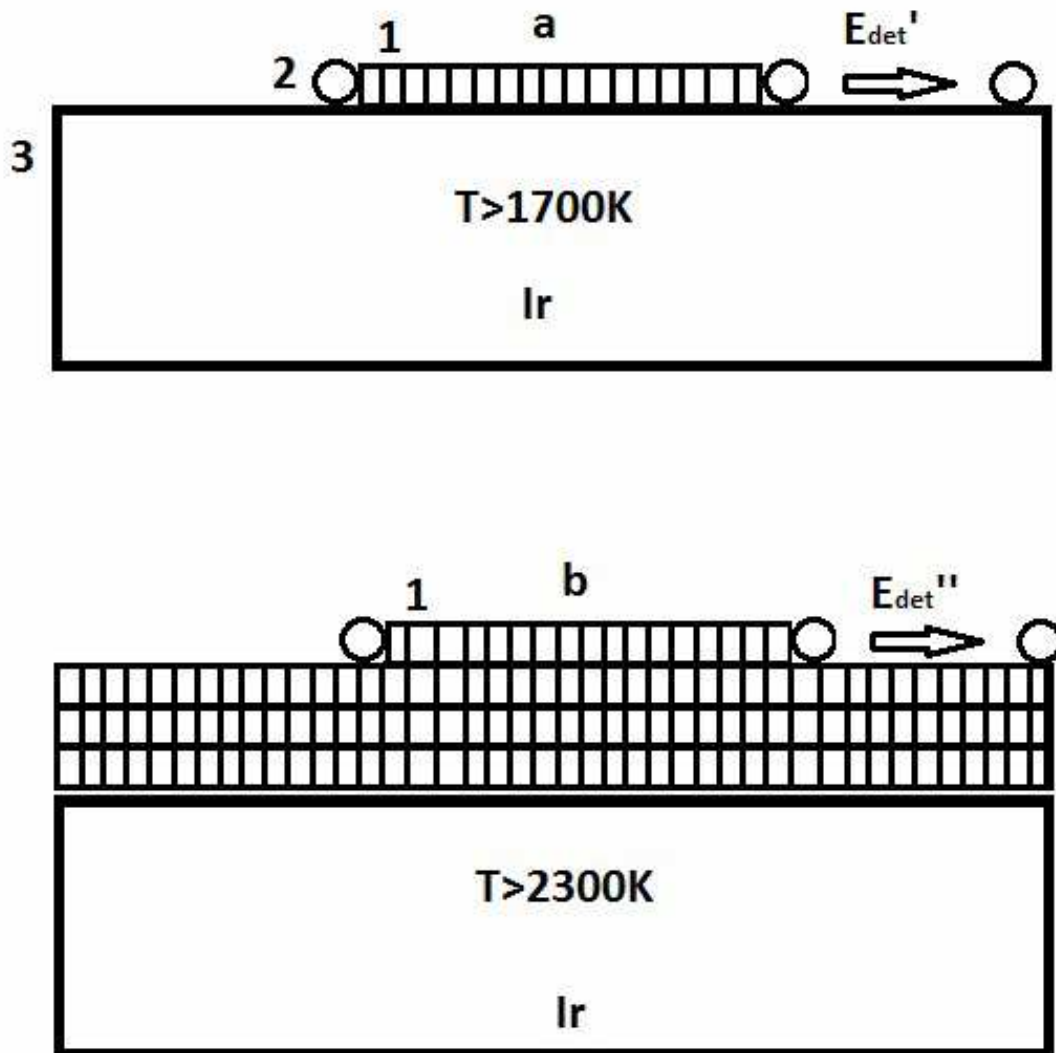


Fig. 32. Schematic representation of atomic carbon interaction with a graphene island on metal surface (a) and on graphite (b). 1 - graphene; 2 - atomic carbon; 3 - substrate.

It appears pertinent to point out here the following significant aspect. The above results relate to the case of the bulk of the metal being practically free of carbon. As carbon is dissolving in the bulk of the metal, the flux of carbon atoms segregating onto the surface increases. This flux enhances noticeably the thermal "lifetime" of the island. To cite an example, on Rh(111) graphene islands start to break up at $T \geq 1000\text{ K}$, with the bulk free of carbon. On carbonization of Rh at $T_C = 1800\text{ K}$, however, one obtains a continuous graphene film, which persists at such high T assisted by a strong carbon flux from the volume of the metal.

5. Adsorption, desorption, and migration on graphene

Valence-bond saturation in the surface layer of a solid should affect noticeably such characteristics as the binding energy of adsorbed particles with the surface, sticking coefficients, adsorption capacity etc. The valence bonds of surface atoms being not saturated, the binding energies of foreign atoms of metals and molecules with atoms of the near-surface metal layer are quite large.

Graphite samples may serve as a good illustrative example of solids with a valence-saturated (passive) surface. Beitel [87] studied adsorption of CO and H₂ on graphite samples. It was demonstrated that the sticking coefficients of CO and H₂ molecules to graphite are very small and decrease with increasing coverage. For instance, at low coverages ($\theta < 10^{-4}$) the sticking coefficients of CO and H₂ molecules to graphite were the highest, (1--5) 10^{-5} . The sticking coefficient was found to decrease rapidly with increasing coverage. Significantly, the number of CO and H₂ molecules chemisorbed on graphite turned out to be ~ 0.01 of the number of molecules chemisorbed on the surface of tungsten. The sticking coefficient of atomic hydrogen to graphite was measured by the same author and found to be $5 \cdot 10^{-3}$ -- $1 \cdot 10^{-2}$ [10].

It is essential that the sticking coefficients of CO and H₂ to pyrolytic graphite ribbons with a precisely adjusted orientation of the (0001) plane of graphite on the surface were smaller than those to other, poorer quality graphite samples. It is suggested [10, 87] that the observed adsorption of gases occurs actually only at defects of the graphite lattice (corner atoms, plane edges, steps, impurity atoms) near which there are empty valence orbitals. Precisely-oriented surface of pyrolytic graphite ribbons containing less structure defects, they are characterized by smaller sticking coefficients than samples of fine-grained graphite. Interestingly, the sticking coefficient of H₂ to graphite heated to $T \sim 1850$ K was $\sim 4 \cdot 10^{-5}$, while that to graphite heated to $T \sim 2400$ K was smaller than 10^{-8} . Quite possibly, high-temperature treatment of graphite samples gave rise to enhanced graphitization, i.e., an increase in the density of surface defects and of the fraction of surface area occupied by them, and this is what caused the decrease of the sticking coefficient. This conclusion matches with our results on graphitization of carbon films on metals studied as a function of sample annealing temperature (§ 11).

Lander and Morrison [88-90] conducted a LEEDS study of the adsorption of O₂, J₂, Br₂, CO, and H₂O molecules on the (0001) face of single-crystal graphite, the most perfect surface of all. It was shown [90] that admission of these gases to pressures $p \leq 1 \cdot 10^{-4}$ Torr and exposure at these pressures of a single crystal for tens of minutes at $T \sim 300$ K did not bring about any change in the diffraction patterns obtained from a clean crystal face. Studies of adsorption of the same gases on other surfaces revealed that a monolayer of gas is easily detectable. The authors offer a conclusion that the substances studied are not chemisorbed on the basal plane of graphite; as for physisorption, it certainly should take place, but at lower substrate temperatures. It was also demonstrated [88,89] that molecules of a number of compounds (FeCl₃, GeI₄, GeI₂, C₆H₆, Xe, ZnI₂) are only physisorbed on the basal plane of single-crystal graphite.

The study of Arthur and Cho [55] occupies a particular place among works dealing with adsorption on the (0001) face of graphite. They investigated the adsorption and desorption kinetics of Cu and Au atoms on this surface. The flash heating method used by them permitted obtaining some quantitative characteristics of desorption. It was shown, for instance, that the coefficient of condensation of Cu and Au increases from ~ 0.05 for $\theta \rightarrow 0$ to 1 for $\theta = 1$. Measurements of the accommodation coefficient of Cu and Au revealed that the small value of the condensation coefficient for a clean surface of the graphite (0001) face is not related in any way with elastic scattering of Cu and Au atoms from the surface; said otherwise, Cu and Au atoms reach thermal equilibrium with the surface prior to desorption. The authors offered the following model to account for the results obtained. Metal atoms reaching the surface of single-crystal graphite have a high mobility and a short average lifetime against desorption. The value of τ determined in the study is in actual fact nothing

else than the upper limit to average lifetime; both for Cu and Au, τ measured at $T = 300$ K and $\theta \approx 0$ was found to be less than 10^{-2} s. Accepting the prefactor in the expression for the lifetime of particles on the surface to be 10^{-13} s, the authors obtained for an estimate of the binding energy of adatoms to the substrate $E_b \leq 0.65$ eV. Such low binding energies should apparently be assigned to the van der Waals character of adatom interaction with the surface, which is possible under valence-band saturation of the graphite surface. This should be contrasted with the activation energy for desorption of Cu and Au atoms from the (110) and (100)W faces, which is $(3 \div 5)$ eV at low coverages [91]. The low binding energy of adatoms with the substrate suggests also a small activation barrier E_{dif} for surface diffusion (estimated by the authors as $E_{dif} \sim kT$), which accounts for the high mobility of the two-dimensional Cu and Au "gas" on graphite. Colliding with one another or with valence-unsaturated surface defects, Cu and Au adatoms can form centers of growth of two- or three-dimensional islands. This is what can underlie the decrease of desorbing flux with time, because islands of adsorbate act as traps for adatoms. The observed increase of the condensation coefficient with increasing atom evaporation time or coverage is attributed by the authors to adatoms escaping from the two-dimensional "gas" phase into close-packed islands, where the lifetime of adatoms exceeds by far the average lifetime in the adsorbed "gas" phase; indeed, the binding energy of a Cu adatom with a copper island was found to be ~ 2.1 eV, and that of Au adatoms with their island, ~ 2.5 eV.

The above data suggest a reasonable conclusion that under the conditions of valence bond saturation in the surface layer of a solid and weak binding of particles with the substrate, particles with free orbitals can form strong bonds with one another. These conditions are conducive to formation of close-packed adsorbate islands, provided the particle mobility on the surface is high enough. An electron microscope study revealed growth of three-dimensional islands of Ag, Au, Pb, Cd, and Zn on amorphous carbon [92-94]. It suggested a conclusion that condensed phase islands nucleate at "particularly active spots" on the surface, i.e., apparently, at valence-active edges of graphite scales on which carbon layers had formed. This suggestion is corroborated by the concentration of adsorbate islands being found independent of the density of the atom flux striking the surface, which appears to indicate that there is no homogeneous nucleation. Growth of three-dimensional Ag and Au islands was observed also on another valence-saturated surface, molybdenum disulfide (MoS_2) [95,96].

Unlike valence-bond-saturated surfaces, adsorption of foreign metal atoms on the surface of metals does not, as a rule, bring about formation of close-packed adsorbate islands [97-99].

It should be noted that amorphous carbon is not a very good model object of valence-bond-saturated surface, because it has a large number of valence-unsaturated defects whose number depends strongly on sample prehistory. Thin carbon films on a metal surface are more stable samples with a reliably controllable surface. McCarthy and Madix [100] studied adsorption of gases and vapors on the surface of a metal coated by a carbon film. Adsorption of CO, H₂, CO₂, and H₂O on clean Ni(110), on carbided nickel, and on the surface of the Ni(110) face coated by a carbon film of graphitic structure was probed by three methods---LEEDS, AES, and heat flashing. Nickel was carbided by cracking of ethylene on the surface at 600 K. The carbon layer on nickel underwent graphitization either under heating of carbided nickel at 775 K, or in ethylene cracking at $T = 700$ -- 800 K, a finding corroborated by other authors as well, e.g., in Refs. [4,5]. In summing up available data, the authors of Ref. [100] came to the conclusion that CO, H₂, CO₂, and H₂O undergo physisorption on a graphite surface, because the heats of adsorption turned out to be too low; for CO₂ and H₂O, for instance, they were found to be ~ 0.35 eV.

Iridium, which does not dissolve carbon, turned out irreplaceable in probing carbon films on metals. Abdullaev *et al.* [101,102] reported on a TESI investigation of the adsorption and initial stages in samarium condensation on iridium ((111)-texture ribbons) and on iridium coated by graphene. The heats of adsorption of Sm atoms on these surfaces at low coverages were found to be 6.0 eV and ~ 1.9 eV, respectively. The large difference between the heats of desorption was attributed to a decrease of the covalent component of adsorption bonding on the passive substrate. The comparatively high desorption heat of ~ 1.9 eV could be assigned to a noticeable contribution to the heat of desorption of the ionic component acting against the mirror image forces [49]. Measurements performed on the same surface [102] demonstrated that the average lifetime of NaCl molecules on graphene-coated iridium, $\tau < 1 \cdot 10^{-5}$ s, even at 300 K, whence for the binding energy of the molecules with the substrate one comes immediately to $E < 0.5$ eV.

It was shown [103] that after formation of graphene on Pt(111) has terminated, the surface becomes passive with respect to adsorption of CO, H₂, and C₆H₆ at $T = 300$ K.

Measurements were conducted [104] of the kinetics of desorption of a number of atoms---Cs, K, Na, Ba, Sr (Table 6)---from both the clean Ir(111) metal and from a graphene film on its surface. It was found that the valence-bond-saturated graphene film on iridium modifies the heats of desorption of particles; in particular, the heats of evaporation E^+ of the monovalent atoms Cs⁺, K⁺, Na⁺ change very little, primarily as a result of a decrease of the polarization

Element	Desorption characteristic $E_{+,0}$ (eV) C, D (s ⁻¹)	Iridium	Graphene on iridium	V (eV)
Cs	E_+	$2,1 \pm 0,1$	$1,8 \pm 0,1$	3,89
	E_0	$4,0 \pm 0,1$	$2,4 \pm 0,1$	
	C	$1,7 \cdot 10^{12}$	$2 \cdot 10^{12}$	
	D	$3,4 \cdot 10^{12}$	$4 \cdot 10^{12}$	
K	E_+	$2,4 \pm 0,1$	$2,2 \pm 0,2$	4,34
	E_0	$3,8 \pm 0,1$	$2,4 \pm 0,2$	
	C	$4 \cdot 10^{12}$	$1 \cdot 10^{14}$	
	D	$8 \cdot 10^{12}$	$2 \cdot 10^{14}$	
Na	E_+	$3,0 \pm 0,1$	$2,9 \pm 0,1$	5,14
	E_0	$3,6 \pm 0,1$	$2,2 \pm 0,1$	
	C	$1 \cdot 10^{13}$	$3 \cdot 10^{11}$	
	D	$2 \cdot 10^{13}$	$6 \cdot 10^{11}$	
Ba	E_+	$5,2 \pm 0,1$	$2,6 \pm 0,1$	5,21
	E_0	$5,8 \pm 0,1$	$1,9 \pm 0,1$	
	C	$2 \cdot 10^{12}$	$1,8 \cdot 10^{10}$	
	D	$1 \cdot 10^{12}$	$0,9 \cdot 10^{10}$	
Sr	E_+	$4,8 \pm 0,1$	$\sim 2,7$	5,70
	E_0	$4,9 \pm 0,1$	$\sim 1,5$	
	C	$6 \cdot 10^{12}$	-	
	D	$3 \cdot 10^{12}$	$\sim 10^{13}$	

Table 6.

interaction between the ion and the metal; indeed, $E^+(\text{Cs}) = 2.1$ eV for Ir(111) and $E^+(\text{Cs}) = 1.8$ eV for Ir(111)-graphene (see Table 6). For the divalent atoms of Ba and Sr, the heats of desorption of Ba^+ and Sr^+ ions decrease strongly, primarily because of the weakening covalent binding forces acting between the s electron of the ion and atomic electrons in the surface layer of the adsorbent. For instance, $E^+(\text{Ba}) = 5.2$ eV from Ir(111) and $E^+(\text{Ba}) = 2.6$ eV from Ir(111)-graphene (Table 6). The large value of $E^+(\text{Ba})$ from graphene should be assigned in the first place to the large "ionic" component of the heats of desorption of alkaline-earth atoms. The Guernsey representation was used [104] to find that the covalent component of the barium heat of desorption decreases from ~ 2.7 eV for clean iridium to a few tenths of eV in the case of graphene coating.

The effect of graphene formation on Ir(111) on the migration characteristics of Cs and Ba was investigated in Ref. [105]. The method was based essentially on continuous irradiation of a ribbon emitter by a flux of atoms on one side only, with detection by surface ionization techniques of the adatoms that have migrated during their lifetime to the other side of the ribbon.

The results of the experiments are presented in Table 7 listing the temperature interval within which the quantities under consideration were measured.

	E_M , eV	Interval of T , K	D_0 , cm^2/s
Ir(111)-Cs	$0,6 \pm 0,1$	860 - 1140	0,23
Ir(111)-C-Cs	$0,5 \pm 0,1$	860 - 1300	0,23
Ir(111)-Ba	$1,0 \pm 0,1$	1980 - 2200	$2,2 \cdot 10^{-2}$
Ir(111)-C-Ba	$\sim 0,5$	950 - 1135	-

Table 7.

We readily see that graphene affects only weakly the migration characteristics of Cs (just as the heats of desorption of Cs^+ ions). The explanation lies in that Cs adatoms on both surfaces reside primarily in ionic state and are constrained mainly by polarization forces, with the influence of the graphene film being very weak. Therefore, the material of the metallic ribbons practically does not

affect the migration characteristics of Cs adatoms; indeed, in the case of Cs diffusion over a tungsten ribbon with uniform emission characteristics, $D = 0.23 \exp^{-0.57/kT} \text{ cm}^2\text{s}^{-1}$ [23] (the study was conducted by the photoemission technique).

Migration of Ba over iridium requires higher temperatures than that of Cs (Table 7). Just as the heat of desorption of Ba^+ ions, the activation energy for migration of Ba adatoms residing primarily in ionic state is higher than that for Cs, which implies the existence, besides the bonding forces of the polarization nature, of covalent forces as well. It turned out that formation of graphene lowers noticeably the temperature region where migration operates, which practically coincides with that for cesium atoms (Table 7), with E_m decreasing down to 0.4–0.5 eV.

Thus, by reducing strongly the covalent components of the binding forces coupling particles to the surface, graphene on iridium gives rise to a substantial decrease of the activation energy for surface migration of polyvalent atoms.

The above literature data on the adsorption of atoms and molecules on valence-saturated surfaces of single-crystal graphite, polycrystalline graphite, graphitized nickel, and graphene on iridium, platinum and other metals suggest a conclusion that the binding

energy of adsorbed particles with atoms of the surface layer is small, which in some cases may give rise to growth of two- or three-dimensional close-packed islands of adsorbate on such surfaces even for submonolayer coverages.

Our studies reveal formation on graphene/iridium of condensed close-packed Pt, Th, Ni, Mo islands [41], tower islands built of fullerene molecules [107], and two-dimensional islands of CsCl molecules [40]. Investigation of the growth and dissolution of CsCl islands, for instance, permitted determination of the migration length $\lambda(T)$ of CsCl molecules during their lifetime on graphene

$$\lambda(T) = B \exp^{\Delta E/kT} = 10 \exp \left[\frac{0,13}{kT} \right].$$

For instance, at $T = 300$ K, $\lambda = 1500$ Å, while at $T = 1500$ K, $\lambda = 27$ Å. We succeeded in determining also the difference $E_{des} - E_{migr} = 0.25$ eV between the activation energies for desorption and migration. It may be added that CsCl molecules desorb easily from the graphene surface even at $T = 300$ K, with their lifetime being <0.01 s [40].

6. Metal-graphene thermal equilibrium

A. Specific features of carbon atom diffusion between the surface and bulk of a metal

Many studies deal with diffusion of carbon atoms in the bulk of solids; see, for instance, Refs. [108-110]. At the same time, literature practically does not contain any reports on such an essential subject as diffusion of atoms between the surface and the bulk of a metal.

Exchange of atoms between the surface and the bulk of a solid is an important aspect of all physico-chemical problems associated with processes occurring on the surface, when the channels involved in dissolution and segregation of atoms operate efficiently. Mass transport of atoms between the surface and the bulk of the metal defines the activation energies for dissolution, E_{S1} , and segregation, E_{1S} ; the latter may differ slightly from E_0 , the activation energy for volume diffusion (Fig. 33). Consider the relevant relations for the fluxes of dissolution, ν_{S1} , and segregation, ν_{1S} , presented in Refs. [27]

$$\nu_{S1} = N_S (1 - N_1 / N_{1lim}) \cdot W_{S1} = N_S (1 - N_1 / N_{1lim}) \cdot C_{S1} \exp^{-E_{S1}/kT} \quad (1)$$

$$\nu_{1S} = N_1 (1 - N_S / N_{Sm}) \cdot W_{1S} = N_1 (1 - \theta) \cdot C_{1S} \exp^{-E_{1S}/kT}, \quad (2)$$

where N_S and N_{SM} are the concentrations of atoms on the surface, both running and in a monolayer (the physical meaning of a monolayer may differ depending on the actual Me-C system discussed); N_1 and $N_{1lim}(T)$ are the concentrations of atoms diffusing in the site plane adjoining the surface, running and at the solubility limit, W_{S1} and W_{1S} are the probabilities of dissolution and segregation, E_{S1} and E_{1S} are the corresponding activation energies, and C_{S1} and C_{1S} are the prefactors. Because desorption involves rupture of all bonds of an adparticle with the surface, and dissolution, of a part of them only, it appears reasonable to expect that $E_{des} > E_{S1}$.

Despite the fairly obvious significance, both for basic science and for the field of applications, of studying diffusion of atoms between the surface and the bulk of a metal, we are aware only of one publication [111] reporting on a quantitative investigation of dissolution of surface carbon in single-crystal W(100) with interesting results, namely, the

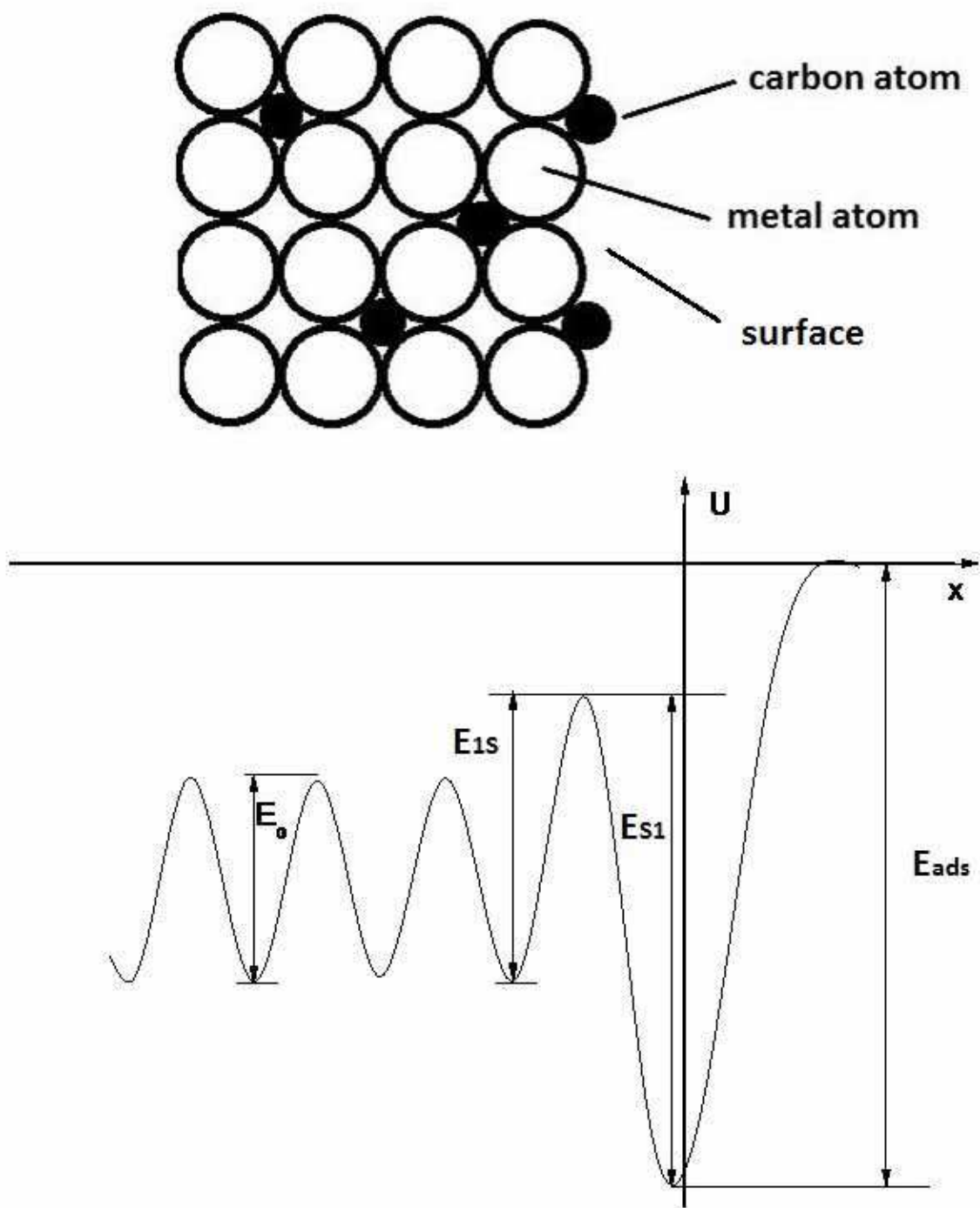


Fig. 33. A model scheme for the surface-bulk interface with diffusing atomic carbon and activation energy barriers for desorption and diffusion:
 E_{ads} - for desorption, E_{s1} - for dissolution into the bulk; E_{1s} - for segregation onto the surface, E_0 - for bulk diffusion.

activation energy for dissolution was found to be high, $E_{S1} = 5.0$ eV, which exceeds by far that of volume diffusion of carbon in tungsten $E_0 = 2.56$ eV. This implies that knowledge of the activation energy for volume diffusion E_0 is not enough by far for adequate description of the diffusion of atoms between the surface and the bulk of a metal; one would need instead the knowledge of E_{S1} and E_{1S} , which should be derived from direct experiments and found readily, besides the energy E_0 , in handbooks on the physics of metals.

The lack of literature data on such a new direction of research as transport processes at the surface/bulk of metal interface can be traced to the following circumstances. To begin with, in order to obtain quantitative data, one has to know exactly the concentration of dissolved carbon in the metal and be able to vary it in a controllable manner. We tackled this problem by employing an absolutely calibrated carbon atom flux and purifying on a qualitative scale the volume of the metal under study from all impurities, including carbon. Apart from this, the use in our experiments of thin (20--50 μm) textured metal ribbons permits one to spread carbon, rapidly and uniformly, over the volume of the metal, as well as to reach in acceptable times equilibrium between the surface carbon and carbon in the bulk of the ribbons; indeed, for a ribbon length of 40--60 mm and a carbon evaporation zone ~ 30 mm long, the effects associated with escape of carbon to cold ends of the ribbons may be neglected. Significantly, we could evaporate carbon onto either side of the ribbon, a factor which in many cases provided supportive evidence for the physical pattern of the processes under study in the Me-C system.

Consider the factors governing diffusion of carbon atoms between the surface and the bulk in the particular case of the (100)Mo-C system.

Distribution of carbon between the surface and volume in a molybdenum ribbon. We have earlier discussed in some detail the physical pattern of the processes involved in the interaction of carbon with heated molybdenum. We recall that if one evaporates carbon atoms on the heated surface of a molybdenum ribbon, say, at $T = 1400$ K, carbon dissolves rapidly in the bulk of the metal, accompanied by a buildup of carbon on the surface in the form of chemisorbed "gas". After carbon has accumulated in the ribbon volume up to a concentration $N_1 \approx 8 \cdot 10^{10}$ at/cm² in each site plane, a carbon film of chemisorbed atoms with $N_c = 1 \cdot 10^{15}$ at/cm² forms on the surface, the surface carbide MoC. One can accumulate SC MoC on the front side of the ribbon by adsorbing carbon at $T = 1400$ K on the rear side of the molybdenum ribbon to the same concentration. But this implies that at $T \geq 1400$ K carbon atoms cross rapidly the thin ribbon. Incidentally, our data fit to the information available in the literature. For instance, it was found [112] that the coefficient of volume diffusion in Mo can be written as $D(\text{cm}^2/\text{s}) = 3,4 \cdot 10^{-2} \cdot \exp\left(-\frac{1,78 \cdot 11600}{TK}\right)$. It is known that the length λ of

the diffusion front in the case of diffusion in one direction is related with the diffusion time t through the expression $\lambda = \sqrt{2Dt}$. [37]. Setting $\varepsilon = h = 20 \mu\text{m} = 2 \cdot 10^{-3}$ cm at $T = 1450$ K, we come to the time $t = 100$ s required for carbon to traverse the ribbon from one side to the other, a figure which fits well to the time experimentally observed in our experiments performed at the same temperature.

Interestingly, it is probably for the first time that one had determined for a Me-C system the carbon distribution between the volume and the surface in molybdenum; it is presented in Table 8. It lists N_{front} and N_{rear} , the carbon concentrations on the surface of the front and rear sides of the ribbon, $N_v = N_{dep} - N_{front} - N_{rear}$, the amount of carbon that dissolved from 1 cm² of the surface into the bulk of the ribbon containing $7 \cdot 10^4$ atomic planes; as well as the

carbon concentration in one site layer $N_1 = \frac{N_v}{n}$ (with the diameter of the Mo atom taken to be 3 Å). N_{dep} is the total amount of the deposited atomic carbon.

N_{dep}, cm^{-2}	$N_{front}, \text{cm}^{-2}$	N_{rear}, cm^{-2}	$N_v = N_{dep} - N_{front} - N_{rear}, \text{cm}^{-2}$	$N_1 = N_v/n, \text{cm}^{-2}$
$5 \cdot 10^{14}$	$1 \cdot 10^{14}$	$1 \cdot 10^{14}$	$4 \cdot 10^{14}$	$6 \cdot 10^9$
$1 \cdot 10^{15}$	$2,5 \cdot 10^{14}$	$2,5 \cdot 10^{14}$	$5 \cdot 10^{14}$	$7 \cdot 10^9$
$3 \cdot 10^{15}$	$7 \cdot 10^{14}$	$7 \cdot 10^{14}$	$1,6 \cdot 10^{15}$	$2,3 \cdot 10^{10}$
$4,5 \cdot 10^{15}$	$9 \cdot 10^{14}$	$9 \cdot 10^{14}$	$2,7 \cdot 10^{15}$	$4 \cdot 10^{10}$
$7,5 \cdot 10^{15}$	$1 \cdot 10^{15}$	$1 \cdot 10^{15}$	$5,5 \cdot 10^{15}$	$8 \cdot 10^{10}$
$8 \cdot 10^{16}$	$1 \cdot 10^{15}$	$1 \cdot 10^{15}$	$7,8 \cdot 10^{16}$	$1,1 \cdot 10^{12}$

Table 8

Consider now these results (Table 8) in more detail. At low concentrations of evaporated carbon, $N_{dep} \leq 5 \cdot 10^{14}$ at/cm², the major part of carbon is confined to the volume of the ribbon, and $N_{front} = N_{rear} < 1 \cdot 10^{14}$ at/cm². At higher concentrations, for instance, for $N_{dep} \leq 1 \cdot 10^{15}$ at/cm², the amount of carbon on the surface of the ribbon grows to $N_{front} = 2,5 \cdot 10^{14}$ at/cm², and that in its bulk, to $N_1 = 7 \cdot 10^9$ at/cm². At still higher concentrations, $N_{dep} = 7,5 \cdot 10^{15}$ at/cm², the carbon concentration on the surface increases to its maximum value $N_{front} = N_{rear} = 1 \cdot 10^{15}$ at/cm², with the attendant formation on the surface of the SC MoC, and carbon in the bulk present in a concentration $N_1 = 8 \cdot 10^{10}$ at/cm². Interestingly, increasing the concentration of evaporated carbon by one more order of magnitude, to $N_{dep} = 8 \cdot 10^{16}$ at/cm², does not initiate growth of surface carbon concentration; indeed, the SC MoC with $N_{front} = N_{rear} = 1 \cdot 10^{15}$ at/cm² persists, while the C concentration in the ribbon bulk grows to $N_1 \approx 1 \cdot 10^{12}$ at/cm².

Diffusion of carbon into molybdenum at surface concentrations $N_s \leq 1 \cdot 10^{15}$ at/cm². A molybdenum ribbon was cleaned thoroughly of impurities by annealing in an oxygen atmosphere ($P_{O_2} \approx 1 \cdot 10^{-5}$ Torr) at $T = 1400$ K, and subsequently, in ultrahigh vacuum at 2200 K to free it of oxygen; thereafter the only peaks left in Auger spectra were those due to molybdenum. Next, carbon was evaporated on the ribbon at 600 K up to the concentration $N_s = 1 \cdot 10^{15}$ at/cm², i.e., to the concentration corresponding to the SC MoC, at which carbon atoms occupy apparently deep hollows between the 4 surface molybdenum atoms. As demonstrated by experiments, heating of such a carbon film to $T \leq 1250$ K does not initiate dissolution of surface carbon. Noticeable dissolution of C in (100)Mo was observed to occur only at $T = 1350$ K, which took a characteristic time of ~ 1 min. This time was found not to depend on the surface concentration of carbon for $N_s < 1 \cdot 10^{15}$ at/cm². Figure 34 shows a typical curve of the kinetics of carbon dissolution in molybdenum for $N_s \approx 6 \cdot 10^{14}$ at/cm². The kinetic parameters describing dissolution of surface carbon can be found using the results published in Ref. [113]. The decrease dN of the surface carbon concentration occurring in a time dt is related with the dissolution flux v_{nl} and the average lifetime $\tau_{S1} = \tau_0 \exp^{E_{S1}/kT}$ of C adatoms with respect to dissolution in the metal through

$$dN = -v_{S1} dt = -\frac{N dt}{\tau_{S1}} . \quad (3)$$

Integration of Eq. (3) in the time t in which the surface concentration of carbon decreases from N_0 to N yields

$$N = N_0 \exp^{-t/\tau_{S1}}. \quad (4)$$

Equation (4) can be used to derive the activation energy for dissolution E_{S1} of surface carbon into the molybdenum

$$E_{S1} = kT \ln \left(\frac{t}{\tau \ln N_0 / N} \right). \quad (5)$$

Upon substitution in Eq. (5) of $\tau_0 = 10^{-13}$ s, $kT(\text{eV}) = \frac{1350 \text{ K}}{11600 \text{ K/eV}}$, and analysis of the initial

parts of the dissolution curves, we come to $E_{S1} = 3.9 \text{ eV}$.

We wish to note the large magnitude of the activation energy for dissolution of surface carbon in (100)Mo, $E_{S1} = 3.9 \text{ eV}$, which exceeds by far, by $\sim 2 \text{ eV}$, that for volume diffusion $E_0 = 1.78 \text{ eV}$ [112]. A similarly large difference between E_{S1} and E_0 was obtained [111] for W-C(100), which is apparently characteristic of such Me-C systems.

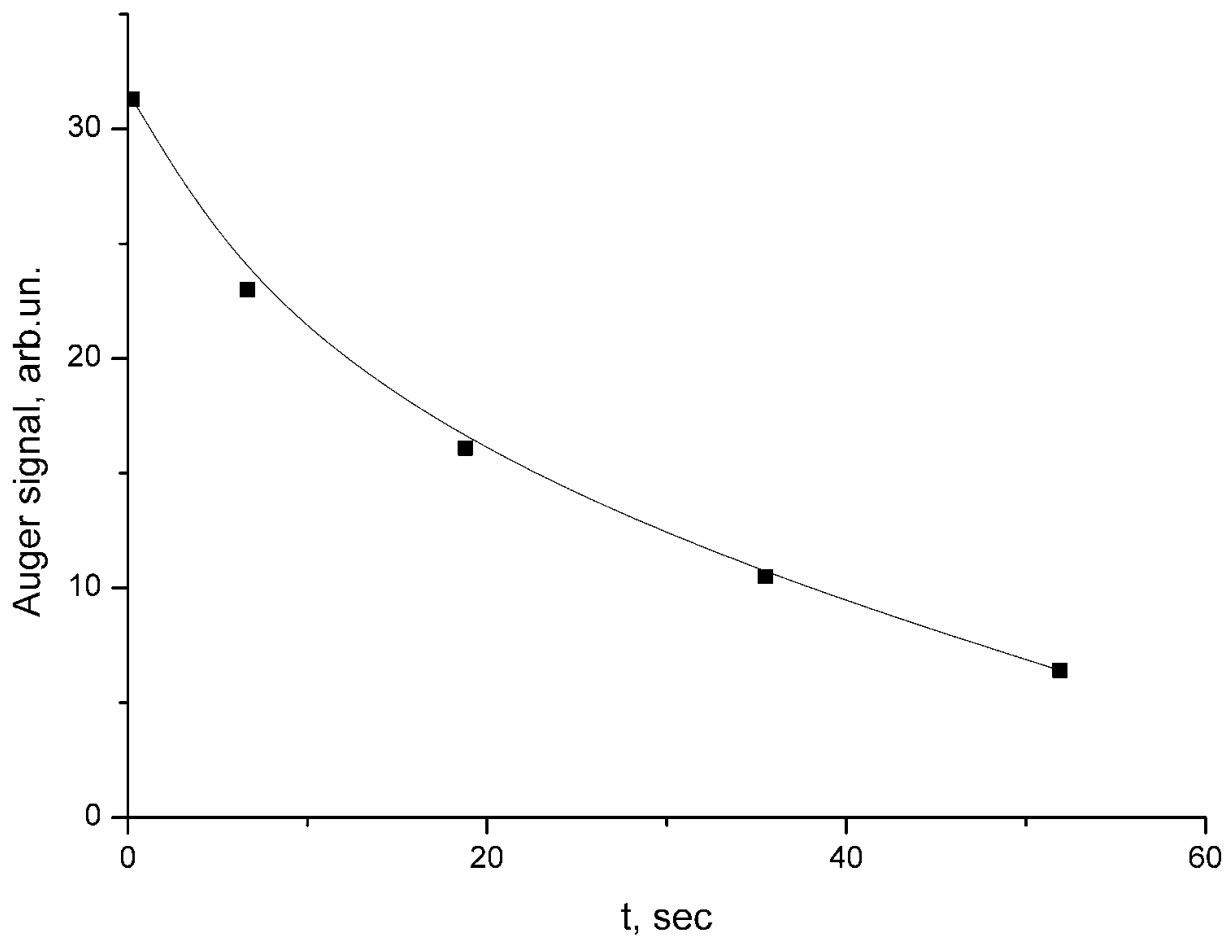


Fig. 34. Carbon Auger signal versus heating time in annealing of carbon film on pure Mo(100) at 1350 K. the film was got by atomic carbon deposition at 300 K using the flux $\nu_C = 6 \cdot 10^{14} \text{ cm}^{-2}\text{s}^{-1}$.

Diffusion into molybdenum of carbon for surface concentrations $N_c > 1 \cdot 10^{15}$ at/cm². It appeared interesting to learn how carbon would dissolve in molybdenum at concentrations higher than that in the SC, when all sites between 4 surface molybdenum atoms are occupied. The study was started by preparing at $T = 1400$ K Mo SC on both sides of the ribbon, as this was described earlier (in the volume, the concentration $N_1 = 8 \cdot 10^{10}$ at/cm²--- see Table 8). After this, carbon was evaporated in an atomic flux on SC MoC at $T = 300$ K to $N_c = 1.5 \cdot 10^{15}$ at/cm², and the ribbon thus treated was annealed at a number of temperatures (Fig. 35). It is seen that now noticeable diffusion of carbon into the bulk of molybdenum occurs at markedly lower temperatures, $T \sim 900$ -- 1000 K, with all *excess* carbon present above that bound in the MoC SC diffusing into the bulk. The dissolution temperature $T = 900$ K was used to estimate the activation energy for dissolution of carbon from centers other than those in SC (we shall refer to them as weakly bound ones). Recalling the relation of Frenkel for average particle lifetimes with respect to dissolution, $\tau = \tau_0 \exp^{E_{S1}/kT}$, accepting $\tau_0 = 10^{-13}$ s and setting for the time of the experiment $\tau \sim 10$ s (at $T = 1000$ K), we come to $E_{S1} = 2.5$ eV.

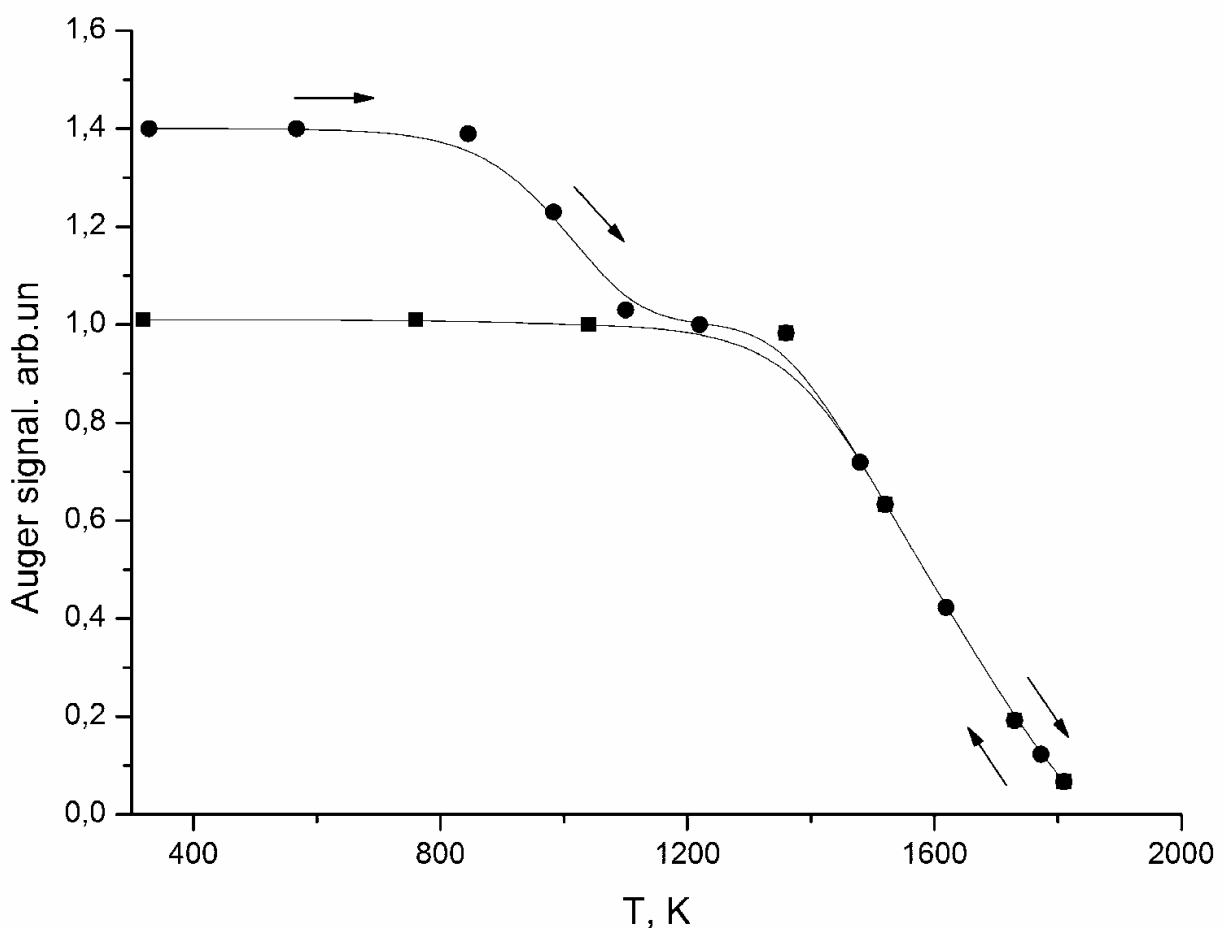


Fig. 35. Carbon Auger signal versus temperature in in annealing of carbon film with $N_c = 1.5 \cdot 10^{15}$ cm⁻², deposited onto Mo(100) with surface carbide at 300 K. Dissolved carbon presented in the substrate bulk in concentration of $N_c = \sim 2 \cdot 10^{11}$ cm⁻², at each interstitial plane.

Consider now the possible nature of these weakly bound dissolution centers. The carbon in SC occupies all deep hollows between the 4 surface Mo atoms, from which it dissolves into the bulk with a high activation energy $E_{S1} = 3.9$ eV. Because C atoms are small, so that the surface area occupied by them is small, $\sim 2 \text{ \AA}$, at a concentration of such atoms in MoC SC $N_c = 1 \cdot 10^{15}$ at/cm² they will cover a surface area of $\sim 2 \cdot 10^{15} \text{ \AA}^2$, which corresponds, for the total area of 1 cm², only 20%. Therefore, the dissolution energy $E_{S1}' = 2.5$ eV relates to adsorption of carbon atoms located closely to the weakly bound MoC SC centers, and it is from here that they apparently diffuse into the metal. We note that the observed strong dependence of the activation energy for dissolution of surface carbon into molybdenum on the nature of adsorption centers has apparently been established for the first time, and that it should be characteristic of other Me-C systems as well.

Interestingly, if one replaces all strongly bound centers on molybdenum by other atoms, e.g., by sulfur or silicon, then the carbon arriving from the outside at $T = 1000$ K will, rather than building up on the surface, dissolve completely in the bulk of the metal [43].

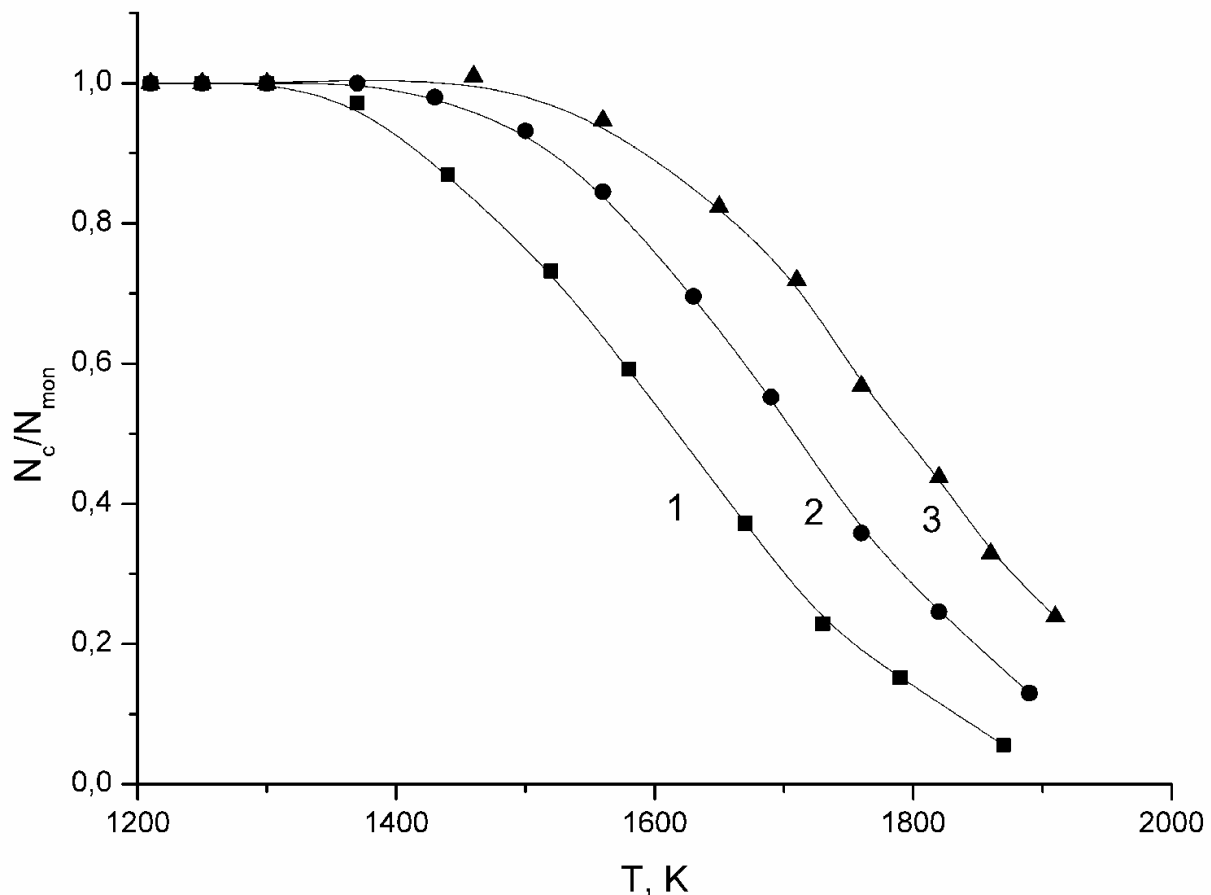


Fig. 36. Equilibrium carbon relative surface concentration (N_c / N_{mon}) versus temperature in Mo-C system. The concentration of dissolved carbon at each interstitial plane is, cm⁻²: 1 - $2 \cdot 10^{11}$; 2 - $4 \cdot 10^{11}$; 3 - $8 \cdot 10^{11}$. $N_{\text{mon}} = 1 \cdot 10^{15}$ cm⁻².

Equilibrium between the fluxes of dissolution and segregation of carbon in the Mo-C system. An intriguing pattern is observed for many Me-C systems on carbonized metal samples at moderate temperatures. Figure 36 plots the variation of the Auger signal intensity due to surface carbon (or, said otherwise, of the surface concentration) with the

temperature of the Mo-C solid solution. Each point on the curve corresponds to equilibrium between the segregation and dissolution fluxes, i.e., $v_{S1} = v_{1S}$, with the surface concentration of carbon being totally independent of the time the sample was kept at the given $T = \text{const}$. The curves obtained under increasing and decreasing temperature are reproducible with a high accuracy. An increase in the concentration of carbon dissolved in the bulk of the molybdenum ribbon brings about an increase of N_1 and, accordingly, as follows from (2), initiates growth of v_{S1} , i.e., of the segregation flux. This is accompanied by growth of the surface concentration N_n of carbon as well (see curves 1--3 in Fig. 36) obtained for $T > 1400$ K, where the carbon concentration in the bulk of the metal serves as a parameter. Crossing these curves by a straight line for $N_S = \text{const}$ and using Eqs. (1) and (2), we obtain, for instance, for curves 1 and 2 the following equilibrium of fluxes for two temperatures, T_1 and T_2 :

$$N_S \left(1 - \frac{N_1(T_1)}{N_{1\text{lim}}(T_1)} \right) \cdot C_{S1} \cdot \exp^{-E_{S1}/kT_1} = N_1(T_1)(1-\theta)C_{1S} \exp^{-E_S/kT_1}, \quad (6)$$

$$N_S \left(1 - \frac{N_1(T_2)}{N_{1\text{lim}}(T_2)} \right) \cdot C_{S1} \cdot \exp^{-E_{S1}/kT_2} = N_1(T_2)(1-\theta)C_{1S} \exp^{-E_{1S}/kT_2}. \quad (7)$$

Assuming C_{1S} and C_{S1} to be temperature independent, and accounting for the volume concentrations of carbon being far from the solubility limit $N_1(T) \ll N_{1\text{lim}}(T)$, an inference drawn from direct experiments on additional adsorption of carbon atoms, we obtain from Eqs. (6) and (7)

$$\exp^{E_{S1}(1/kT_2 - 1/kT_1)} = \frac{N_1(T_1)}{N_1(T_2)} \exp^{E_{1S}(1/kT_2 - 1/kT_1)}$$

or

$$\exp^{\Delta E(1/kT_2 - 1/kT_1)} = \frac{N_1(T_1)}{N_1(T_2)}$$

or again

$$\Delta E = \frac{\ln \frac{N_1(T_1)}{N_1(T_2)}}{1/kT_2 - 1/kT_1} \quad (8)$$

Thus, $E_{S1} - E_{1S} = 2.0$ eV. Because $E_{S1} = 3.9$ eV, $E_{1S} = 3.9 - 2.0 = 1.9$ eV, a point appearing reasonable enough and matching the magnitude of $E_0 = 1.8$ eV reported in Ref. [111]. The relative similarity of the energies $E_{1S} = 1.9$ eV and $E'_{1S} = 2.5$ eV for the surface concentration of carbon $N_S > 1 \cdot 10^{15}$ at/cm² accounts for the weak growth of the surface concentration of carbon for $T < 1400$ K considered against the large "base" of the surface carbide MoC; this is why the Auger signal intensity of carbon at $T < 1400$ K is practically constant (Fig. 36). Thus, the energies mediating transport processes in the Mo-C system could be arranged in the following way:

1. Activation energy for dissolution E_{1S} of carbon atoms in Mo(100) for surface concentrations $N_S \leq 1 \cdot 10^{15}$ at/cm²: $E_{1S} = 3.9$ eV.

2. Activation energy for dissolution E'_{1S} of carbon atoms in (100)Mo for surface concentrations $N_S > 1 \cdot 10^{15}$ at/cm², when all the strongly bound centers are already occupied: $E'_{1S} = 2.5$ eV.
3. Activation energy for carbon segregation E_{1S} from the near-surface region: $E_{1S} = 1.9$ eV,
4. Activation energy for volume diffusion E_0 of carbon in molybdenum: $E_0 = 1.8$ eV [112].

The very close values of E_{1S} and E_0 do not give us sound grounds to consider these quantities as radically different. It appears reasonable presently to accept $E_0 \approx E_{1S}$.

Dissolution of carbon in (1010)Re. Carbon atoms dissolve actively in rhenium which contains carbon neither on the surface nor in the bulk of the metal at $T \sim 1000$ K. Study of the kinetics of dissolution provided an estimate $E_{S1} \approx 2.6$ eV for low carbon surface concentrations $N_c \approx 5 \cdot 10^{14}$ at/cm². Formation of rhenium SC with $N_c \approx 1.4 \cdot 10^{15}$ at/cm², when the concentration of carbon in the bulk of rhenium is far from the solubility limit, displaces the threshold of active carbon diffusion into the bulk of the metal to $T \sim 800$ K, which matches with the estimated activation energy for dissolution for the case of $N_c > 1.4 \cdot 10^{15}$ at/cm², $E'_{S1} \approx 2.2\text{--}2.4$ eV. Literature suggests $E_0 = 2.3$ eV for volume diffusion of carbon in the unsaturated Re-C solid solution [114]. The closeness of the E_{1S} and E_0 values implies virtual independence of the equilibrium surface concentration of carbon on temperature in the Re-C system after the formation of rhenium SC ($T > 1800$ K) and accounts for the weak temperature dependence of the equilibrium carbon concentration on the rhenium surface N_c in the high temperature domain ($T > 1900$ K), when $N_c < 1.4 \cdot 10^{15}$ at/cm², which should be contrasted, for instance, with the Mo-C system, with $N_c \sim \exp^{\Delta E/kT}$, where $\Delta E = E_{S1} - E_0$.

B. Equilibrium of graphene islands in the Me-graphene system

The two-dimensional phase transition in a carbon layer on Me involving formation of graphene islands (§ 5) at moderate and high temperatures assumes dynamic equilibrium between the chemisorbed carbon "gas" and graphene islands. Incidentally, the equilibrium of the islands rests on the peripheral, edge carbon atoms of the islands.

Figure 37 displays an equilibrium curve of the dependence of the relative area of graphene islands S_0 on substrate temperature for Ir(111). The curve does not change shape with the temperature increased to $T = 1950$ K followed by its decrease; equilibrium obtains on a time scale of a few seconds to a few tens of seconds. For $T > 1950$ K, the $S_0 = f(T)$ curve becomes irreversible, because of noticeable desorption of carbon atoms from iridium setting in.

Figures 38 and 39 present similar $S_0 = f(T)$ curves for the Re(1010)-graphene and Rh(111)-graphene systems. The parameter of the curves is the amount of carbon in the bulk of the metal; for better visualization, the concentration of carbon dissolved in the bulk is given for each atomic plane of the metal (in at/cm²). The curves reflect strict equilibrium, because maintaining the sample for a long time at each $T = \text{const}$ does not result in a change of the graphene island area. Obviously enough, the lifetime of graphene islands at high T depends directly on the carbon flux from the bulk of the metal to the surface; as the concentration of dissolved carbon increases, the flux to the surface grows, with equilibrium shifting to higher temperatures (Figs. 38 and 39).

One can readily estimate that, for instance, for the Re-graphene system at $T = 1400$ K the islands would have broken up in a few hundredths of a second without adequate supply from the chemisorbed "gas" phase [115].

The equilibrium in the Me-graphene case resembles that in a vapor-liquid system (Fig. 40). There is, however, a radical difference also in that in the Me-graphene case there is the metal

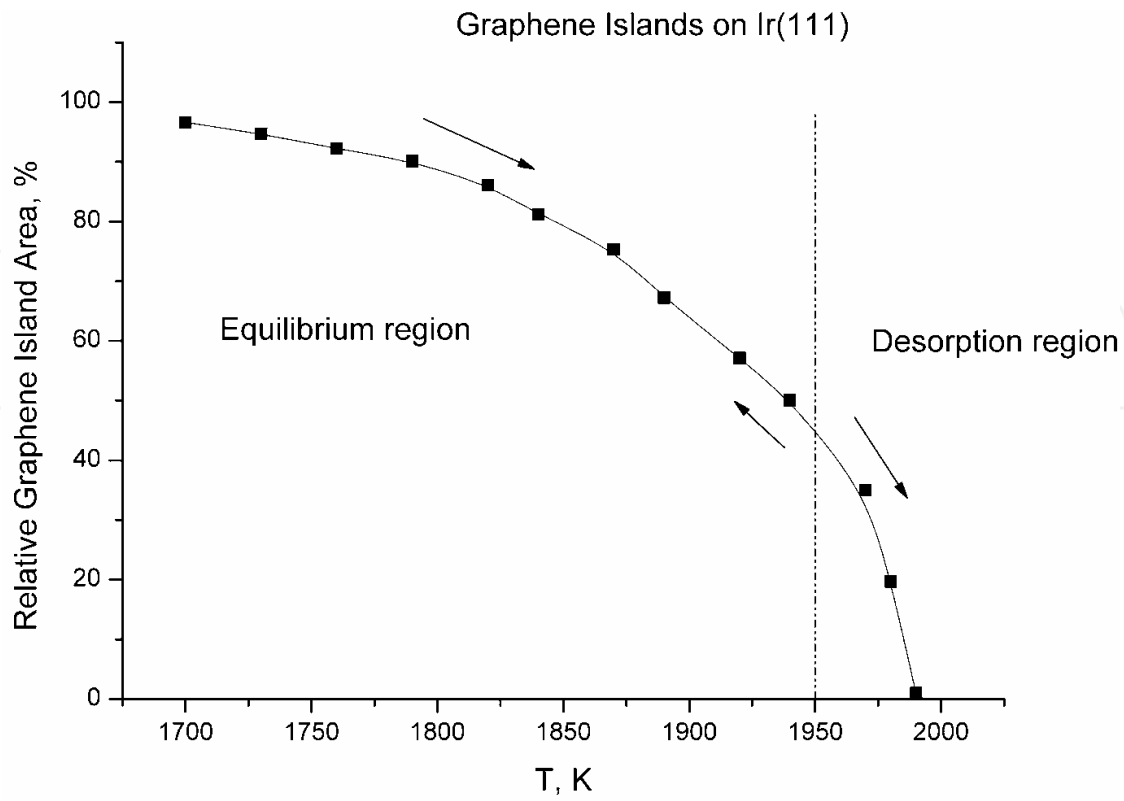


Fig. 37. Relative graphene island area versus annealing temperature for Ir(111).

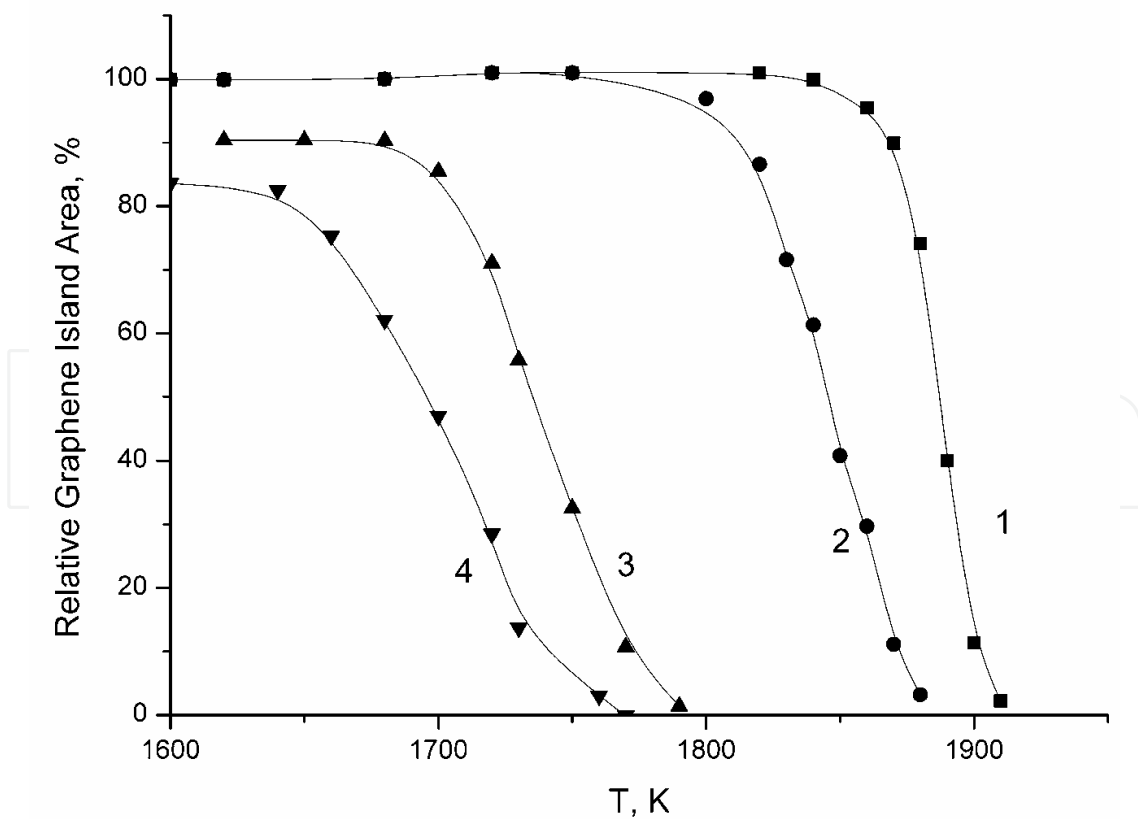


Fig. 38. Equilibrium relative graphene island area versus annealing temperature for Re (10-10). Carbonization temperature T_c , K: 1 - 1840, 2 - 1790, 3 - 1670, 4 - 1640.

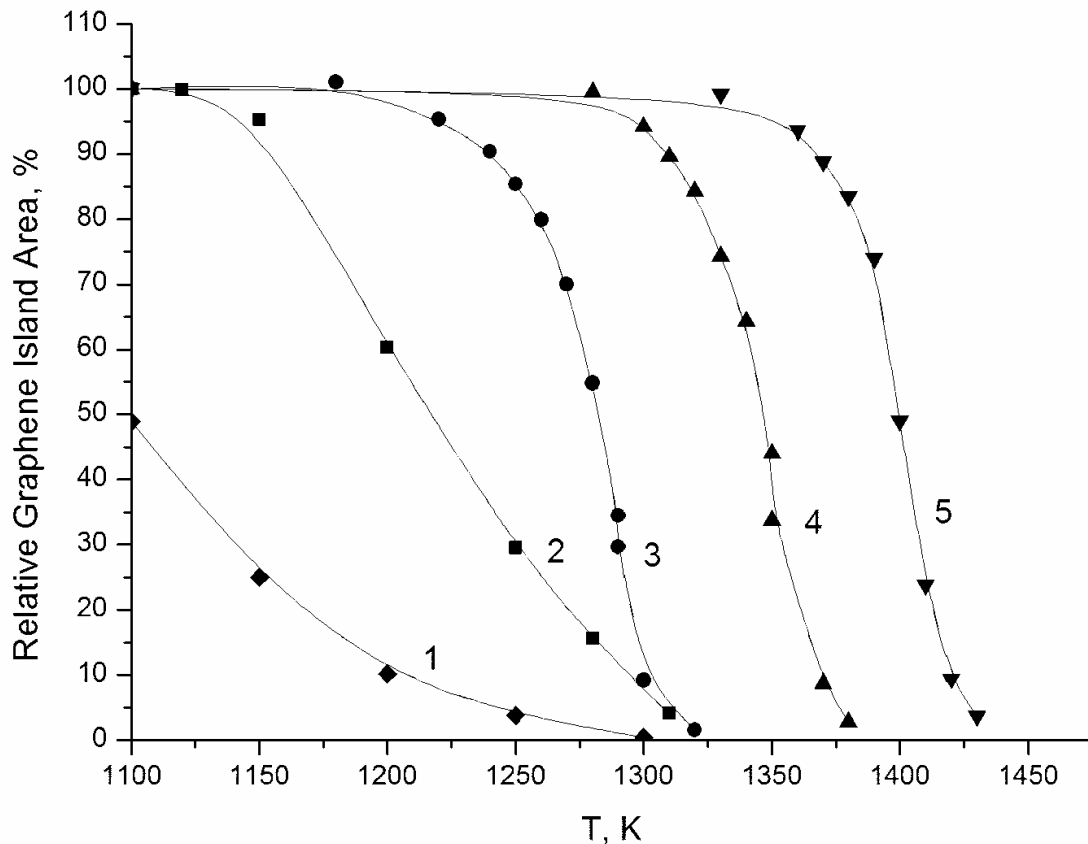


Fig. 39. Equilibrium relative graphene island area versus annealing temperature for Rh(111). The concentration of dissolved carbon at each interstitial plane is, at. %: 1 - 0.035; 2 - 0.045; 3 - 0.06; 4 - 0.075

surface separating the two phases of carbon (Fig. 40). In this case, the equilibrium is mediated by the chemisorbed carbon "gas" on the metal surface and edge carbon atoms in the graphene islands.

Consider the extent to which the concepts developed here agree with the universally accepted thermodynamic description of equilibrium systems, in particular, with the Gibbs phase rule. The rule postulates that $W=U+2-V$, where W is the number of phases, U is the number of components, and v is the number of thermodynamic degrees of freedom.

At zero pressure and a fixed component composition, the conditions corresponding to the standard experimental arrangements, when carbon neither enters the system nor leaves it, $V = 1$, because the only thermodynamic degree of freedom is here the temperature. Apart from this, one may consider the above system as a single-component one ($U = 1$); indeed, the metal itself is not involved in any chemical transformation and is not modified in the course of experiments, so that it may be considered as just an external limitation similar, say, to walls, flasks etc. With this in mind, we come to $W = 2$, i. e., one can expect that TWO volume phases can be in equilibrium here. And we have here indeed TWO such phases---carbon dissolved in the metal (metal-C solid solution) and GRAPHENE (graphite).

It appears, however, that, staying in the context of phase equilibrium, graphene should be considered not as an independent chemical form of carbon but rather as the initial stage of growth of the volume phase, which is graphite. This approach is attested by its being virtually impossible to locate the point in an experiment where growth of a graphene film

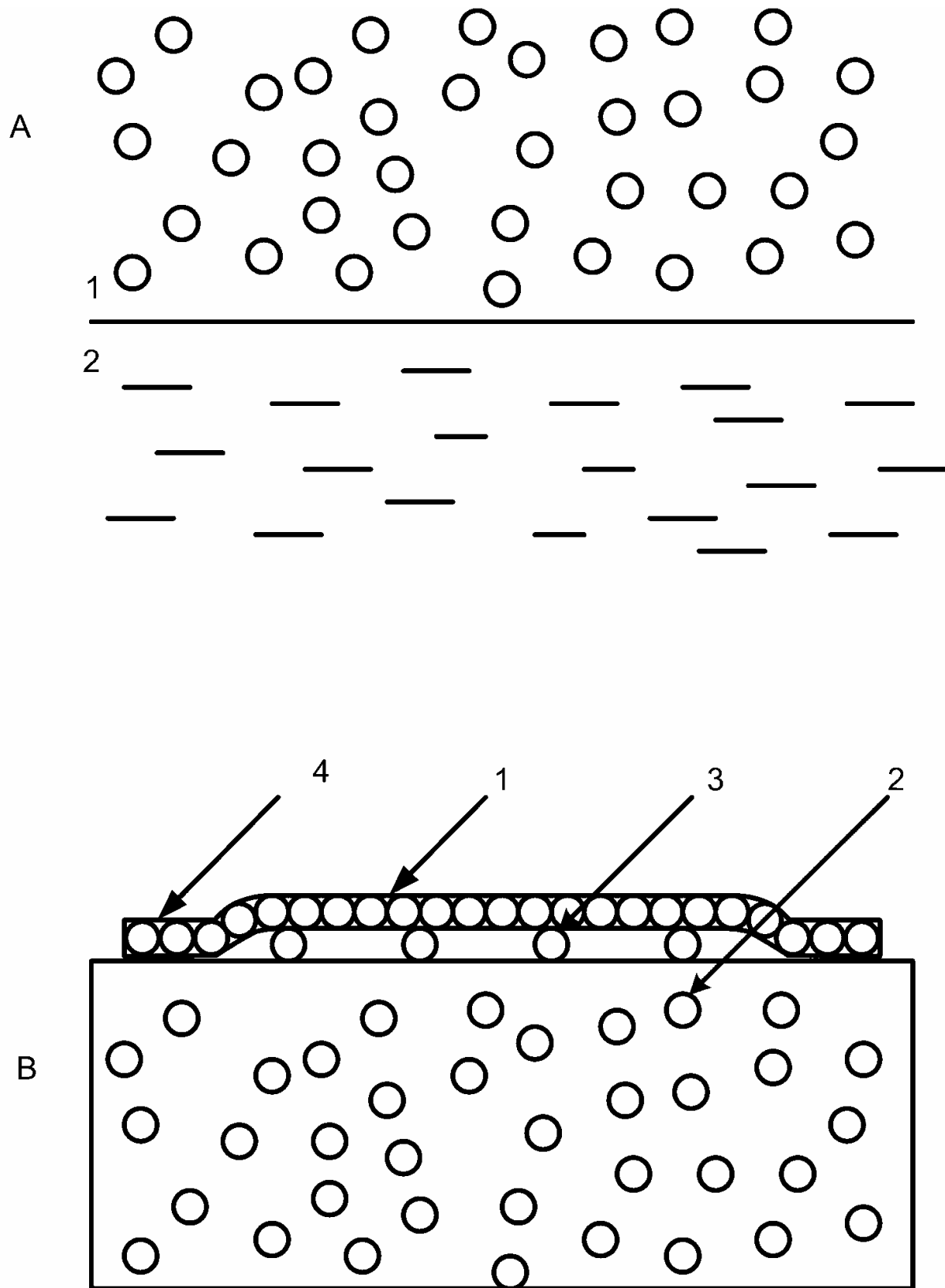


Fig. 40. A model scheme illustrating details of the phase transition for graphene - metal system: A - vapor (1) over the substrate (2); B - graphene (1); dissolved atomic carbon (2); chemisorbed atomic carbon (3); chemisorbed graphene island edges (4).

transforms to that of a multilayer graphite film. We showed [11] that the reason for it is rooted in the mechanism itself of nucleation and growth of the second and subsequent layers.

In the above consideration we have missed, however, a very important phase, namely, that of carbon atoms chemisorbed on the surface. It might seem at first glance that its existence is in contradiction with the Gibbs phase rule. This is, however, not so. Indeed, accepted in its classical form, this rule relates only to volume phases. To take due account of the part played by the surface, one has to add to the number of independent degrees of freedom also surface tension, a two-dimensional analog of pressure. With this correction included, it is THREE surface or volume phases that can be in equilibrium, a conclusion corroborated by experiment.

§ 8. Growth of graphite on a metal surface

A graphene film of a given thickness can be readily produced by segregation of carbon from a Me-C solid solution onto the surface of a metal.

1. Segregation of carbon onto the nickel surface [36]

The solubility limit of carbon in nickel is high [114]. For instance, at $T = 1170$ K, $N_{lim} = 1$ at. %, to be contrasted with rhenium, in which at the same temperature $N_{lim} < 0.01$ at. %. Figure 41 visualizes the kinetics of carbon segregation on the surface of nickel at $T = 900$ K obtained by AES; the carbonization temperature $T_c = 1100$ K. Interestingly, accepting the reference of nickel substrate screening ($E_{Ni} = 61$ eV) by a graphene (\sim a factor two), we come to the conclusion that assuming layer-by-layer film growth the time taken by each layer to form is the same (Fig. 41). This means that the flux of carbon atoms arriving from the bulk of nickel onto its surface is constant, $v_c = \text{const} = 2.4 \cdot 10^{13}$ at./cm² s. The constancy of the flux suggests both fast migration of carbon from central regions of the ribbon to its surface and a large amount of carbon accumulated in the bulk of nickel. For $T \leq 800$ K, diffusion of carbon in Ni freezes out, with no carbon segregation to the surface of nickel observed.

Figure 15 in § 1 visualizes the behavior of nickel carbonized at $T_c = 1375$ K at different T translated by AES (equilibrium curve). The initial state is a graphene layer at $T = T_c = 1375$ K. Now if we raise the temperature to $T > T_c + 15^\circ$, graphene breaks down, and the carbon left on the surface at $T \geq T_c + 40^\circ$ will be surface carbide with $N_c \approx (2 \div 3) \cdot 10^{14}$ at./cm². If we lower the ribbon temperature, it is only a graphene layer which will grow at $(T_c - 40^\circ) \leq T \leq T_c$ (Fig. 15, § 1). One can readily see in Fig. 15 a small, but well reproducible wing in the temperature region $T_c \div (T_c - 40^\circ)$ which can be identified with one graphene layer. A similar wing is observed in spectra of many metal-carbon systems: Re-C, Rh-C, Mo-C.

One may forward the following assumption as a reasonable explanation. The conditions in which the first and the subsequent graphene layers grow are essentially different. Indeed, while the first layer grows on a metal, the second layer, while it has been nucleated on the metal too, but it was under the first graphene layer (the physical processes involved in the growth of thick graphite layers are discussed at length in § 9). It appears that in order for the second layer to start growing, the concentration of surface carbon should be higher by some amount than θ_c , which is made possible by setting the temperature of the ribbon below the carbonization temperature. For $T < T_c - 40^\circ$, a thick film of graphite grows; in our case, its thickness can be readily estimated knowing the dependence of the limiting solubility of carbon on temperature and the ribbon thickness [36].

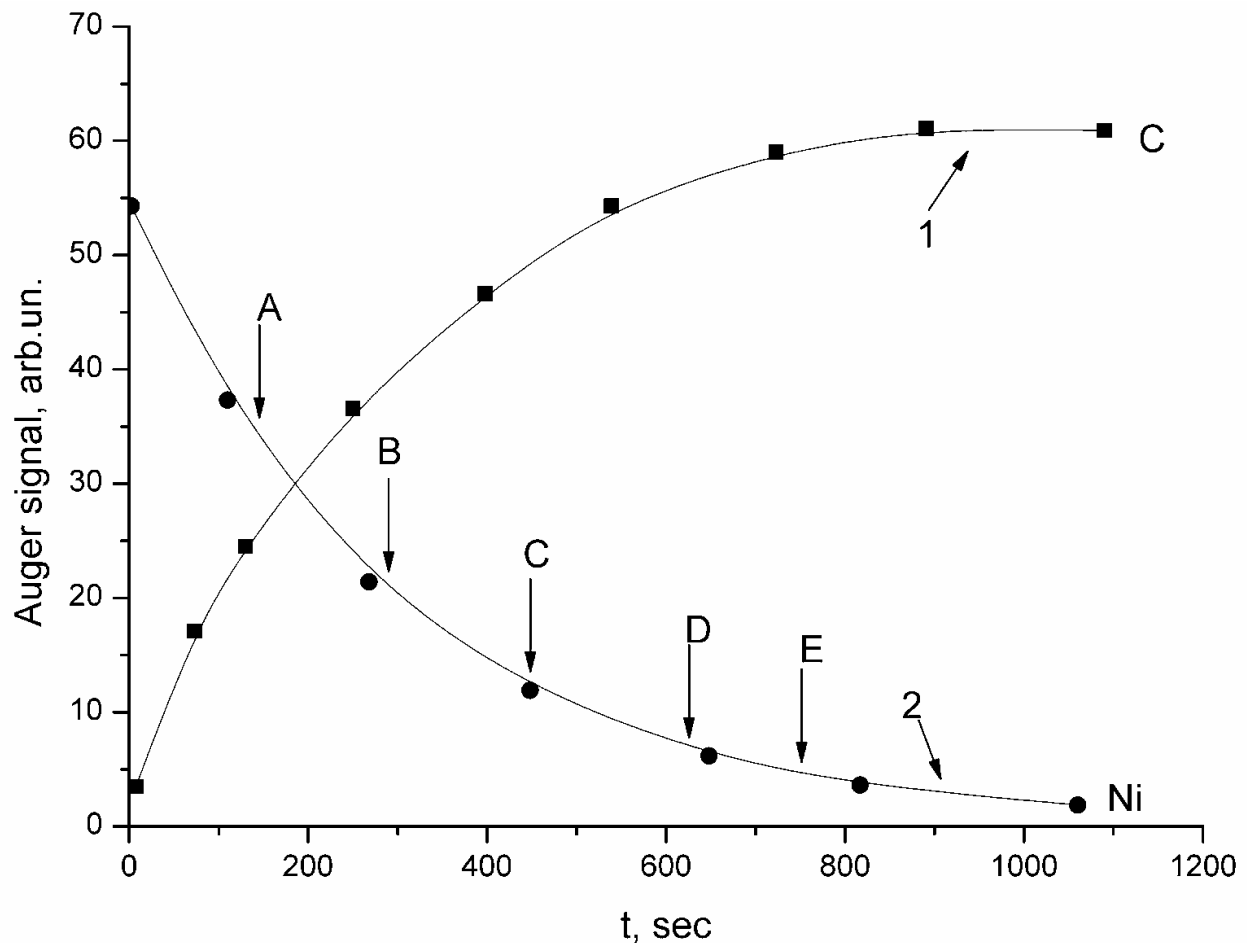


Fig. 41. Auger signals of carbon (1) and Ni (2) versus time in carbon precipitation from the Ni-C solid solution at 900 K. Carbonization temperature is 1100 K, initial carbon concentration in the substrate bulk is $N_C = 4 \cdot 10^{12} \text{ cm}^{-2}$ per each interstitial plane. A, B, C, D, E - correspond to the formation of the first, second, etc. graphene layer

2. Segregation of carbon onto the surface of rhodium, rhenium, and platinum [27,41]

If rhodium is carbonized in the region of moderate and high temperatures, $T_c = 1400\text{--}1800$ K, and thereafter the temperature is lowered, for instance, down to $T = 1100$ K, a graphite film will also grow on the surface of rhodium, with its thickness depending on T_c . Figure 6 (§ 1) plots the behavior of the intensity of the Auger signal of carbon and rhodium under decreasing temperature of a sample carbonized at $T = 1400$ K. As with the Ni-C system, one observes an equilibrium wing $\Delta T \approx 50^\circ$ wide corresponding to one graphene layer, for $T \leq T_c$ -- 50° , a thick graphite film grows rapidly and the Auger signal of rhodium melts into background noise, with the Auger spectrum of carbon acquiring the typically "graphitic" shape (spectrum 3 in Fig. 7).

A similar wing in the behavior of the carbon Auger signal intensity with temperature of a carbonized sample is observed with the Re-carbon system as well (Fig. 42). At $T < 1710$ K, intensive growth of a thick graphite film becomes evident.

For the Pt-carbon system, however, there is no wing, and the intensity of the carbon Auger signal grows monotonically with decreasing temperature (Fig. 43).

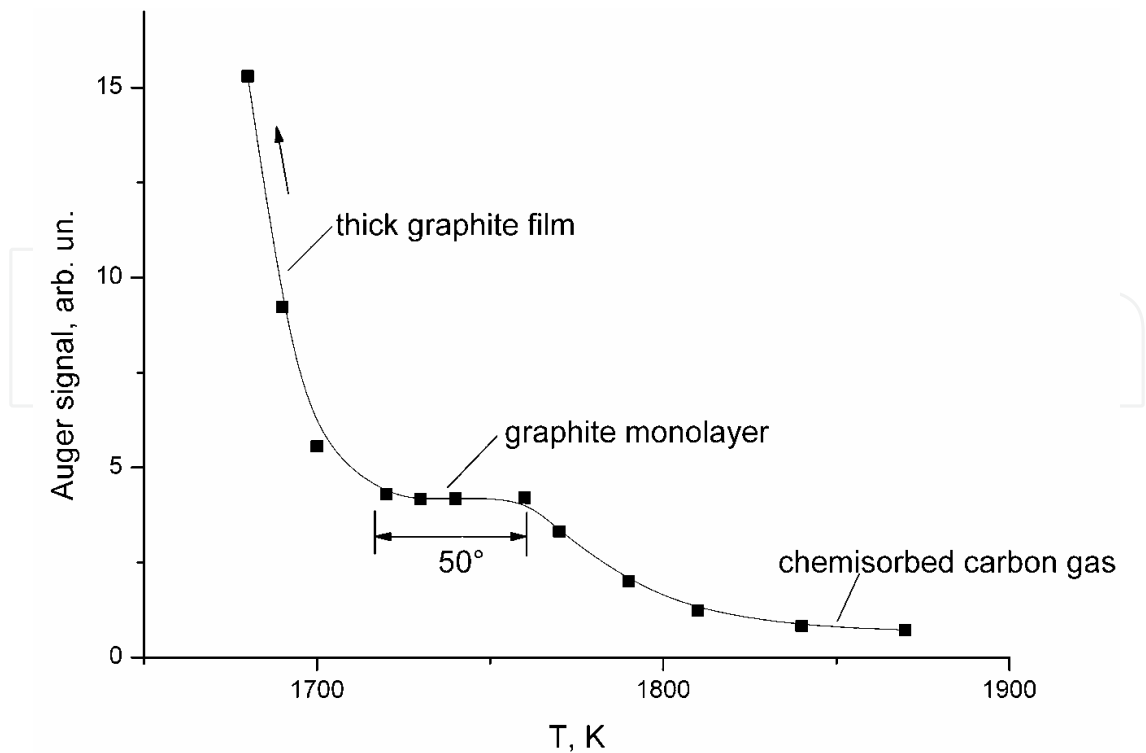


Fig. 42. Carbon Auger signal versus heating time in annealing of polylayer graphite film of about 8 layer thick. Carbonization time is 1770 K, time delay at each temperature is 5 min.

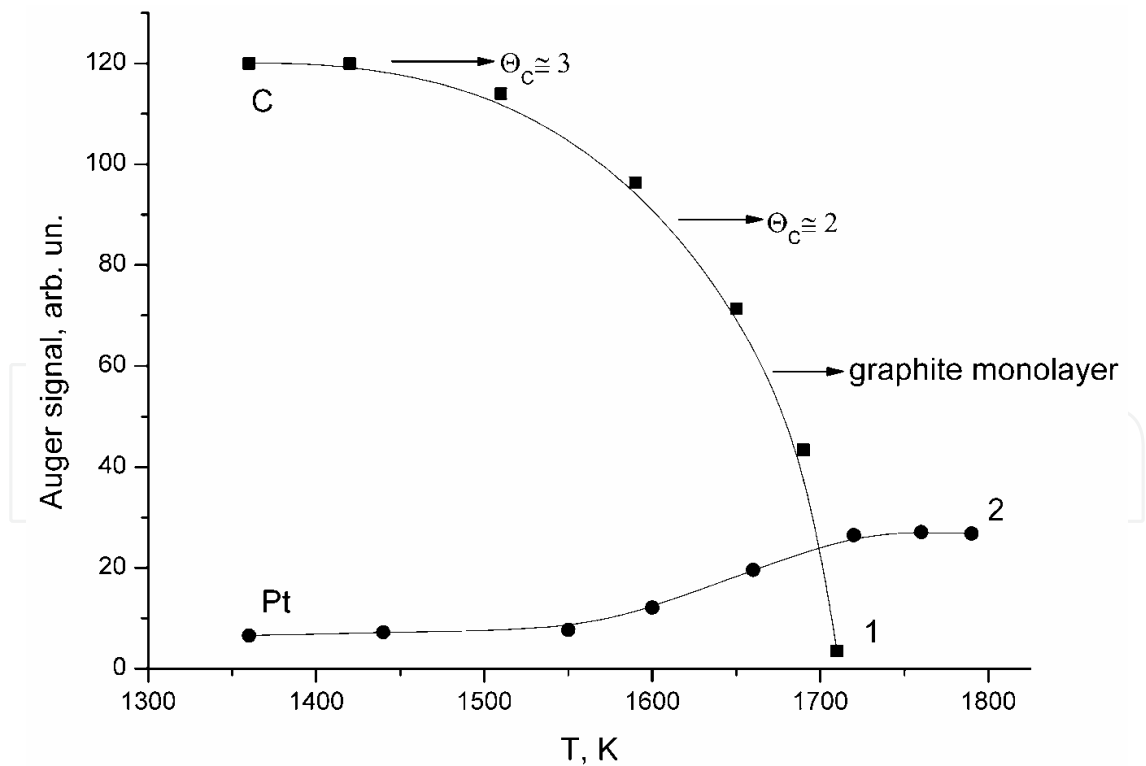


Fig. 43. Auger signals of carbon (1) and Pt (2) versus annealing temperature in carbon precipitation from the solid solution Pt-C. Carbonization temperature is 1670 K, initial carbon concentration in the substrate bulk is $N_C = 1 \cdot 10^{11} \text{ cm}^{-2}$ per each interstitial plane. $I_C = 55 \text{ a.u.}$ corresponds to the graphene layer with the surface carbon concentration $N_C \sim 3.5 \cdot 10^{15} \text{ cm}^{-2}$.

3. Carbon segregation onto the surface of molybdenum [9]

In contrast to rhenium, rhodium, and nickel, carbon segregates to molybdenum surface only after formation of the $\text{Mo}_2\text{-C}$ volume carbide has come to an end over all of the ribbon thickness (§ 1). Therefore, in this case we deal actually with a solid solution of carbon in the Mo_2C volume carbide. The kinetics of carbon segregation at $T = 1200$ K to the surface of molybdenum ($T_c = 1670$ K) obtained by AES at $T = 1200$ K is visualized in Fig. 44. The falloff of the molybdenum Auger signal intensity down to background level implies growth of a thick graphite film.

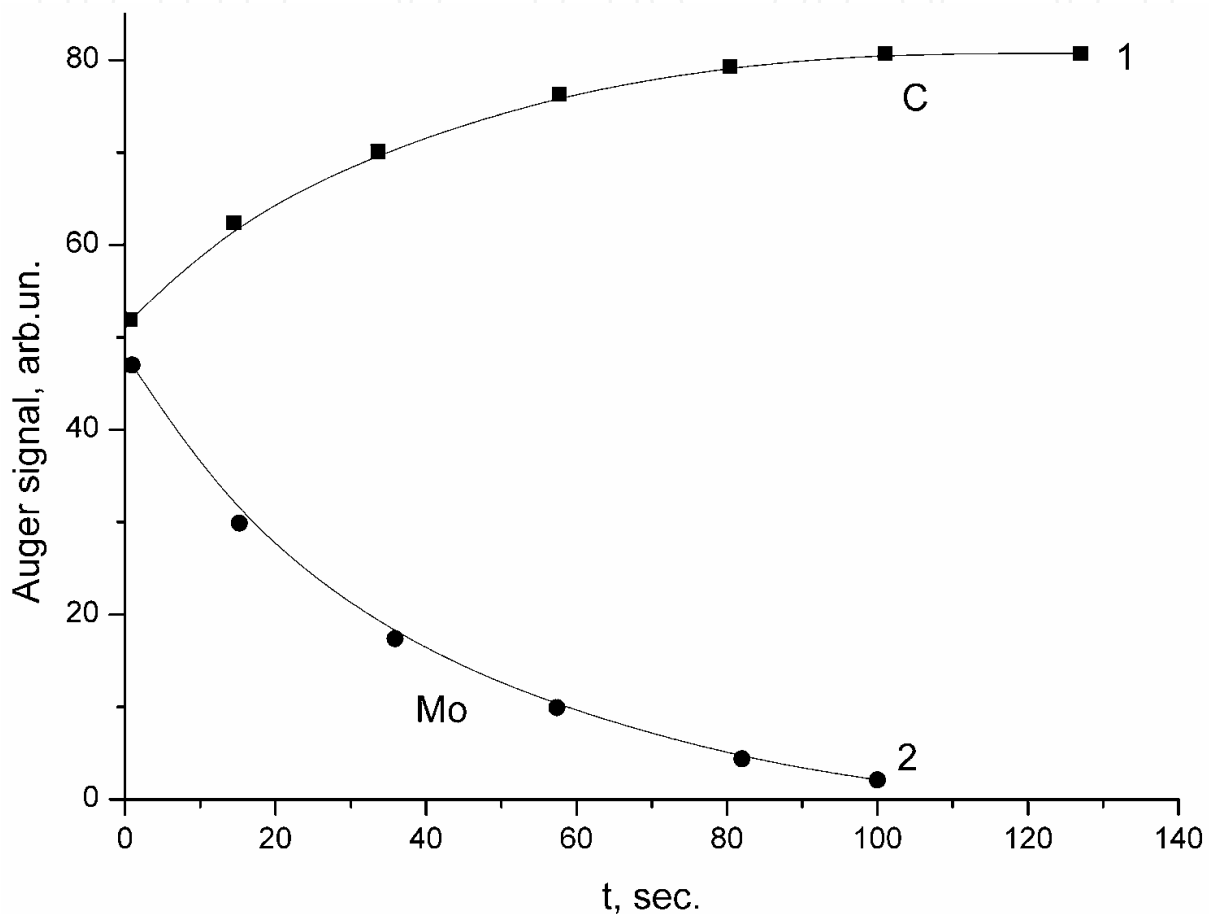


Fig. 44. Auger signals of carbon (1) and Mo (2) versus heating time in annealing of the carbonated Mo at 1200 K. Carbonization temperature is 1670 K.

4. Formation of thick graphite films on iridium [41]

As already pointed out, exposure of heated iridium samples to benzene vapor brings about formation of one graphene layer only. Experiments revealed that a thick film of carbon grows under incidence of a flux of carbon atoms. Figure 45 displays graphs relating the Auger peak intensities of carbon and iridium with the time of evaporation of carbon atoms at $T = 1600$ K. We readily see that the iridium Auger peak intensity falls by a factor of 16 for $t = 600$ s, to melt into the background for $t > 800$ s. The Auger spectrum of carbon obtained from a thick ($\theta_c \sim 4$) graphite film presented in Fig 46 (spectrum1) is completely similar in shape to that of single-crystal graphite. Close results are obtained when carbon atoms are evaporated onto iridium in the 1100--1900-K region.

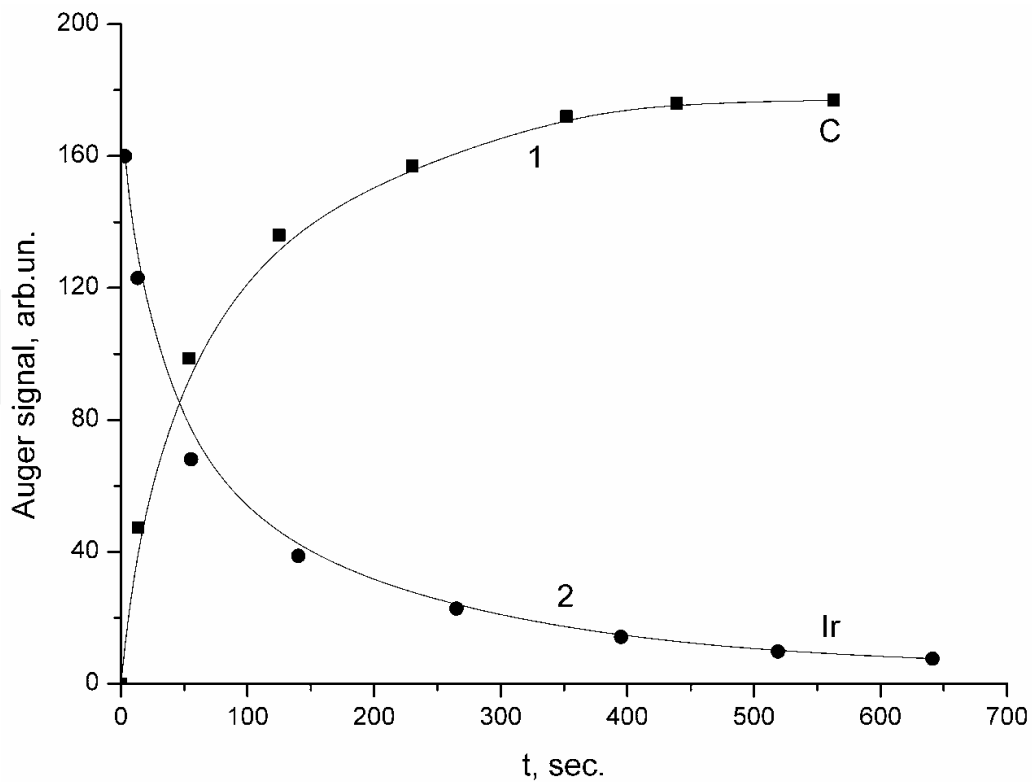


Fig. 45. Auger signals of carbon (1) and Ir (2) versus deposition time in atomic carbon deposition on Ir(111) at 1600 K. The deposition flux is $v_C = 7 \cdot 10^{13} \text{ cm}^{-2}\text{s}^{-1}$, $I_C = 85 \text{ a.u.}$ corresponds to the graphene layer.

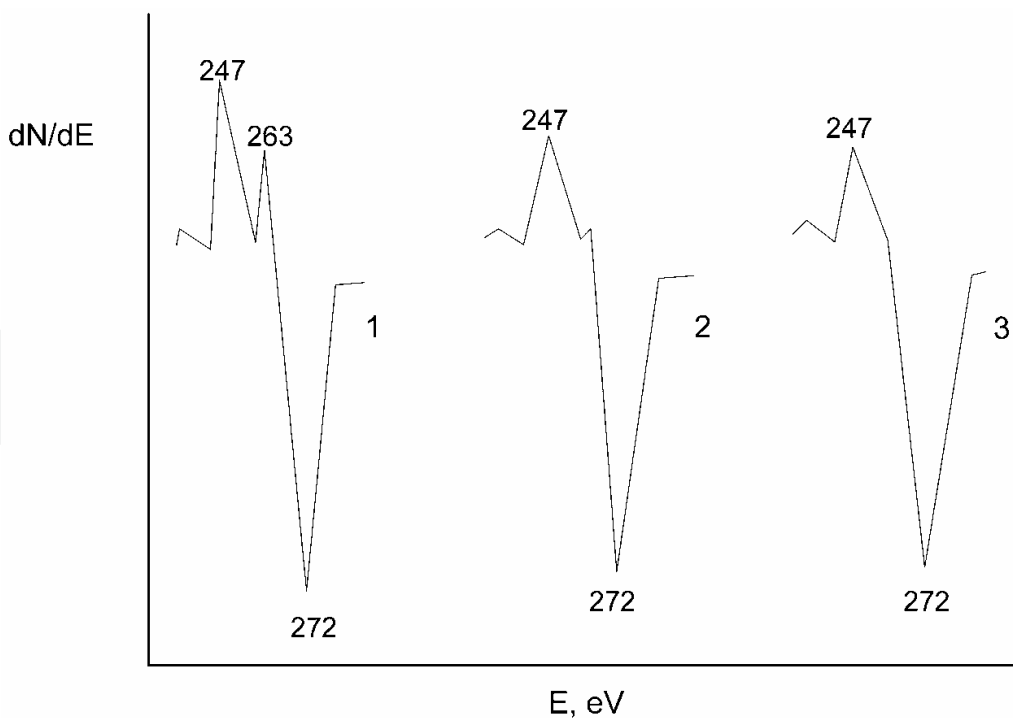


Fig. 46. Carbon KVV Auger spectra for carbon films of about 4 layer thick, deposited onto Ir(111) at the various temperatures, K: 1- 1800, 2 - 900, 3 - 300. the spectra are identical for the range 1100 - 1800 K.

Evaporation of carbon on graphene-coated Ir(111) at $T < 1000$ K initiates growth of a disordered carbon film atop the graphene, with the carbon Auger spectrum acquiring the typical shape of pyrographite (spectra 2 and 3 in Fig. 46).

When carbon is evaporated at $T \geq 1100$ K, its atoms migrate actively under the graphene film to form the second layer of graphene on the surface of iridium. In this case, the growth rate of graphene layers at $v_c = \text{const}$ falls off with increasing thickness of the graphene film, because the probability for a carbon atom to be desorbed from the surface of the graphite film increases progressively compared with that to migrate under the film down to the metal.

For $T \leq 1000$ K, the rate of growth of a carbon layer is constant for $v_c = \text{const}$.

§9. Mechanism of growth of a thick graphite film on the surface of supersaturated solid solution of carbon in a metal

The graphene film “raised over” the metal does not interfere with nucleation and growth of subsequent layers through segregation of carbon from a supersaturated Me-C solid solution.

It is common knowledge that such atoms as C, Si, B, P, S, H, N, O diffuse over the volume of the metal by migrating over the interstitial sites of the metal lattice [117]. Segregation of “non-gas” atoms from the volume onto the surface culminates most frequently by formation of a diffusant monolayer. Then why do we observe on the surface of carbon-containing metals and alloys whose volume is supersaturated with carbon formation of a thick graphite film?

Information on the structure of a carbon adlayer on metals accumulated recently provide an explanation for the anomalous behavior of carbon. We are going to use also present concepts of the first-order phase transition of the type of two-dimensional condensation in a carbon adlayer on metals, which suggests the possibility of coexistence on the surface of two carbon phases, more specifically, of chemisorbed “gas” and two-dimensional graphene islands. In the initial stage of film growth on a heated metal, as long as the critical coverage θ_c has not been reached, carbon resides on the surface in the form of chemisorbed “gas” (A in Fig. 47a). For $\theta > \theta_c$, close-packed carbon islands form and attain equilibrium with the chemisorbed carbon “gas” (B in Fig. 47a). A small enough carbon island may not have yet graphitic structure and rests chemisorbed on the surface. On reaching a certain critical size, the island acquires graphitic structure and becomes coupled to the metal by van der Waals forces (C in Fig. 47a). Therefore, the adlayer under the graphite islands becomes filled by chemisorbed carbon “gas” through diffusion of carbon from the bulk of the metal until second-layer islands start to grow on having reached a certain coverage (D in Fig. 47a). The central part of such an island rises from the metal surface up to the equilibrium height defined by van der Waals forces. A first-layer graphene island may interfere with this process, and the second-layer island will try to force it out of the way (E in Fig. 47b). As a result, the first-layer graphene island will be acted upon by two forces, namely, that of expulsion $F_{ex} \sim R^2$ (R is the island radius) and the other, from attraction from the side of the metal $F_{att} \sim R$, which acts along the island periphery. As the area of the second-layer island grows, the expulsive force may become larger than the attractive one, which will culminate in the first-layer graphene island tearing away from the metal surface (F in Fig. 47). Thus, this mechanism operating on the metal surface may give rise to growth of a thick graphite film through segregation of carbon out from the bulk of the metal.

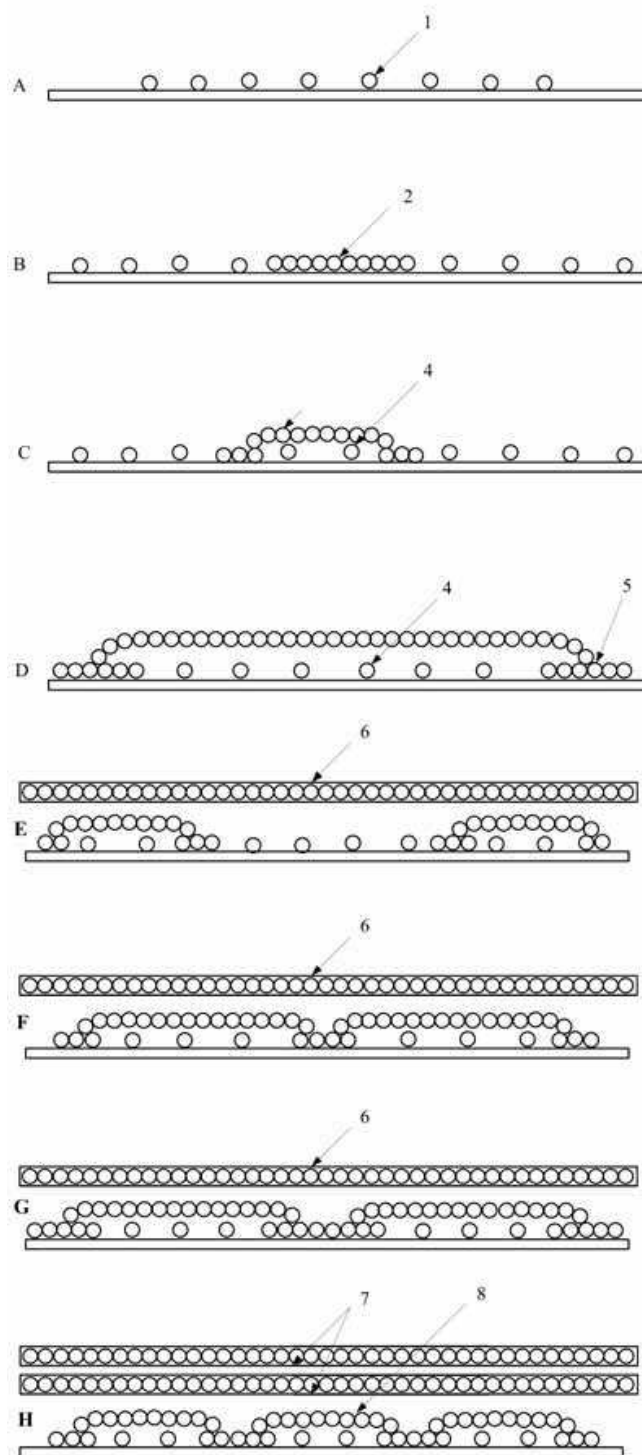


Fig. 47. A model scheme showing sequential growth of a polylayer graphite film on a metal by carbon precipitation from the substrate bulk: 1 - chemisorbed 2D carbon 'gas'; 2 - nucleation of a carbon island; 3 - graphene island; 4 - carbon 2D 'gas' under the graphene island; 5 - non-graphitic edge of the island; 6 - finalization of the first layer growth and nucleation of the second layer; 7 - finalization of the two graphene layers and nucleation of the third layer; 8 - graphene islands of the third layer.

This mechanism is supported by the observation of the edges of first-layer graphene islands detaching from the surface during carbon segregation from a supersaturated Re-C solid solution. In this experiment, rhenium was carbonized in benzene vapor at $T_c = 1800$ K up to formation of graphene on its surface, after which it was cooled rapidly down to 300 K, Cesium atoms were adsorbed to saturation on the graphene film at 300 K, with the cesium becoming distributed equally between the α -phase (atop graphene) and γ -phase (cesium buried under the graphene film), with $N_\alpha = N_\gamma \approx 5 \cdot 10^{14}$ at/cm² (see below). After this, the rhenium ribbon was heated rapidly to $T = T_c = 1800$ K. It was found that all of the cesium desorbed from the α phase, leaving cesium buried in the γ phase under the graphene layer with a concentration $N_\gamma \approx 8 \cdot 10^{13}$ at/cm². This cesium could be removed in one of two ways. In the first way, the ribbon temperature was raised to $T = 2200$ K, where the graphene film broke down completely. Incidentally, if one intercalates a thick graphene film on a metal at 300 K with Cs atoms and raises thereafter the temperature to $T \sim 1000$ K, all of the intercalated cesium will end up desorbed, as this was observed with single-crystal graphite [62]; in this case, the graphene layer edges will not close onto the surface. Cesium will remain buried under the graphene islands only in the lowest layer contacting the metal. In the second approach, cesium could be removed completely from the surface by lowering T below T_c ! In this case, at $T < T_c$, the Re-C solid solution supersaturates, thus initiating carbon segregation to the surface, which brings about detachment of the edges of first-layer graphene islands, with the attendant escape of cesium atoms from under the graphene traps and desorption from the surface (Fig. 48). The desorption of cesium was followed by measuring the Cs⁺ ion current, a highly sensitive method, because each cesium atom desorbed in the form of the Cs⁺ ion as a result of surface ionization [39]. Figure 48 displays in graphical form the dependence of the Cs ion current on time after the lowering of T from $T_c = 1800$ K to $T = 1570$ K. This procedure removes all of cesium from the γ phase, and the variation of the Auger peak intensities of carbon and rhenium visualized growth of the graphite film thickness.

The proposed mechanism of growth of a thick graphite film on the surface of a metal rests on a number of conditions. First, carbon islands growing in the adlayer should have graphitic structure, because only graphite is a valence-saturated state of carbon, in contrast, for instance, to chemisorbed atoms and clusters or carbides. Second, for a thick graphite film to grow, the edges of first-layer graphene islands should be able to break off the surface of the metal. If the island edges detach at $\theta_c < 1$, a multilayer graphite "tower" will grow over each graphene island, with the result that the graphite film will not be continuous in the initial stages of its growth. Incidentally, in Me-C systems two types of carbon segregation on the surface were observed. In segregation of the first type, the dependence of the carbon Auger signal on substrate temperature T has three characteristic regions (Fig. 49A). In region "A", the Me-C solid solution is not saturated, with chemisorbed carbon "gas" present on the surface. In region "B" ($T < T_c$), extending over ~ 40 -- 70° , the surface is coated by a graphene layer (see, e.g., Fig. 49A). In this region, the solid solution becomes supersaturated with decreasing temperature, and the graphite film will not grow above one monolayer thickness. It appears reasonable to assign the absence of growth of a graphite film above monolayer thickness to the observation that in order for the second-layer graphene islands to nucleate, the coverage θ_c should exceed a critical level which is larger than that required for the first layer to form. Therefore with T decreasing still more, supersaturation grows to an extent where the required coverage θ_c is reached, at which the second-layer islands grow, $F_a > F_b$, and the edge of a first-layer graphene island detaches from the surface. Therefore, in region "C" in Fig. 49A a multilayer graphite film grows layer by layer.

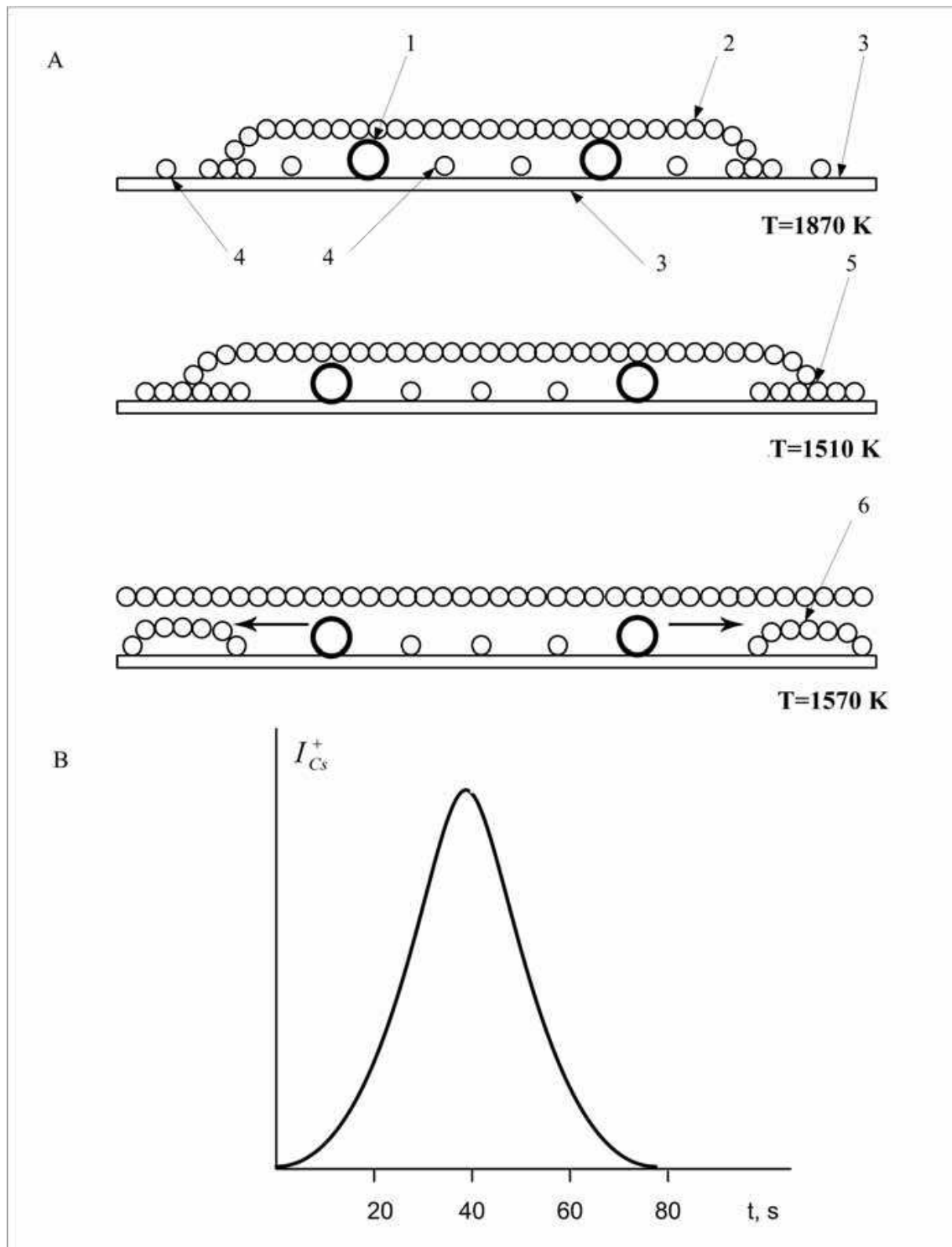


Fig. 48. Desorption of Cs⁺ ions in their release from the graphite island at temperature decrease from 1870 K to 1570 K. A - thermal desorption spectrum. B - A model scheme showing oversaturation of the solid solution Me-C, carbon precipitation onto the surface and Cs⁺ release. 1 - Cs atom under a layer of graphene - the output of cesium from the islands is difficult; 2 - graphene island; 3 - rhenium substrate; 4 - carbon atoms in the phase of two-dimensional "gas"; 5 - carbon atoms at the edges of graphene islands; 6 - graphene islands of the second layer - the output of cesium greatly facilitated.

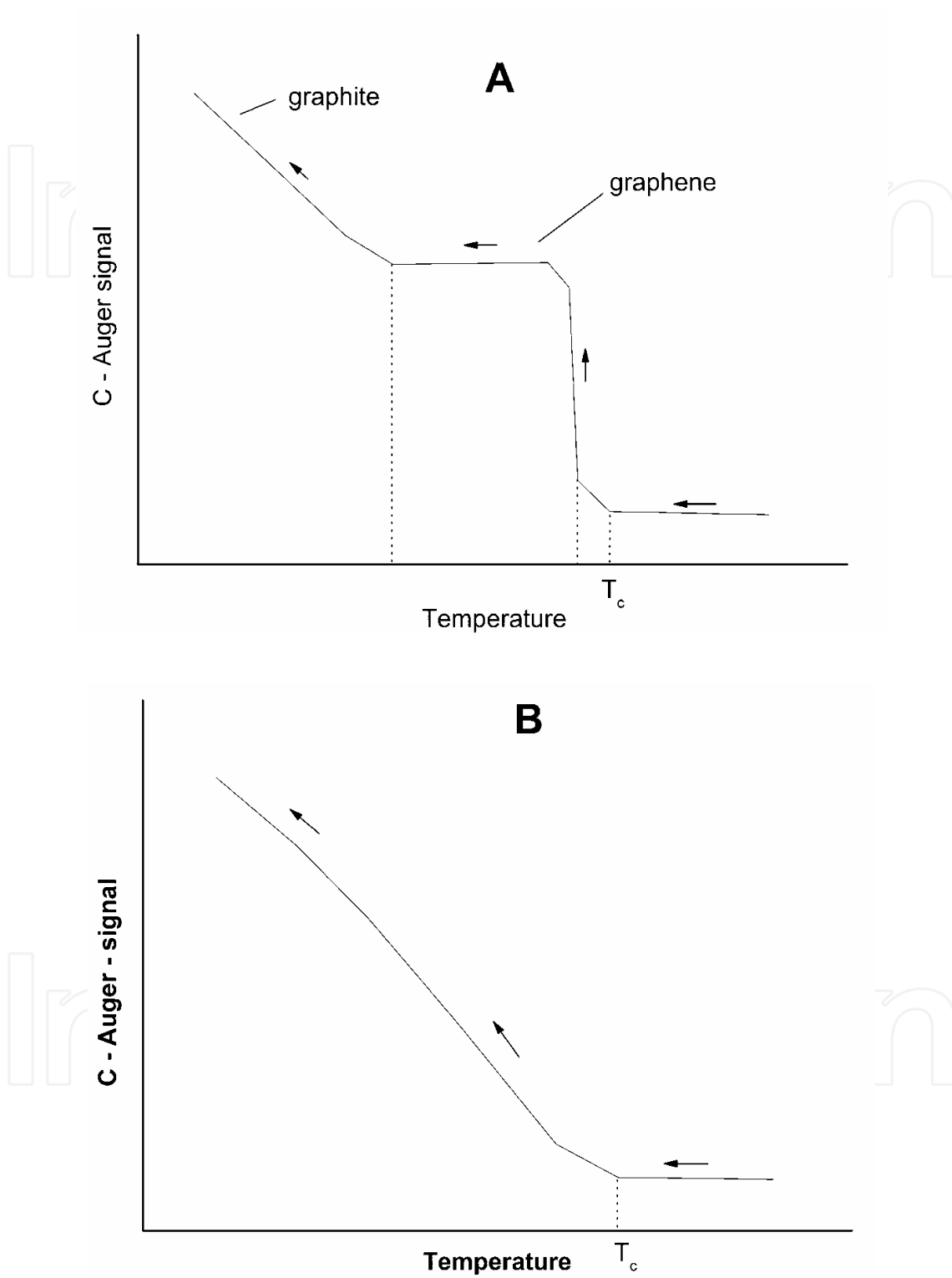


Fig. 49. A model carbon Auger signal versus temperature and film structure for two possible variants of carbon precipitation from the substrate bulk onto the surface: A - the first type; B - the second type.

Carbon segregation of the first type from supersaturated Me-C solid solutions was observed on Ni(111) [118], Pd(100) [7], Pd(111) [7], polycrystalline Pd [16], Co(0001) [7], Mo(100) [8], Re(1010) [11], polycrystalline Re [119], and Rh [27].

The dependence of the carbon Auger signal intensity on T in segregation of the second type is displayed graphically in Fig. 49B. The carbon signal continues to grow as T decreases, because in these conditions multilayer graphite towers surrounded by chemisorbed carbon "gas" grow on the metal surface. Film growth does not pass here through the stage of formation of a graphene film. This growth may be expected if the $F_a > F_b$ condition is reached before the formation of the graphene film came to an end. Segregation of the second type was observed to take place on Pt(100) [7], Fe(100) [120], and Pt(111) [2].

§10. Three-dimensional phase transition in the Me-graphite system

This transition gives rise to growth of
the volume graphite phase, i.e., polylayer graphite films.

The two-dimensional phase transition in a carbon layer on a metal was studied in considerable detail for the Ir(111)-C system (§5). It appeared reasonable to expect that under certain conditions a three-dimensional phase transition would occur, in which volume graphite phase of carbon would form. As pointed out in §8, many Me-C systems exhibit a stable temperature interval $\Delta T \approx 40\text{--}70^\circ$ within which a continuous graphene film can exist (Figs. 6 and 15 in §1). Further cooling of the carbonized metal initiates intense growth of graphite films. For illustration, consider the physical processes occurring in the Rh(111)-C system as visualized by studying thermionic emission. Rhodium was carbonized at $T_c = 1720$ K, after which the temperature was increased to $T = 1820$ K, and lowered subsequently in small temperature steps. Figure 50 plots variation of the thermionic current in $\log I$ -vs. ribbon heating current coordinates, with the top scale referring to the sample temperature. Now what do we see? In region AB, the low-density chemisorbed carbon "gas" covering the surface practically does not change the surface work function $e\phi = 4.95$ eV, and the current I falls off in accordance with Eq. (1) of §5. Point B identifies the two-dimensional phase transition, graphene islands form and thermionic emission rises, because for graphene islands $e\phi = 4.35$ eV.

In region BC, islands grow in area and coalesce to form a continuous graphene layer (C in Fig. 50). In region BC, equilibrium obtains among the graphene islands (§7, item 6).

In region DC, the graphene layer is stable, with AES producing a wing (Figs. 6 and 15 in §1).

An intriguing and important feature is awaiting us at point D: lowering the temperature by 3-5° brings about a drop of the thermionic current by nearly four orders of magnitude! Auger electron spectroscopy reveals a thick graphite film to have grown on the surface, which suppresses the strong rhodium Auger signal. In region DE, the brightness temperature of the sample decreases by $\Delta T \sim 300^\circ$ too (sic!); this effect is seen by naked eye. A sharp decrease of the brightness temperature was observed for the Rh-C and Re-C systems earlier [121,122] and attributed to formation of a thick graphite film, which reduces markedly the spectral coefficient of emissivity from $\varepsilon_\lambda = 0.24$ characteristic of clean rhodium to $\varepsilon_\lambda \approx 0.8$ for graphite [123]. Now the true ribbon temperature decreases strongly too, which initiates a drop in thermionic emission by several orders of magnitude. Therefore the ribbon temperature for region EF in Fig. 50 is not specified. Nevertheless, if we repeat a pyrometric measurement of ribbon temperature in region EF with due account of $\varepsilon_\lambda = 0.8$ and construct a Richardson graph, the graphite work function can be found, which turned out to be 4.65 eV (§7).

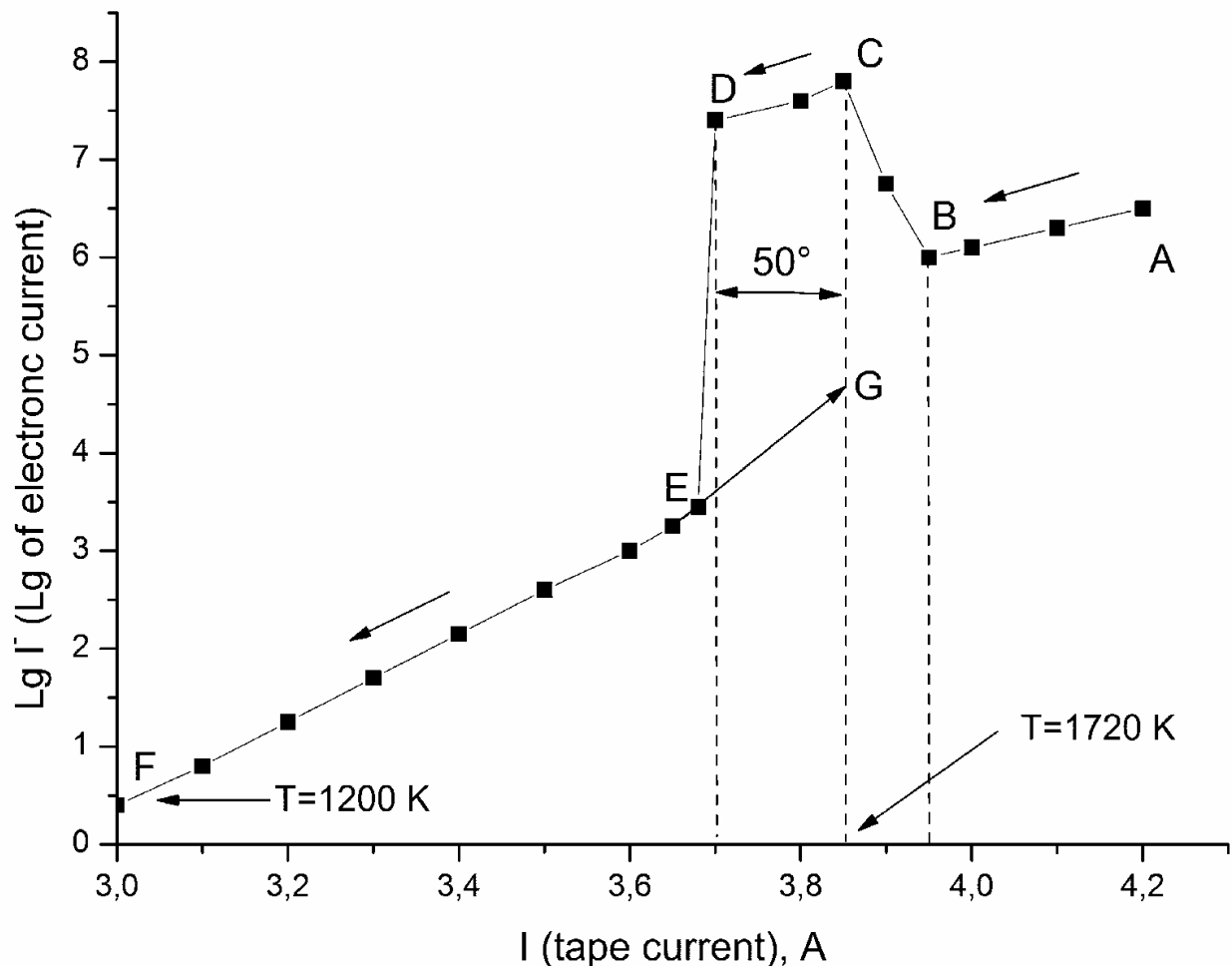


Fig. 50. Thermionic current from the surface of carbonated Rh ($T_C = 1720 \text{ K}$) in decreasing of the current heating the ribbon.

Reverse heating ($F \rightarrow E$) reveals a noticeable hysteresis, with the curve choosing region EG, because the true temperature at point E is lower now by a few hundred degrees than the former value of $T = 1680 \text{ K}$, and additional heating is required to destroy the graphite film.

Knowing the solubility limit of carbon in rhodium and varying properly the carbonization temperature T_c (§1), one can readily calculate the number of "excess" carbon atoms freed by the decrease of temperature ($T < T_c$) and determine the effect of the thickness of a graphite layer on variation of the brightness temperature. Experiments showed that for thicknesses below 10 layers the sample temperature does not change. For thicknesses above 40--50 layers, the emissive optics of the system is governed by the graphite film.

§11. Graphitization of carbon films on a metal surface

Temperature is a major factor
mediating graphitization

Significantly, adsorption of carbon on a metal at low T either does not initiate formation of graphene films or such films turn out to be heavily defective. This should apparently be attributed to the large number of carbon clusters in the layer and the islands being too small and not graphitic yet. Consider an illustrative example of graphitization of carbon films

adsorbed at a low temperature on Ir(111) [114]. Obviously enough, these conditions depend strongly on carbon layer thickness.

Recall, necessarily briefly, the methods used to detect the presence of graphene on the surface of a metal.

1. Through catalytic dissociation of CsCl molecules. This method, proposed by A. Ya. Tontegode [27], consists in probing the surface with a flux of CsCl molecules. One of the products of dissociation of these molecules are cesium atoms. On the surface of refractory metals, graphite, and other carbon films the relation $V_{Cs} < \varphi$ holds, and, therefore, each cesium atom desorbs from a heated surface in the form of the Cs^+ ion, which facilitates markedly detection of one of the products of dissociation and makes the method highly sensitive.

As shown earlier, it is only carbon present in the form of graphite that reduces markedly the efficiency of dissociation of CsCl molecules. Therefore, the degree of dissociation $\omega = I^+/I_0^+$ can be found by measuring the total cesium current from a clean iridium surface, $I_0^+ = evS$, and the current $I^+ = evS\omega$ from the surface of iridium coated by a carbon film (v is the CsCl flux density). On clean metals, a chemisorbed carbon film, carbon clusters, and surface carbide $\omega \sim 1$. By contrast, on the graphene phase of carbon $\omega = 10^{-3}$ – 10^{-5} , thus making it possible not only to detect the presence itself of graphite on the surface but to determine the relative area occupied by this phase. The shortcoming of this method is its becoming inapplicable at $T < 900$ K, when cesium atoms no longer desorb from a metal coated by a carbon film.

2. From the shape of the carbon Auger spectrum. The shape of the Auger spectrum of carbon is extremely sensitive to the chemical state in which it resides on the surface (§3). This method is applicable over a wide range of temperatures (in the present study, 300–2500 K).

3. From a change in the shape of carbon Auger spectrum in adsorption of alkali metals. It was shown that adsorption of Cs, K, and Na on a graphene film atop a metal modifies strongly the shape of the high-energy part of the carbon Auger spectrum, more specifically, the negative spike in the spectrum splits into three peaks located energy-wise at 272, 276.5, and 281 eV (Fig. 14, spectrum 5). At the same time, adsorption of alkali metals on a monolayer of chemisorbed (non-graphite) carbon does not initiate such changes. This method turned out fruitful in detection of the graphite phase.

4. By application of TDS. It is known that cesium present on refractory metals desorbs completely from the surface at $T \leq 900$ K. Cesium atoms adsorbed on carbon (non-graphite) films are desorbed totally in the 900–1100-K interval. If, however, cesium atoms are adsorbed at 300 K on graphene-coated iridium to saturation, the TD spectrum will reveal two phases: a low-temperature (~ 900 K) and a high-temperature (~ 2000 K) ones, the latter being associated with cesium escaping from under the graphene film in the course of its destruction. Thus the presence in a TD spectrum of the high-temperature phase implies unambiguously the presence of the graphene phase of carbon on the metal surface in submonolayer coverages.

5. From the work function. The work function of a chemisorbed carbon film, for instance, on iridium is larger by 0.3 eV than that of graphene film. Therefore, graphitization should be accompanied here by a decrease of the work function.

Graphitization of a film evaporated on iridium. Carbon atoms were evaporated at 300 K on iridium up to $\theta \approx 1.5$; this coverage implies complete filling of the first layer with carbon, the second layer containing carbon to $\theta = 0.5$. At $\theta = 1.5$, the surface work function varying from 5.75 eV to 4.75 eV becomes stabilized. Tests for graphite (involving cesium adsorption)

demonstrated that the film prepared by this method is non-graphitic (Fig. 51, spectrum 2). After this, the carbon film was annealed for 10 min at each temperature point and analyzed again. It was found that only after annealing at $T = 1300$ K did adsorption of cesium atoms initiate noticeable appearance of a fine structure in the carbon Auger spectrum (3 in Fig. 51). The degree of graphitization increased with increasing temperature, until at $T = 1500$ K graphitization of the carbon film came to completion; indeed, adsorption of Cs atoms brought about now the appearance of a fine structure in the Auger spectrum of carbon like that from a graphene film (Fig. 51, spectrum 5). The onset of complete graphitization is corroborated also by a decrease of the surface work function from 4.75 down to 4.45 eV.

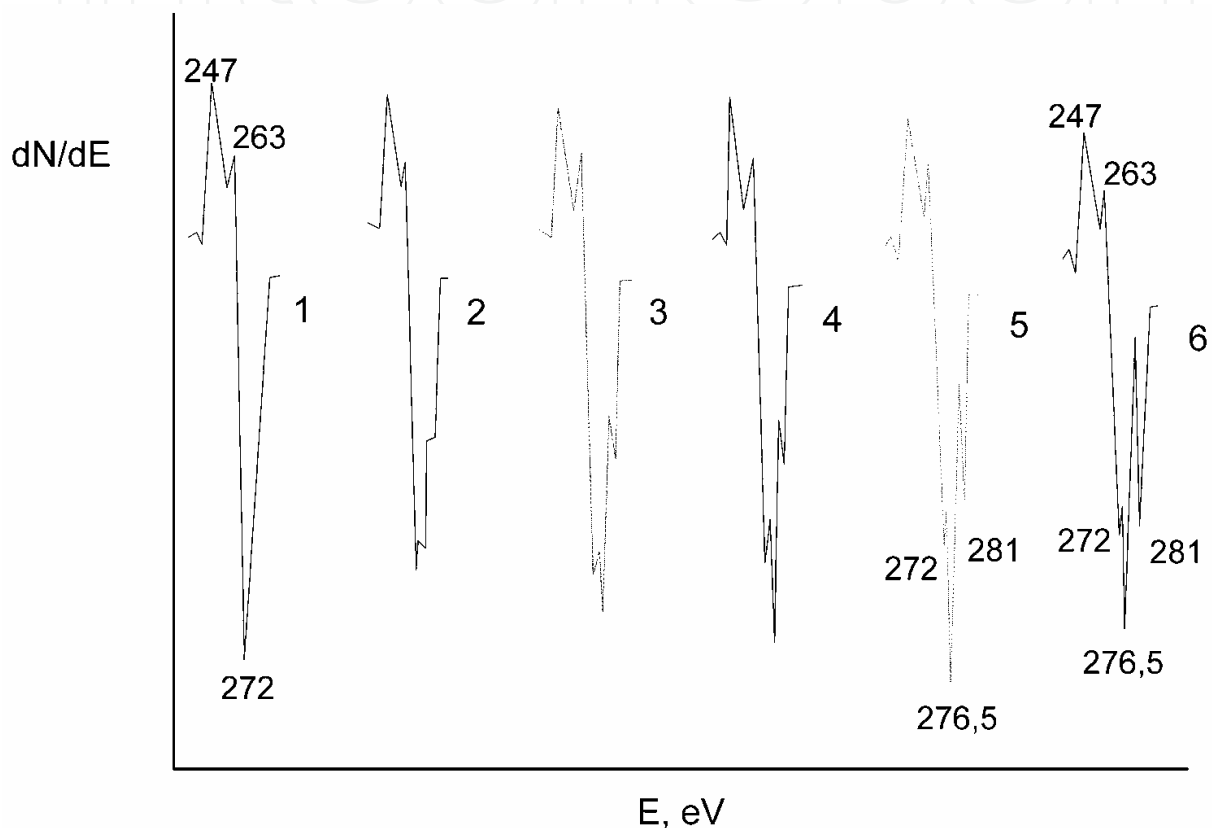


Fig. 51. Transformation of carbon KVV Auger spectra in adsorption of atomic Cs to saturation. The carbon film was got by atomic carbon deposition at 300 K ($\theta_C \sim 1.5$) with sequential annealing at various temperatures, K: 1- 300, 2 - 800, 3 - 1300, 4 - 1400, 5 - 1500, 6 - 1600. The total amount of the adsorbed Cs in saturation for the spectrum 6 is twice as high as for the spectrum 2.

The processes involved in graphitization can be studied through dissociation of CsCl molecules too. Figure 52 plots the variation of the degree of dissociation ω with the heating time of a chemisorbed carbon layer ($\theta \sim 1.5-2$) for two substrate temperatures. We readily see that the major changes take place during $t \approx 30$ s of heating, while subsequent heating (~ 10 min) produces very little effect. At $T = 1300$ K, ω drops to $\omega = 0.1$ only, which suggests incomplete graphitization. At $T = 1600$ K, the graphitization comes to completion, with $\omega = 10^{-3}$, which corresponds to a graphene film. Figure 53 illustrates the behavior of the $\omega(T)$ relation for a carbon film with $\theta = 1.5$ chemisorbed at 300 K, which was studied under stepped heating from 1200 to 1600 K (at each point, ω was measured 30 s after the

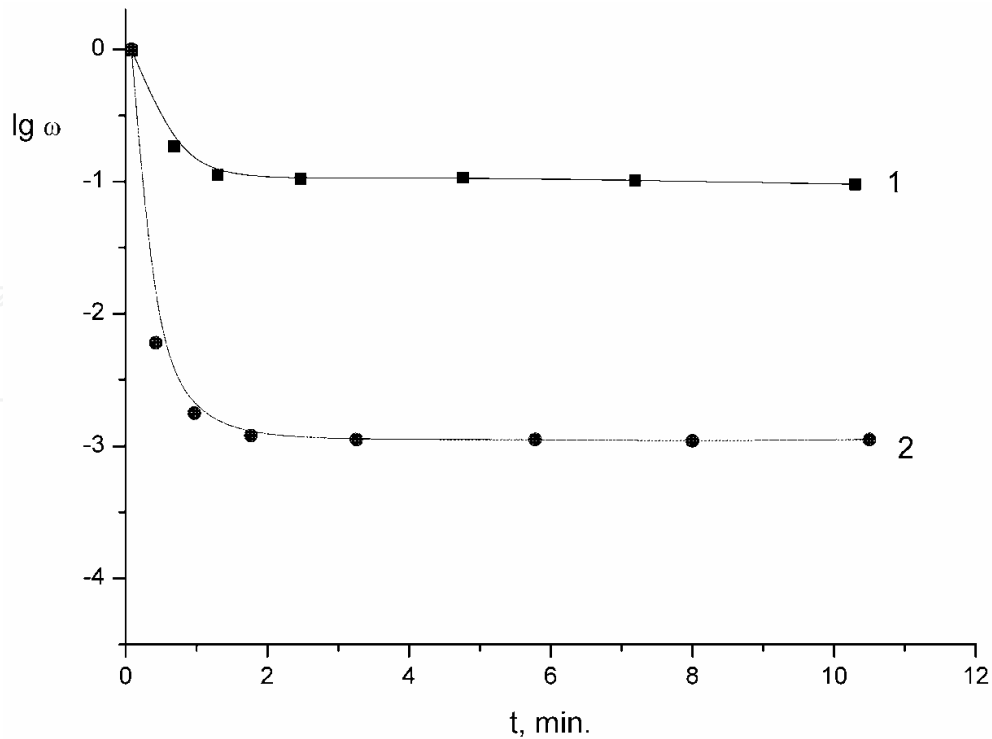


Fig. 52. The dependence of $\lg \omega$ for molecular CsCl from annealing time of the carbon layer deposited at 300 K with $\theta_C \sim 1.5$ for two substrate temperatures, K: 1 - 1300; 2 - 1600. The deposition flux of molecular CsCl is $v_{\text{CsCl}} = 1 \cdot 10^{12} \text{ cm}^{-2} \cdot \text{s}^{-1}$.

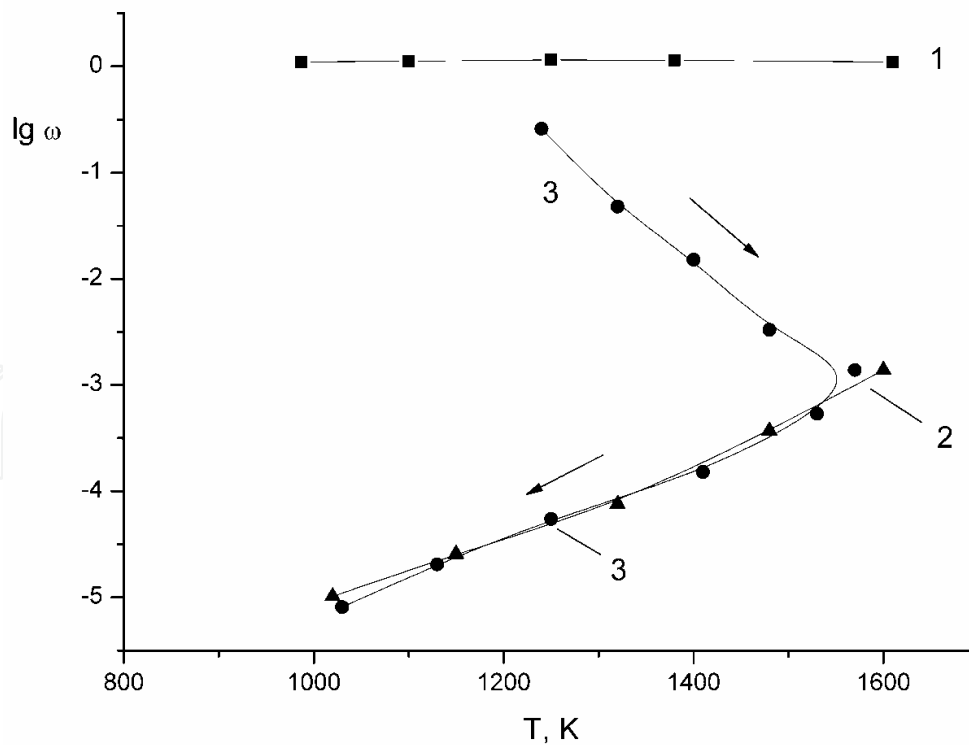


Fig. 53. The dependence of $\lg \omega$ for molecular CsCl from temperature for three surfaces: 1 - pure Ir(111); 2 - graphene single layer on Ir(111); 3 - carbon layer deposited at 300 K with $\theta_C \sim 1.5$. Exposure at each point is 10 s; $v_{\text{CsCl}} = 1 \cdot 10^{12} \text{ cm}^{-2} \cdot \text{s}^{-1}$.

temperature had been raised). On reaching complete graphitization, decrease of temperature reproduces the $\omega(T)$ relation obtained with a graphene film (Fig. 53). This suggests that graphitization of a carbon film with $\theta = 1.5$ chemisorbed at 300 K occurs in the 1300--1500-K temperature interval. Interestingly, evaporation of carbon atoms on heated iridium affects favorably graphitization, in that its temperature interval shifts toward lower temperatures, 950--1100 K, and comes to completion at 1100 K.

One can reasonably suggest that carbon atoms adsorbing on a heated substrate at $T \sim 1000$ K fit immediately into the thermally favorable graphite phase. In the case of a carbon film chemisorbed at 300 K, a variety of different carbon structures form on the surface, and, therefore, graphitization requires expending an activation energy to break different C-C bonds, a factor that curtails graphitization.

Graphitization of a carbon layer formed on a graphene film atop iridium. The experiment was started by producing a graphene film on iridium at $T = 1700$ K in benzene vapor, after which carbon was evaporated at 300 K on the graphene to $0.1 \leq \theta \leq 150$. The graphitization of the carbon films thus formed was studied at $T = 1300$ K by CsCl dissociation (Fig. 54). We readily see that evaporation on a graphene film of carbon atoms stimulates growth of ω , which is the more pronounced, the larger the evaporated carbon dose. For instance, for $\theta \sim 100$, $\omega = 0.6$, and this carbon film approaches in its catalytic properties a metal, for which $\omega = 1$. To make graphitization of thick carbon films with $\theta \approx 100$ complete, temperatures in excess of 2200 K were required.

The decrease of $\omega(T)$ for $T = \text{const}$ evident in Fig. 54 can be assigned to partial graphitization of carbon films.

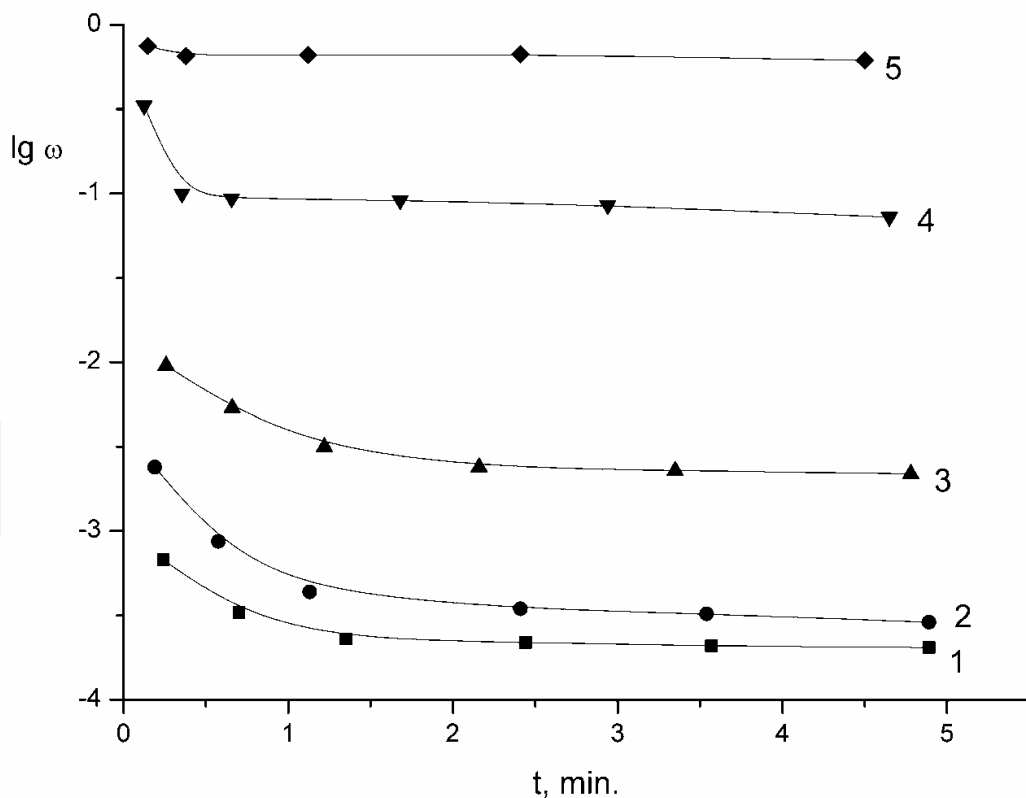


Fig. 54. The dependence of $\lg \omega$ for molecular CsCl from annealing time of the carbon layer deposited at 300 K with θ_C , arb.un.: 1 - 1.1; 2 - 1.4; 3 - 2.6; 4 - 9, 5 - 100. Annealing temperature is 1300 K; $v_{\text{CsCl}} = 1 \cdot 10^{12} \text{ cm}^{-2} \cdot \text{s}^{-1}$.

Graphitization of carbon films on iridium prepared by adsorption of benzene molecules.

Experiments demonstrated adsorption of benzene vapors on a heated iridium surface at high temperatures, 1500--1800 K, to culminate in formation of a graphene film. At lower temperatures, the carbon film prepared by adsorption of benzene undergoes graphitization in the temperature region $1100 < T < 1400$ K, with the process being only partial at $T < 1400$ K, to become complete for $T \geq 1400$ K (the test for graphite was effected by adsorption at 300 K of Cs atoms which brought about the change of the carbon Auger peak shape, namely, the appearance of "splitting").

It is instructive to follow the process of graphitization occurring in adsorption of benzene molecules on iridium at 300 K to saturation, with subsequent annealing of the film. Spectrum 1 in Fig. 55 corresponds to a benzene monolayer. At $T \sim 800$ K, desorption of hydrogen [124] produced in the breakup of benzene molecules on iridium sets in, and a carbon film, consisting apparently of carbon cores of benzene molecules and their cluster fragments, forms on the surface. Tests on graphite performed after the annealing of such a film at 900 and 1000 K (spectra 2 and 3) showed the film to be non-graphitic. Graphitization starts at anneal temperatures $T > 110$ K, with the process coming to completion at $T = 1400$ K. The end result is formation on the surface of graphene islands over a relative area $s_0 \sim 0.5$. The graphitization is accompanied by a slight modification of the carbon Auger peak shape (spectra 4 and 5 in Fig. 55).

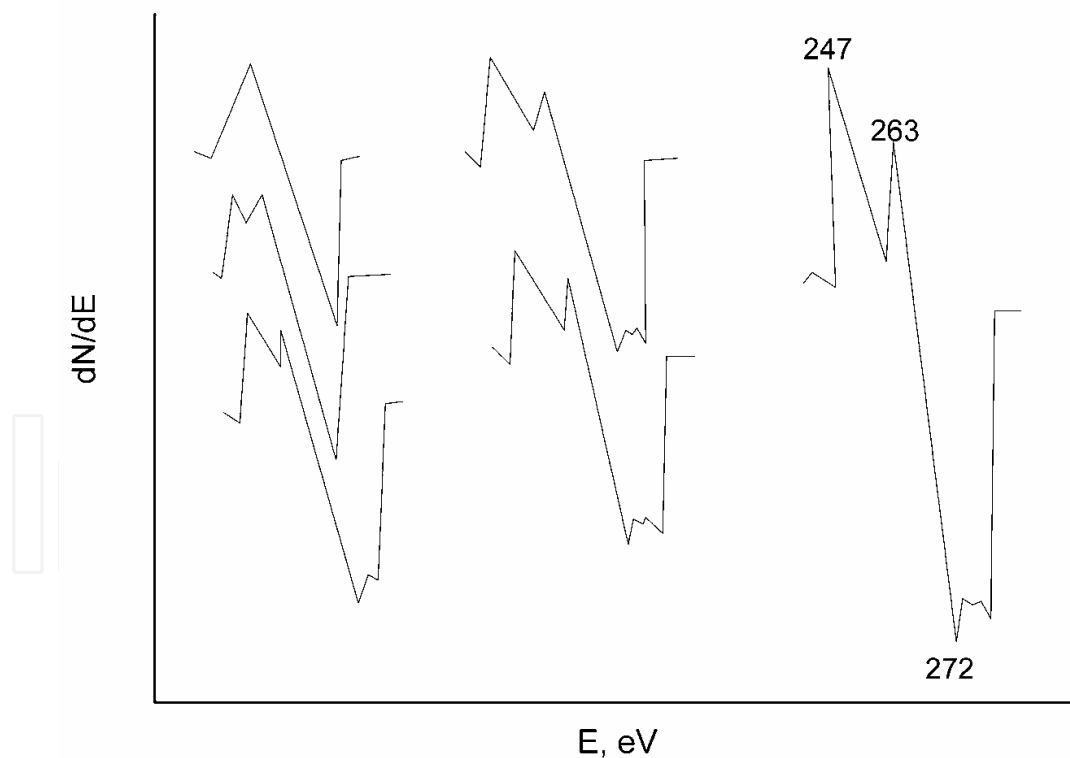


Fig. 55. Transformation of carbon KVV Auger spectra for benzene vapor adsorbed to saturation onto Ir(111) at 300 K in surface heating at various temperatures, K: 1 - 300 (spectrum remains unchanged up to 600 K); 2 - 900; 3 - 1040; 4 - 1280; 5 - 1400 (spectrum remains unchanged up to 1850 K). the spectrum 6 corresponds to the single graphene layer on Ir(111).

Significantly, the high temperature ($T \approx 1400$ K) required for complete graphitization of carbon films prepared by low-temperature adsorption of benzene suggests that it is indeed rupture of C-C bonds in carbon clusters that is the limiting stage of the process, because complete graphitization of films of atomic composition takes place at $T \approx 1100$ K. Clusters may form on the surface through adsorption of already existing clusters in evaporation, say, of carbon from pyrographite ribbons, association of carbon atoms in the layer, and adsorption and breakup of molecules of hydrocarbons producing cluster fragments.

A. Ya. Tontegode [27] and N. R.Gall, E. V. Rut'kov and A. Ya. Tontegode [41] studied the conditions favoring graphitization on other substrates as well, namely, Re, Pt, and Ni, which are among the most widely used industrial catalysts. It was shown that thin carbon films (one to two layers thick) undergo graphitization at moderate temperatures $T \sim (1100 \pm 250)$ K. Listed below in Table 9 are the temperature intervals within which one layer of carbon chemisorbed at 300 K on different metals can be graphitized, with the upper T referring to the onset of graphitization, and the lower one, to complete graphitization of the layer.

Examining the table shows that the conditions favoring graphitization are different for different metals. On nickel, graphitization occurs at the lowest temperatures of all.

Me	Ir(111)	Re(1010)	Pt(111)	Ni(111)
T, K	1200	1100	950	750
	1500	1500	1100	850

Table 9.

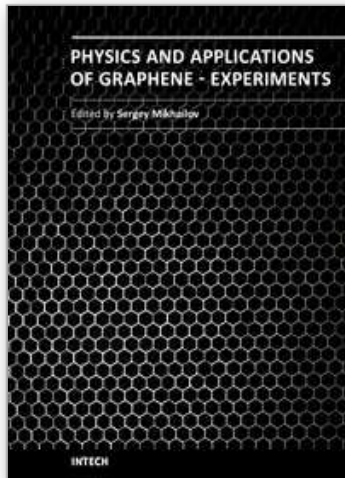
12. References

- [1] Palmberg P.W. In: The Structure and Chemistry of Solid Surfaces. Eds. G.A. Somorjai, J. Wiley. N.Y., 1969.
- [2] Hamilton J.C., Blakely J.M. J. Vacuum Sci. Technol. 1978. V.15. P. 559-562.
- [3] Grant J.T., Haas T.W. Surf. Sci. 1970. V. 21, P. 76-85.
- [4] Coad J.P., Riviere J.C. Surf. Sci. 1971. V. 25. P. 609-624.
- [5] Shelton J.C., Patil H.R, Blakely J.M. Surf. Sci. 1974. V. 43. P. 493-503.
- [6] Eizenberg M., Blakely J.M. Surf. Sci. 1979.V. 82(1). P. 228-236.
- [7] Humilton J.C., Blakely J.M. Surf. Sci. 1980. V. 91(1). P. 199-217.
- [8] Gillet E.J. Less-Common. Met. 1980. V. 71(1). P. 277-291.
- [9] Rut'kov E.V., Tontegode A.Ya., Usufov M.M., Gall N.R. ЖТФ. 1992. V. 62(10). P. 148-153.
- [10] Beitel G.A. J. Vac. Sci. and Technol., 1969. V. 6. P. 224-228.
- [11] Gall N.R., Mikhailov S.N., Rut'kov E.V., Tontegode A.Ya. Surf. Sci. 1987. V. 191. P.185-202.
- [12] Rut'kov E.V., Gall N.R., Physics of the Solid State, 2009, Vol. 51, No. 8, pp. 1738-1743
- [13] Kholin N.A., Rut'kov E.V., Tontegode A.Ya. Surf. Sci. 1984. V.139. P. 155-172.
- [14] Tontegode A.Ya., Rut'kov E.V. Surf. Sci. 1985. V. 161. P. 373-389.
- [15] Ageev V.N., Rut'kov E.V., Tontegode A.Ya., Kholin N.A. Fiz. Tverd. Tela, 1982. V. 24(3). P. 780-786.
- [16] Abdullaev R.M., Tontegode A.Ya. Zh.Tech. Fiz. 1980. V. 50. P. 577-581.
- [17] Tilley B., Aizava T., Souda R., Hayami W., Otani S., Ishizava Y. Solid State Communications. 1995. V. 94. P. 685.
- [18] Nagashima A., Itoh H., Ishinokava T., Oshima C, Otani S. Phys. Rev. B. 1994. V. 50. P. 4756.
- [19] M.W.Roberts, C.S.McKee "Chemistry of the metal-gas interface", Clarendon Press, Oxford, 1978, pp.300-331

- [20] Gall N.R., Makarenko I.V., Titkov A.N., Waqar Z., Rut'kov E.V., Tontegode A.Ya., Usufov M.M., Poverhnost, 1999. V. 7. P. 39-42.
- [21] Waqar Z., Makarenko I.V., Titkov A.N., Gall N.R., Rut'kov E.V., Tontegode A.Ya. J. of Materials Research (JMR). 2004. V 19(4). P. 1058-1061.
- [22] Klusek Z., Kozlowski W., Waqar Z., Patta S., Buenell-Gray J.S., Makarenko I.V., Gall N.R., Rut'kov E.V., Tontegode A.Ya., Titkov A.N. Applied Surface Science. 2005. V. 252. P. 1221-1227.
- [23] Makarenko I.V., Titkov A.N., Rut'kov E.V., Gall N.R. Izvestia RAN (Seria fizicheskays) 2007. V. 71(1). P. 57-60.
- [24] Rut'kov E.V., Tontegode A.Ya. Fiz. Tverd. Tela, 1996. V. 38(2). P. 635-639.
- [25] E.Fromm, E.Gebhardt "Gase und Kohlenstoff in Metallen", Springer-Verlag, Berlin, 1976
- [26] Gall N.R., Rut'kov E.V., Tontegode A.Ya., Kuznetsov P.B., Gall R.N. J. Chemical Vapor. 1997. V. 6(10). P. 72-75.
- [27] Tontegode A.Ya. Progress in Surface Science. 1991. V. 38(3-5). P. 429.
- [28] Fomenko V.S. Electronic properties of materials. Reference-book, Kiev< Naukova Numka, 981, 336 c.
- [29] Gall N.R., Rut'kov E.V., Tontegode A.Ya. Rossiiski Himichesky Zurnal, 2003. V. 47(2). P. 13-22.
- [30] Ageev V.N., Afanasieva E.Yu., Gall N.R., Mikhailov S.N., Rut'kov E.V., Tontegode A.Ya. Poverkhnost. 1987. V. 5. P. 7-14 (in Russian).
- [31] Gall N.R., Rut'kov E.V., Tontegode A.Ya. Zh.Tech. Fiz., 1990. V. 60(4). P. 125-130.
- [32] Gall N.R., Rut'kov E.V., Tontegode A.Ya., Usufov M.M. Pisma v Zh.Tech. Fiz., 1994. V. 20(18). P. 65.
- [33] Gall N.R., Rut'kov E.V., Tontegode A.Ya., Usufov M.M. Applied Surface Science. 1996. V. 93. P. 353-358.
- [34] Gall N.R., Rut'kov E.V., Tontegode A.Ya., Usufov M.M. Applied Surface Science. 1994. V. 78. P. 179-184.
- [35] Shank F.A. Structure of Binary Alloys Moscow, Metallurgia, 1973, 568 p. (in Russian)
- [36] Rut'kov E.V., Tontegode A.Ya., Usufov M.M. Известия РАН (серия физическая). 1994. V. 58. P. 102-105.
- [37] Schulze G. Metallophysika. M.: Mir, 1971. 404 p. (in Russia)
- [38] Anderson J. Structure of Metal catalysts, Mocsow, MIR, 1978. 482 p (in Russian).
- [39] Zandberg E.Ya. and Ionov N.I. Surface Ionization. Israel Program for Scientific Translation. Jerusalem, 1971.
- [40] Nasrullaev N.M., Rut'kov E.V., Tontegode A.Ya. Zh.Tech. Fiz.. 1987. V. 57(2). P. 353-356.
- [41] Gall N.R., Rut'kov E.V., Tontegode A.Ya. Int. J. of Modern Physics B. 1997. V. 11(16). P. 1865-1911.
- [42] Ageev V.N., Rut'kov E.V., Tontegode A.Ya., Kholin N.A. Fiz. Tverd. Tela, 1981. V. 23(8). P. 2248-2254.
- [43] Gall N.R., Rut'kov E.V., Tontegode A.Ya., Usufov M.M. Zh.Tech. Fiz. 1997. V. 67(7). P. 137-140.
- [44] Methods of Surface Analysys, ed. by A.W.Zanderna, N.Y., 1975.
- [45] Shrednik V.N. ФТТ. 1961. V. 3. P. 1750-1761.
- [46] Shrednik V.N., Odishariya G.A. Izvestia AN USSR (Seria fizicheskays). 1969. V. 33. P. 536-543.
- [47] Odishariya G.A., Shrednik V.N. Dokladi AN USSR, 1968. V. 182. P. 542-544.
- [48] Shrednik V.N., Odishariya G.A. Fiz. Tverd. Tela, 1969. V. 11. P. 1844-1853.
- [49] Shrednik V.N. Cristal Growth and Field Ion Microscopy, Moscow, Nauka, 1975. P. 150-171. (in Russian)

- [50] Zandberg E.Ya., Tontegode A.Ya., Yusifov F.K. Zh.Tech. Fiz.. 1971. V. 41. P. 2420-2427.
- [51] Zandberg E.Ya., Tontegode A.Ya., Yusifov F.K. Zh.Tech. Fiz.. 1972. V. 42(1). P. 171-174.
- [52] Potekhina N.D., Tontegode A.Ya. Zh.Tech. Fiz. 1972. V. 42. P. 162-170.
- [53] Medvedev V.K., Naumovets A.G., Fedorus A.G. Fiz. Tverd. Tela, 1970. V. 12. P. 375-385.
- [54] Vedula Yu.S., Naumovets A.G., Ukrainski Fizicheski Zurnal, 1973. V. 18. P. 1000-1007.
- [55] Arthur J.R., Cho A.Y. Surf. Sci. 1973. V.36. P. 641-660.
- [56] Bol'shov L.A., Napartovich A.P. Fiz. Tverd. Tela, 1971. V. 13. P. 1679-1684.
- [57] Bol'shov L.A., Napartovich A.P. Zh. Exp. Tech. Fiz. 1973. V. 64. P. 1404-1413.
- [58] R.Defay, I.Prigogine, A.Bellmans, D.H.Everett Surface tension and Adsorption, N-Y, Willey and Son, 1966, 274 p..
- [59] Thermodynamic constants of matter, V. IV, part I. M. Ussr Academy of Sciences. 1970. 383 p (in Russian).
- [60] Dobretsov L.N. Zh.Tech. Fiz.,. 1934. V. 4. P. 783-795.
- [61] Potekhina N.D. Poverhnost, 1987, No 4, P. 14- 21
- [62] Rut'kov E.V., Tontegode A.Ya. Uspekhi Fiz. Nauk. 1993. V. 163. P. 57.
- [63] Gall N.R., Rut'kov E.V., Tontegode A.Ya. Pisma v Zh.Tech. Fiz., 1988. V. 14(6). P. 527-532.
- [64] Rosei R., De Cresceci M., Sette F., Quaresima C., Savoia A., Perfetti P. Phys. Rev. 1983. V. 28. P. 1161-1164.
- [65] Efimov A.I., Belorukova L.P., Basil'kova I.V., Chechev V.P. "Properties of Nonirganic Compounds", Handbook, Leningrad , Khimia, 1983 (in Russian)
- [66] Zi-Pu Hu, Ogletree D.F., Van-Hove M.A., Somorjai G.A. Surf. Sci. 1987. V.180. P. 433-459.
- [67] Ageev V.N., Soloviev S.N., Tontegode A.Ya. Fiz. Tverd. Tela, 1981. V. 23. P. 2280-2289.
- [68] Meksted E.B. in Problems of catalysis, Moscow, Inostrannaia Literatura, 1955. 100 p.(in Russian)
- [69] Fogel Ya.M., Nadytko V.T., Rybalko V.F., Slabospitsky R.P., Korobchanskaya I.E. ДАН СССР. 1962. V.147. P. 414-417.
- [70] Wilhoff M.A. Trahs. Farad. Soc. 1968. V.64. P. 1925-1933.
- [71] Zandberg E.Ya., Tontegode A.Ya. Zh.Tech. Fiz.. 1970. V. 40. P. 626-630.
- [72] Zandberg E.Ya., Tontegode A.Ya., Yusifov F.K. Fiz. Tverd. Tela, 1970. V. 12. P. 1740-1744.
- [73] Zandberg E.Ya., Tontegode A.Ya. Zh.Tech. Fiz. 1968. V. 38. P. 763-766.
- [74] Abdullaev R.M. "Growth of carbon films on Ir, Re, and Pd, and its role in their adsorption, catalytic, and emission properties". Candidate thesis, Leningrad, 1983. 194 p (in Russian).
- [75] Mc Carty J.G., Madix R.J. J. of Catalysis. 1975. V. 38. P. 402-409.
- [76] Goodman D.W., Kelley R.D., Madey T.E., Yates J.T. J. of Catalysis. 1980. V. 63. P. 226-231.
- [77] Bonzel H.P., Krebs H.J. Surf. Sci. 1980. V. 91. P. 499-513.
- [78] Tontegode A.Ya. Pisma v Zh.Tech. Fiz., 1977. V. 3. P. 635-639.
- [79] Bonzel H.P. J. Vacuum Sci. Technol. 1984. V. A2(2). P. 866-872.
- [80] Holmlid L. J. Chem. Phys. 1974. V. 61. P. 1244-1245.
- [81] Zandberg E.Ya., Nasrullaev N.M., Potekhina N.D., Rut'kov E.V., Tontegode A.Ya. Kinetika i Kataliz. 1991. V. 32(1). P. 92-97.
- [82] Zandberg E.Ya., Nasrullaev N.M., Rut'kov E.V., Tontegode A.Ya. Kinetika i Kataliz. 1986. V. 27(5). P. 1170-1173.
- [83] Zandberg E.Ya., Nasrullaev N.M., Rut'kov E.V., Tontegode A.Ya. Dokladi AN USSR. 1987. V. 295(3). P. 633-636.
- [84] Zandberg E.Ya., Nasrullaev N.M., Rut'kov E.V., Tontegode A.Ya. Himicheskaya Fizika. 1988. V. 7(7). P. 962-969.
- [85] Potekhina N.D. Kinetika i Kataliz. 1990. V. 31. P. 72-78.

- [86] Wakar Z., Gall N.R., Makarenko I.N., Rut'kov E.V., Titkov A.N., Tontegode A.Ya., Usufov M.M. *ФТТ*. 1998. V. 40(8). P. 1570-1573.
- [87] Beigel G.A. *J. Vac. Sci. and Technol.* 1972. V. 9. P. 370-372.
- [88] Lander J.J., Morrison J. *Surf. Sci.* 1966. V. 4. P. 103-107.
- [89] Morrison J., Lander J.J. *Surf. Sci.* 1966. V. 5. P. 163-169.
- [90] Lander J.J., Morrison. *J. Appl. Phys.* 1964. V.35. P. 3593-3599.
- [91] Baner E., Bonczek F., Poppa H., Todd G. *Surf. Sci.* 1975. V. 53. P. 87-109.
- [92] Hamilton J.F., Logel P.C., Baetzold R.C. *Thin Solid Films.* 1976. V. 32. P. 233-236.
- [93] Hamilton J.F., Logel P.C. *Thin Solid Films.* 1974. V. 23. P. 89-100.
- [94] Hamilton J.F., Logel P.C., Baetzold R.C. *Thin Solid Films.* 1973. V. 16. P. 49-63.
- [95] Pashley P.W., Stowell M.F., Jacobs M.H., Law T.J. *Phil. Mag.* 1964. V. 10. P. 127-158.
- [96] Corbett J.M., Baswell F.W. *J. Appl. Phys.* 1969. V. 40. P. 2663-2669.
- [97] Fedorus A.G. "Electronic and adsorption properties and the structure of Cs and Na films on W surface" Doctor thesis, Kiev, 1970. 160 p.
- [98] I.F.Luksutov, A.G.Naumovetz, V.L.Pokrovsky, "Two-Dimensional Crystals", Kiev, Naukova Dumka, 1988, p.20. (in Russian)
- [99] Ionov N.I., Mittsev M.A. *Fiz. Tverd. Tela*, 1975. V. 17. P. 1607-1612.
- [100] Mc Carty J.G., Madix R.J. *Surf. Sci.* 1976. V. 54. P. 121-138.
- [101] Abdullaev R.M., Tontegode A.Ya., Yusifov F.K. *Fiz. Tverd. Tela*, 1978. V. 20. P. 2343-2356.
- [102] Abdullaev R.M., Tontegode A.Ya., Yusifov F.K. *Fiz. Tverd. Tela*, 1978. V. 20. P. 3217-3224.
- [103] Abon M., Billy J.C., Bertolini J.C., Jardy B. *Surf. Sci.* 1986. V. 167. P. L187-L193.
- [104] Zandberg E.Ya., Rut'kov E.V., Tontegode A.Ya. *Zh.Tech. Fiz.* 1975. V. 45. P. 1884-1891.
- [105] Zandberg E.Ya., Potekhina N.D., Rut'kov E.V., Tontegode A.Ya. *Zh.Tech. Fiz.* 1982. V. 52. P. 2398-2404.
- [106] Love H.M., Wiederick H.D. *Canad. J. Phys.* 1969. V. 47. P. 657-663.
- [107] Rut'kov E.V., Tontegode A.Ya., Usufov M.M. *Phys. Rev. Letters.* 1995. V. 74(5). P. 758-760.
- [108] Burrer R.M. *Diffusion in and through Solid.* Cambridge. 1941.
- [109] Shumon P. *Diffusion in Solids.* Moscow, Metallurgia, 1966. 195 p. (in Russian)
- [110] Seach M.P. In: *Practical Surface Analysis by Auger and X-ray Photoelectron Spectroscopy.* John Willey&Sons Ltd., 1983. P. 277-317.
- [111] Rawlings K.J., Foulis S.D., Hopkins B.J. *Surf. Sci.* 1981. V. 109. P. 513-521.
- [112] Rudman P.S. *TMS-AIME.* 1967. V. 239. P. 1949.
- [113] Tontegode A.Ya., Yusifov F.K. *Poverhnost*, 1994. V. 4. P. 20-24.
- [114] Samsonov G.V., Vanitsky I.M. *Refractory Compounds, Reference-book*, Moscow, Metallurgia, 1976, 558 p.
- [115] Gall N.R., Lavrovskaya N.P., Rut'kov E.V., Tontegode A.Ya. *Phys. Rev. Letters.* 1995. V. 74(5). P. 758-760.
- [116] Rut'kov E.V., Gall N.R. *Fiz. Tverd. Tela*, 2008.
- [117] Goldschmidt H.J. *Interstitial Alloys*, Moscow, MIR, 1971. 424 p. (in Russian)
- [118] Shelton J.C., Patil H.R., Blakely J.M. *Surf. Sci.* 1974. V. 43. P. 493-505.
- [119] Tontegode A.Ya., Abdullaev R.M., Yusifov F.K. *Zh.Tech. Fiz.* 1975. V. 45. P. 1904-1914.
- [120] Panzner G., Diekmann W. *Surf. Sci.* 1985. V. 160. P. 253-270.
- [121] Tontegode A.Ya., Yusifov F.K. *Zh.Tech. Fiz.* 1973. V. 43. P. 1106.
- [122] Pallmer P.G., Jr., Gordon R.L. *J. Appl. Phys.* 1980. V. 51(3). P. 1798-1801.
- [123] Espe V. *Technology of electronic vacuum materials*, Moscow, State Electronics Publishing, 1962. V. 1. 631 p. (in Russian)
- [124] Gall N.R., Mikhailov S.N., Rut'kov E.V., Tontegode A.Ya. *Kinetika i Kataliz.* 1988. V. 29. P. 1196-1201.



Physics and Applications of Graphene - Experiments

Edited by Dr. Sergey Mikhailov

ISBN 978-953-307-217-3

Hard cover, 540 pages

Publisher InTech

Published online 19, April, 2011

Published in print edition April, 2011

The Stone Age, the Bronze Age, the Iron Age... Every global epoch in the history of the mankind is characterized by materials used in it. In 2004 a new era in material science was opened: the era of graphene or, more generally, of two-dimensional materials. Graphene is the strongest and the most stretchable known material, it has the record thermal conductivity and the very high mobility of charge carriers. It demonstrates many interesting fundamental physical effects and promises a lot of applications, among which are conductive ink, terahertz transistors, ultrafast photodetectors and bendable touch screens. In 2010 Andre Geim and Konstantin Novoselov were awarded the Nobel Prize in Physics "for groundbreaking experiments regarding the two-dimensional material graphene". The two volumes *Physics and Applications of Graphene - Experiments* and *Physics and Applications of Graphene - Theory* contain a collection of research articles reporting on different aspects of experimental and theoretical studies of this new material.

How to reference

In order to correctly reference this scholarly work, feel free to copy and paste the following:

E.V.Rut'kov and N.R.Gall (2011). Equilibrium Nucleation, Growth, and Thermal Stability of Graphene on Solids, *Physics and Applications of Graphene - Experiments*, Dr. Sergey Mikhailov (Ed.), ISBN: 978-953-307-217-3, InTech, Available from: <http://www.intechopen.com/books/physics-and-applications-of-graphene-experiments/equilibrium-nucleation-growth-and-thermal-stability-of-graphene-on-solids>

INTECH
open science | open minds

InTech Europe

University Campus STeP Ri
Slavka Krautzeka 83/A
51000 Rijeka, Croatia
Phone: +385 (51) 770 447
Fax: +385 (51) 686 166
www.intechopen.com

InTech China

Unit 405, Office Block, Hotel Equatorial Shanghai
No.65, Yan An Road (West), Shanghai, 200040, China
中国上海市延安西路65号上海国际贵都大饭店办公楼405单元
Phone: +86-21-62489820
Fax: +86-21-62489821

© 2011 The Author(s). Licensee IntechOpen. This chapter is distributed under the terms of the [Creative Commons Attribution-NonCommercial-ShareAlike-3.0 License](#), which permits use, distribution and reproduction for non-commercial purposes, provided the original is properly cited and derivative works building on this content are distributed under the same license.

IntechOpen

IntechOpen